ADVANCED CHARACTERIZATION OF GLUCAN PARTICULATES: SMALL-GRANULE STARCHES, RETENTION OF SMALL MOLECULES AND LOCAL SPATIAL ARCHITECTURE DEFINED BY MOLECULAR ROTOR

by

Xingyun Peng

A Dissertation

Submitted to the Faculty of Purdue University

In Partial Fulfillment of the Requirements for the degree of

Doctor of Philosophy

Department of Food Science

West Lafayette, Indiana

December 2018

THE PURDUE UNIVERSITY GRADUATE SCHOOL
STATEMENT OF COMMITTEE APPROVAL

Dr. Yuan Yao, Chair
Department of Food Science
Dr. Bruce R. Hamaker
Department of Food Science
Dr. James R. Daniel
Department of Nutrition Science
Dr. Owen G. Jones
Department of Food Science

Approved by:

Dr. Arun K. Bhunia
Head of the Graduate Program

I dedicate my dissertation work to my family and many friends. A special feeling of gratitude to my loving parents, Jian Peng and Hejun Wu whose unconditional love support me throughout my 18-year-long student life away from home. My wife, Ru Shen, who has been a constant source of support and encouragement during the challenges of research and life. The distance between University of Illinois and Purdue has never set us apart in the past four years but jointed us as dearest life partners in Summer 2018. I believe our love will last forever. I also dedicate this dissertation to my families and friends who have supported me throughout the process. In my every step forward, my grandparents, Ze Peng, Yimin Liu, Weimin Wu; my sisters and brothers, Kai Yu and Yu Yan, Zhaoxiong Wu, Jing Que and Hongliang Li, and Yuli Shen; my aunt, Ling Peng, I have so much precious memories that you gave me support, encouragement, guidance and confidence in facing any challenges. I only hope that someday I can make you proud of me.

ACKNOWLEDGMENTS

I would like to express my gratitude to many people who are my families, friends, and academic mentors. I couldn't get through all challenges in the process of my research and life without your help and support. First and foremost, I would like to thank my parents and my wife for their unconditional love, patience and support. I would also like to express my gratitude to my sincerely advisor, Dr. Yuan Yao, whose guidance has helped me in many fields of researches and life at Purdue University. I also give my sincerely gratitude to my advisory committee members, Dr. Andrea M. Liceaga, Dr. Bruce R. Hamaker, Dr. James R. Daniel and Dr. Owen G. Jones. Without your assistance and encouragement, I couldn't have gone so far with my research. I would like to give my very special thanks to my dear labmates, past and present, including Ying Xie, Randol J. Rodriguez, Yezhi Fu, Jingfan Chen and Miguel A. Gonzales for their strong supports throughout my work at Purdue. I will never forget the precious memories in the past four years with you lovely guys. I sincerely hope your life will be full of happiness and love. Last but not the least, I would like to thank to the financial supports from China Scholarship Council and Bilsland Dissertation Fellowship.

TABLE OF CONTENTS

LIST OF TABLES

LIST OF FIGURES

LIST OF ABBREVIATIONS

AS: Amaranth starch

ANBPC: Average number of branches per cluster

AP: Amylopectin

AP-BLD: β-limit dextrin of amylopectin

BLD: β-limit dextrin

CCS: Cow cockle starch

CCVJ: 9-(2-carboxy-2-cyanovinyl) julolidine

CL: Chain length

CLD: Chain length distribution

$\overline{CL_n}$: Number-average chain length

d_{32}: Sauter mean diameter

d_{43}: Volume mean diameter

DE: Dextrose equivalent value

DP: Degree of polymerization

DMSO: Dimethyl sulfoxide

DSC: Differential scanning calorimetry

EG_b: Emission strength gradients per unit molar of branch points

GCWS starch: Granular cold-water swelling starch

HC setting: High-contrast setting

HPSEC: High performance size exclusion chromatography

I: Fluorescent emission response

IBD: Intra-cluster branch distance

ICL_{B2}: Internal chain length of B2 chain

LC setting: Low-contrast setting

LE state: Locally excited state

LM: Light microscopy

LMW, IMW, HMW: Low, intermediate and high molecular weight

$mMDC_{ums}$: Mass of maltodextrin components retained in unit mass of starch granules

MDC_f: Maltodextrin component in the free water phase

MR: Molecular rotor

n_b: Molar number of branch points per liter of glucan dispersion

NaAc: Sodium acetate

NCS: Normal corn starch

NG starch: Non-granular starch

NRS: Normal rice starch

PG: Phytoglycogen

PG-BLD: β-limit dextrin of phytoglycogen

PS: Potato starch

RFU: Relative fluorescence unit

RI: Refractive index

RVA: Rapid viscosity analyzer

R_Z: Z-average root mean square radius

SCS: Sweet corn starch

SEM: Scanning electron microscopy

SGS: Small-granule starch

SP: Swelling power

SS: Swellable starch

TICT state: twisted intramolecular charge transfer state

WCS: Waxy corn starch

WRS: Waxy rice starch

WSI: Water soluble index

λ_{max}: Peak emission wavelength

η: Viscosity

ABSTRACT

Author: Peng, Xingyun PhD
Institution: Purdue University
Degree Received: December 2018
Title: Advanced Characterization of Glucan Particulates: Small-granule Starch, Retention of Small Molecules, and Local Architecture Defined by Molecular Rotor
Committee Chair: Yuan Yao

The discovery and utilization of novel starches with unique superb properties are highly demanded for modern industrial uses. Small-granule starch (SGS) is a category of unconventional starches with the granular size smaller than 10 μm. The potential use of SGS includes many conventional and novel high-value applications, such as texturizing, fat replacement, encapsulation, controlled delivery and nano-engineering. In the present work, we focused on three SGS isolated from amaranth (*Amaranth cruentus*), cow cockle (*Saponaria vaccaria*) and sweet corn (*sugary-1* maize mutant). The basic structural and unique physical properties of SGS were characterized and compared to common large-granule food starches. It was found that (1) the highly branched amylopectin contributed to low crystallinity and pasting viscosities of sweet corn starch, (2) cow cockle starch exhibited high shear-resistance and low retrogradation in prolonged storage, and (3) the amylopectin for amaranth starch was less branched with small clusters, which was associated with the high crystallinity, medium shear-resistance and low pasting viscosity of amaranth starch. Despite the small size of starch granules, SGS in both native and swelling states showed the capacity of retaining small molecules. Compared to large-granule starch, native SGS are more difficult for small molecules to reach an equilibrium permeation. This work provides insights to the fine structure and physicochemical behaviors of selected high-potent SGS, which is believed to support the industrial production and application of SGS in the future.

The characteristics of local polymeric structure dominate many critical properties of glucan particles, such as starch retrogradation and the loading and stabilizing of active substance. Molecular rotor (MR), a fluorescent probe, was proposed to fulfill the simple, high-sensitive, and quantitative-based characterization of local glucan architecture (LGA). In the present work, two innovative studies relevant to this novel method were conducted: (1) MR was able to characterize glucans based on its unique fluorescent response to characteristic LGA, (2) MR was

able to sensitively probe and visually demonstrate the transition of LGA induced by starch retrogradation. This novel MR-based approach is expected to advance carbohydrate-related researches in the future.

Keywords: Small-granule starch; Molecular rotors; Amylopectin branching; Retention of small molecules; Glucan structure transition

CHAPTER 1. LITERATURE REVIEWS

1.1 Introduction

The discovery and utilization of novel starches with unique properties are highly demanded for modern industrial uses (Ellis et al., 1998; Muth et al., 2008). There is an ongoing trend in food industry for phasing out artificial food ingredients, such as chemically modified starch (McDonagh, 2012; Woodhouse, 2017). As one of the most important food ingredients, native and modified starches are conventionally used as thickener, stabilizer, gelling agent and bulking agent. These functionalities are relying on the physicochemical properties of starch, such as swelling, gelatinization and retrogradation (Singh et al., 2003). In most cases, chemical modifications are used to overcome the shortcomings of native starch and target on: (1) strengthening starch integrity, (2) enhancing the resistance to reverse processing or storage conditions (e.g. shearing and freezing), (3) functionalize starch matrix with hydrophobic, hydrophilic or charged groups (Bemiller, 1997).

Small-granule starch is a category of unconventional starches with the granular size smaller than 10 μm (Lindeboom et al., 2004). Compared to conventional large-granule starches (e.g. corn and potato starches), small-granule starches often exhibit large specific surface area, outstanding stability and high resistance to shear (Biliaderis et al., 1993; Goering and DeHaas, 1972; Juszczak et al., 2002). These superb properties may highlight the potential use of native small-granule starch not only for the replacement of chemically modified starch, but also for novel high-value applications, such as encapsulation, controlled delivery and nano-engineering.

There are economic, scientific and technological hurdles in the industrial production and utilization of small-granule starches. First, many small-granule starches are obtained from unconventional and less accessible botanic sources that are often belonging to either wild-type plants or local cultivars and are of course not suitable for industrial production (Goering and DeHaas, 1972; Jane et al., 1992, 1994). Second, it is still lack of scientific understanding on the structure, property and biogenesis of small-granule starches that impedes the breeding of small-granule starch bearing plants (Ao and Jane, 2007). Third, the small size of small-granule starch can make the isolation and purification process challenging as conventional hydrocyclones are not effective in recovering small starch granules (Lindeboom et al., 2004). From another

perspective, the three hurdles in fact establish the criteria that can help to identify high-potential small-granule starch and small-granule starch bearing plants.

In the present work, we focused on three small-granule starches isolated from amaranth (*Amaranth cruentus*), cow cockle (*Saponaria vaccaria*) and sweet corn (*sugary-1* maize mutant), because they are traditionally consumed as food or animal feed and the seeds (or grains) are currently commercially available (Azanza et al., 1996; Caselato-Sousa and Amaya-Farfán, 2012; Willenborg and Johnson, 2013). Therefore, the three starches are readily commercialized and utilized for food applications without accessibility or regulation hurdles. However, the basic property and the characteristic behaviors of the three selected starches for food uses remain unclear.

The fine structure of starch and starch-based matrix is closely relevant to its macroscale properties and potential applications. However, the routine methods for the characterization of the fine structure of starch is very complex, which usually involves tedious sample preparation and advanced chromatography equipment (Bello-Pérez et al., 1996; Klucinec and Thompson, 2002). Thus, a simple, rapid and non-invasive method for the characterization of starch fine structure is highly demanded in relevant research areas. Molecular rotor (MR) is a group of special fluorophores that release florescence after excitation and the quantum yield quantitatively correlates with the spatial restriction of the MR molecules (Haidekker and Theodorakis, 2010). Starch and starch-based matrix are polymeric networks exerting different extent of spatial restriction on small molecules. When MR is incorporated in starch or starch-based matrix, it is possible to use MR as a polymeric structure probe and characterize starch structures based on their spatial restriction to MR. This novel approach may also provide innovative insights into the fine structure and fine-structure related properties of starch.

In the present work, our overall goal was to carry out a comprehensive characterization of the selected small-granule starches from amaranth, cow cockle and sweet corn and to establish a novel fluorescent-based approach for the characterization of fine structure and fine structure-related properties of starch. The outcomes of the study could support the future utilization of small-granule starch and fundamental studies of starch.

1.2 Starch

Starch is one of the most abundant natural carbohydrate polymers produced by plants as energy storage. Starch has been consumed by human since ancient times and now is demanded by many important modern industries, such as the food, pharmaceutical and biofuel industries.
The chemical nature of starch is simply α-D-glucan that is a polymer of α-D-glucopyranose connected with α -1, 4 or α-1, 6 linkages. However, starch can possess highly diversified structure and physicochemical properties since the degree of polymerization and the supramolecular arrangement of starch molecules seriously differ among different starches.

1.2.1 Diversities of starch

Starch naturally presents in the microparticulate form, termed as 'granule'. There are two types of starch molecules that are responsible for constructing starch granules (Pérez and Bertoft, 2010). The linear-type starch molecule, amylose, has the molecular weight of 10^5-10^6 Daltons (Ong et al., 1994), whereas the branching-type starch molecule, amylopectin, has the molecular weight of 10^7-10^9 Daltons (Yoo and Jane, 2002). The diversity of native starch exists at different levels:

1.2.1.1 Molecular level

The starch biosynthesis genes determine the diversity of native starch at the molecular level. Three critical enzymes, the starch synthases (SS), starch branching enzyme (SBE), and starch debranching enzyme (SDE), are involved in the starch biosynthesis (Martin and Smith, 1995). SS is responsible for the elongation of α-1,4-linked glucan chain. SBE creates a branch by cleaving an α-1,4-linked glucan chain and forming an α-1, 6 linkage between the reducing end of the cut chain and the C6 of another glucose residue in an α-1, 6-linked chain. SDE trims off excessive branches to maintain the characteristic branching pattern of amylopectin (Ball et al., 1996). Therefore, structural characteristic of amylose and amylopectin are determined by the overall function of three enzymes (Buléon et al., 1998). In sum, starches from different botanic sources often exhibit diversities in amylose content and characteristic structure of amylopectin (Jane et al., 1999).

The gene expression and the activity of the starch biosynthesis enzymes are dominated by the genotype of plants. Starches isolated from different mutants show large variations in the composition and structure (Wang et al., 1993). For example, the waxy mutant (*wx*) is lack of SS yielding the absence of amylose in final starch. In contrast, the amylose-extender mutant (*ae*) is lack of SBE yielding unusual high amylose content (50-75%) and the presence of intermediate materials in addition to amylose and amylopectin.

1.2.1.2 Granular level

The granular structure on the basis of amylose and amylopectin also exhibits great diversities.
Crystalline structure Native starch granules show various polymorphic types of semi-crystalline structure. Based on the wide-angle X-ray scattering diffraction patterns, native starches are mainly divided into A- and B- types (Zobel, 1988). Cereal starches, such normal corn starch, wheat starch and rice starch, are often belong to A-type, whereas tuber and amylose-rich starches, such as potato starch and *ae* maize starch, are often belonging to B-type (Lourdin et al., 2015). The crystallinity of native starch granules exhibits strong dependence on the source of starch.
Size and shape The size of starch granules vary greatly from less than 1 μm to 100 μm showing strong dependence on the botanic source. Both monomodal and bimodal size distribution of starch granules are widely reported for different starches. Native starches are also found to show different shapes, such as oval (potato starch), round (pea starch), disc (wheat starch), polygonal (corn starch) granules (Jane et al., 1994). Sometimes aggregated starch granules may be observed (e.g. in sweet corn starch) (Peng and Yao, 2018).
Granular ultra-structures Starch granules from different sources may exhibit characteristic ultra-structures. A number of ultra-structure types have been identified on different starch granules, including pores and openings, channels, central hilium and layered structure (or ‘growth ring’) (Buléon et al., 1998; Fannon et al., 1992; Tester et al., 2004). These ultra-structure features are more likely found in larger starch granules since such structures (usually in microscale) are too large to be formed in small starch granules.

1.2.2 Fundamental properties of starch

1.2.2.1 Gelatinization

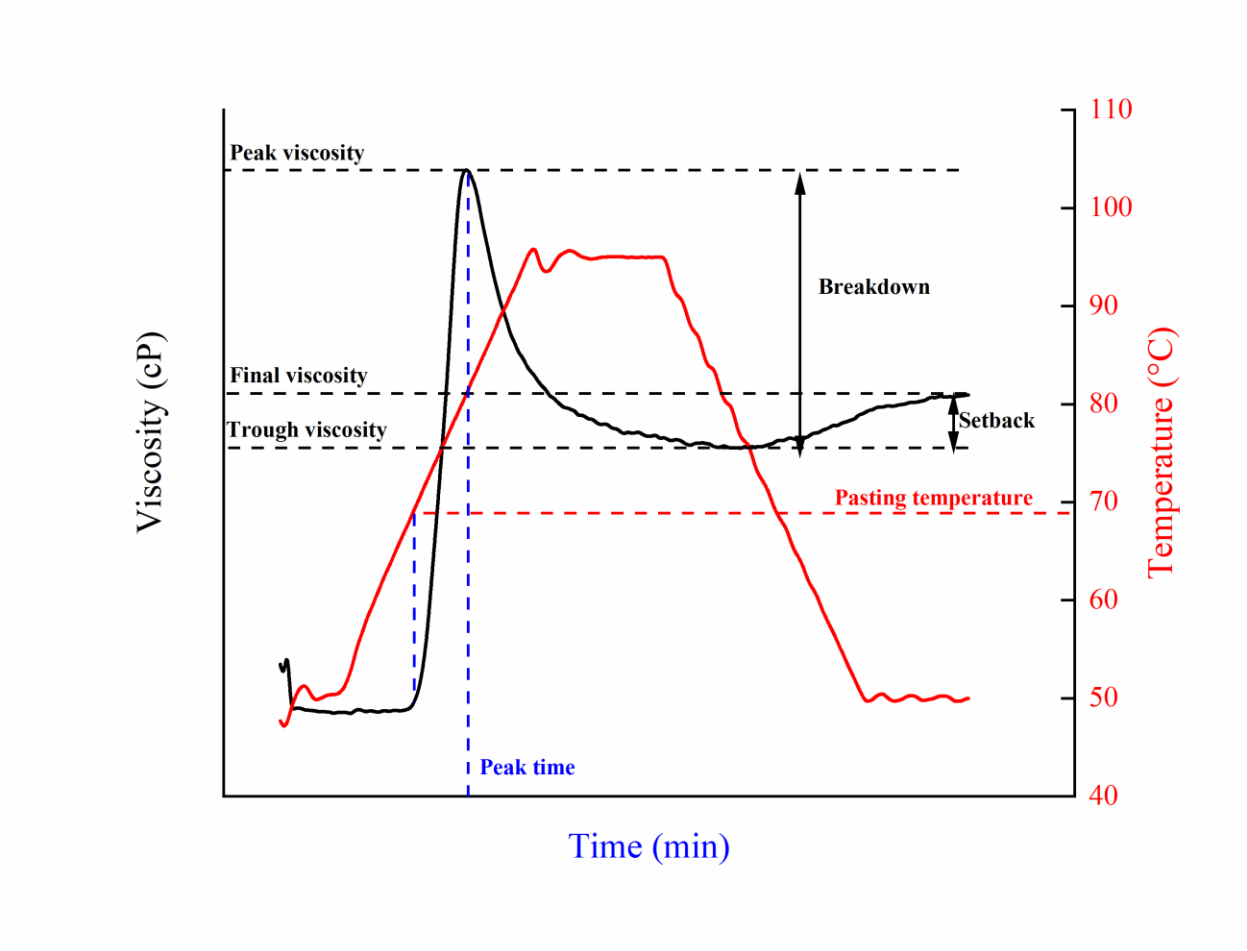

Figure 1-1.Typical Rapid Viscosity Analyzer (RVA) viscograph. Waxy rice starch was used as an example. RVA parameters are depicted on the viscograph, including peak viscosity (the maximum hot paste viscosity), trough viscosity (the minimum hot paste viscosity); final viscosity (the viscosity at the end of test), breakdown (the difference between peak viscosity and trough viscosity), setback (the difference between final viscosity and trough viscosity), pasting temperature (the temperature where viscosity first increases by > 25 cP over a 20-s period), and peak time (the time needed to reach peak viscosity).

One of the most representative property of starch is gelatinization, which involves a series of complex physical changes of starch granules upon hydrothermal treatment, such as the swelling of granules, the melting of crystalline structure, and the full dispersion of starch molecules (Hoover, 2001). From the broader perspective, the gelatinization properties of starch are most relevant to the rheological property, volume expansion, phase stability and digestibility of starch-

containing systems, thus indicating the potential application of starch (Biliaderis et al., 1980; Holm et al., 1988; Lee et al., 2002; Singh et al., 2003). Moreover, the structural diversities render distinct gelatinization behaviors for various starches, which can be used to characterize and differentiate starches (Singh et al., 2003).

The gelatinization properties of starches are usually characterized using mechanical rheology tests (Hsu et al., 2000; Wiesenborn et al., 1994). Rapid viscosity analyzer (RVA) is one of the most widely accepted and standardized tool for the evaluation of gelatinization properties (Bahnassey and Breene, 1994). It measures the viscosity of a starch slurry (≥ 6%, w/w) with the change of temperature and constant shear (Batey and Curtin, 2000). A set of parameters (**Fig. 1-1**) are used to report the gelatinization, anti-shear and rapid retrogradation properties of a starch and indicate its potential functions. For example, viscosity breakdown shows the extent of starch granules disruption upon shearing, and low viscosity breakdown means a shear-resistance function (Ragaee and Abdel-Aal, 2006).

1.2.2.2 Retrogradation

Retrogradation is the other aspect of fundamental property of starch and is of course a hot spot in starch-related research. It is a process during which gelatinized starch reassociate to form ordered structures (Wang et al., 2015). Starch retrogradation mainly occurs at the cooling and prolonged storage stages after gelatinization often yielding detrimental effects on food quality, such as staling (bread hardening) and syneresis (loss water holding capacity) (Gray and Bemiller, 2003). Retrogradation can also be beneficial in some cases. Retrograded starch is more resistant to human digestion than fresh-gelatinized starch rendering healthy benefits for the control of glycemic response (Sajilata et al., 2006). On the other hand, retrograded starch is a good material for the incorporation of active compounds and is intensively studied for the use of encapsulation and controlled delivery (Ding et al., 2018).

Amylose and amylopectin usually show different tendency to retrogradation (Wang et al., 2015). As a linear polymer, the retrogradation of amylose often occurs in the cooling of hot amylose-containing starch paste, facilitating the gelation by forming three-dimensional starch network. In contrast, the retrogradation of highly-branched amylopectin usually occurs at a slower rate during prolonged storage, so that is more relevant to food quality in shelf-life.

At the molecular level, starch retrogradation is driven by the hydrogen bonds that induce the formation of double helical associations among different glucan chains of starch molecules. For amylose, such association requires the presence of linear regions with the degree of polymerization (DP) of 40- 70 (Jane and Robyt, 1984; Leloup et al., 1992). For amylopectin, such association occurs among the short branching chains with DP ~12-22 (Vandeputte et al., 2003; Wang et al., 2015). Studies also showed that the optimum chain length favoring starch retrogradation is ~ DP12- 24 (Shi and Seib, 1992; Vandeputte et al., 2003). In sum, fine molecular structure of starch molecules is an important factor in deciding the retrogradation property of a starch.

Routine tools for evaluating retrogradation include RVA, textural analyzer, electron microscopy, NMR and thermal analysis, etc. (Wang et al., 2015). Differential scanning calorimetry is the most common approach in the evaluation of starch retrogradation properties (Karim et al., 2000), however, the tests are usually run at very high starch concentrations (20%-50%) and indicate little about the case of a dilute starch system.

1.2.3 Fine structures of amylopectin

Amylopectin comprises over 70% of the total mass of a native starch granule. Most characteristic properties of starch are attributed to the unique structure and supramolecular arrangement of amylopectin. Compared to amylose, amylopectin in different starches exhibits much more complexities and diversities. The studies on the fine structures of amylopectin are of great importance for (1) the discovery and utilization of novel starches, (2) the prediction on the potential applications of starch, and (3) advancing our understanding on starch biosynthesis as well as the unique functions of related genes and enzymes.

1.2.3.1 Cluster model of amylopectin

Amylopectin is a huge branched macromolecule (10^7-10^9 Da), in general possessing 4-5% of α-1, 6 branches (Manners, 1989). To describe the fine structure of amylopectin, a cluster model for amylopectin was proposed based on the hypothesis that the whole amylopectin molecule is composed of the interconnected and periodically occurring clusters (Thompson, 2000). A schematic model is usually applied to show the clusters and the detailed branch pattern within a cluster (**Fig. 1-2A**). Three different types of unit chains are defined in a cluster model (Peat et al.,

1952): (1) ***A chains***, are the outmost short chains without carrying other chains; (2) ***B chains***, are the internal chains carrying other chains; (3) ***C chain***, is the single chain that carry the reducing end of the whole amylopectin molecule.

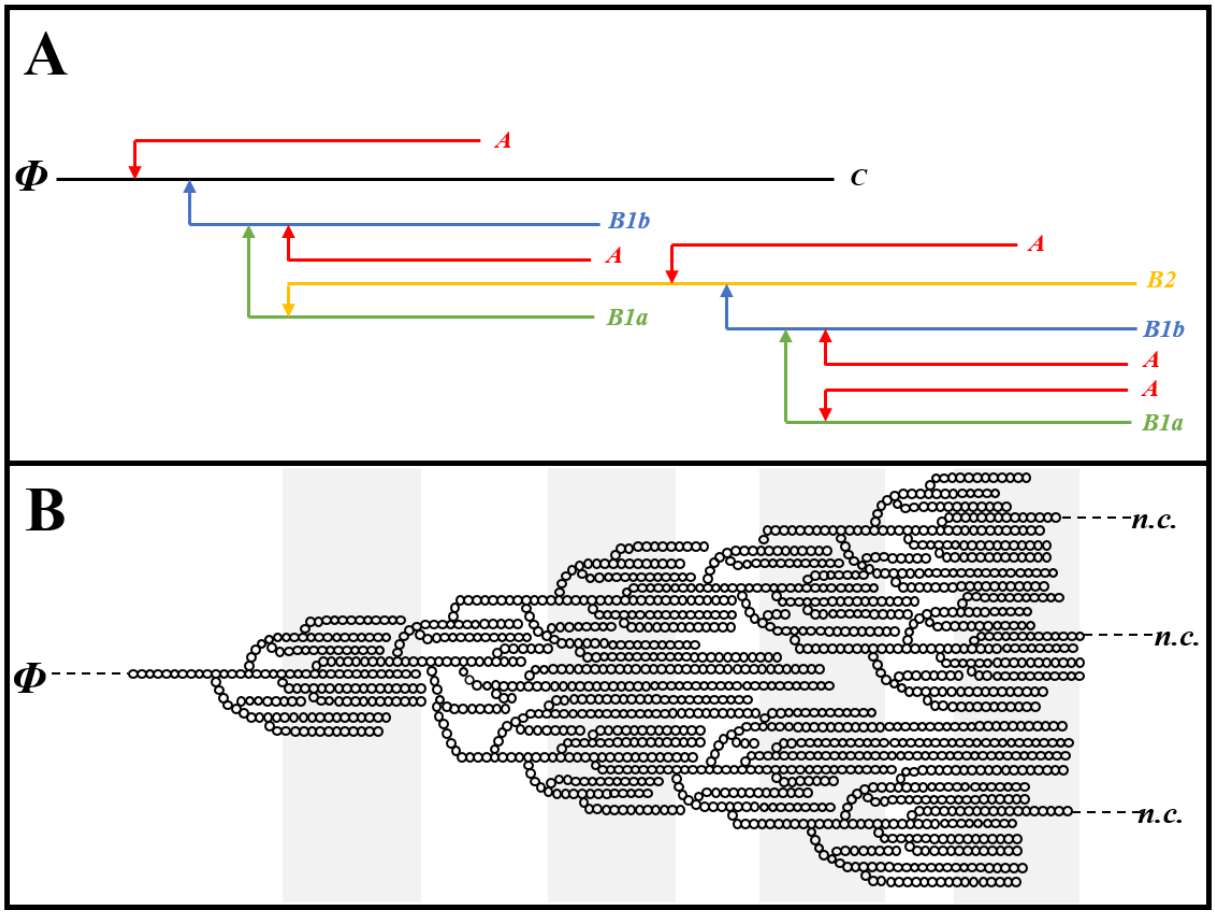

Figure 1-2. Schematics showing the different unit chains of amylopectin **(A)** and the periodically occurring linear and branching regions (labelled with shaded background) of amylopectin **(B)**. *Φ*, the reducing end of amylopectin; *n.c.*, new cluster.

A number of different B chains are further defined based on their different contributions to the intra- and inter-cluster structure (Hizukuri, 1986; Manners, 1989): (1) ***Intra-cluster chains***, include B1a chain (carrying one branch point) and B1b chain (carrying two branch points); (2) ***Inter-cluster chains,*** include B2 chain (connecting two adjacent clusters) and B3 chain (connecting three adjacent cluster) and etc..

It is worthy to note that amylopectin is non-randomly branched which makes its structure differ from the regularly branched dendrimer-like structure (e.g. phytoglycogen) (Huang and Yao, 2011). In fact, the branching points are clustering in the local regions that forms the amorphous

region (~ 2 nm thick) of a cluster while the chains extending to the non-branched linear region forms the crystalline region of a cluster (~5 nm thick) (**Fig. 1-2B**) (Tester et al., 2004; Thompson, 2000). With the periodically occurring clusters, amylopectin thus forms a growth ring (120-400 nm thick) and semi-crystalline structure of starch granules (French, 1972).
The cluster model permits multi-respects of structural flexibility that are in general determined by the length of unit chains, the abundance of branching points in a cluster and the distance between adjacent branches. **Table 1-1** summarized the structural features of some typical amylopectin reported in previous literature. It is clear that large diversities in fine structures exist among different amylopectin.

Table 1-1. Structural features of selected amylopectin (adapted from previous literatures)

Source	$\overline{DP_w}$[1]	DP of unit chains	A:B molar ratio
Maize[2]	23.5-24.4	DP13 (short), DP48 (long)	1.3[5]
Potato[3]	22-23.9	DP16 (A), DP24 (B1), DP48 (B2), DP75 (B3), DP104 (B4)	0.79
Waxy rice[3]	17.5-18.3	DP13 (A), DP22 (B1), DP42 (B2), DP69 (B3), DP101 (B4)	2.2
Wheat[4]	25	DP13 (A), DP22 (B1), DP43 (B2), DP79 (B3), DP140 (B4)	1.7

[1]Weight Average chain length.

[2]Data adapted from (Jane et al., 1999).

[3]Data adapted from (Morrison and Karkalas, 1990).

[4]Data adapted from (Hizukuri and Maehara, 1990).

[5]Data adapted from (Yao et al., 2004)

1.2.3.2 Characterization methods

A series of amylolytic digestion followed by size exclusion chromatography (SEC) is usually applied to characterize the fine structure of amylopectin. First, amylopectin is subjected to

debranching enzymes, such as isoamylase, pullulanase or the both, followed by SEC (Yuan et al., 1993). The two enzymes specifically cleave α-1, 6 linkages, producing linear α-1, 4 linked chains (Taniguchi and Honnda, 2009). After the exhaustive hydrolysis, the whole amylopectin molecule can be degraded into different linear chain populations with various DP, which is subsequently separated by SEC. The average chain length and representative chain populations for certain amylopectin could be identified this way. In general, two populations of chains are responsible for constructing amylopectin: the short chain population is ~17 DP for cereal starches and 19 DP for tuber starches; the longer chain population is ~54 DP for cereal starches and 62 DP for tuber starches; and in overall, longer average chain length is often observed for tuber starches (26 DP) than cereal starches (36 DP) (Manners, 1989). Similar difference in the chain length of unit chains are observed between cereal and tuber starches (Biliaderis et al., 1980).

The branch pattern of amylopectin is usually investigated by determining the chain length profile of β-limit dextrins of amylopectin. The exhaustive β-amylolysis removes the external (linear regions) portions of A and B chains while preserving the intact internal branching regions (Lee, 1971). After the subsequent debranching of the β-limit dextrins of amylopectin and the SEC separation, the residual DP values for the characteristic chains (B1a, B1b, B2, B3 and etc.) and the mass or molar ratios of different chain populations are used for representing the branch pattern of a particular amylopectin (Xia and Thompson, 2006). Based on this method, several parameters are developed to describe the basic branch features of amylopectin: (1) the internal branch distance represents the distance between two adjacent branches, (2) the average number of branches per cluster depicts the size and complexity of a cluster, and (3) internal chain length measures the distance between two consecutive clusters (Yao et al., 2004; Yuan et al., 1993).

1.3. Small-granule starch

1.3.1 Overview of small granule starch

In general, the granular size of starch varies from less than 1 μm to over 100 μm mostly depending on the biological source of plants. While no clear definition can be found in literatures, native starch granules can be classified into four categories: large (> 25 μm, e.g. potato starch), medium (10- 25 μm, e.g. maize starch), small (2- 10 μm, e.g. rice starch) and very

small (< 2 μm, e.g. amaranth starch) granular starches (Bhosale and Singhal, 2007; Hoover, 2001; Jane et al., 1994).

Small-granule starch is a category of starches with their granular size smaller than <10 μm. Natural small-granule starch can be isolated from particular botanic sources or fractionated from commercial starches. The widely reported sources of small-granule starches include rice, amaranth, cow cockle, quinoa, taro and some special genotypes of common crops (e.g. sweet corn) (Lindeboom et al., 2004). Common industrial starch production procedure cannot handle small-granule starch mainly due to the difficulty in fractionating starch from aqueous phase and proteinaceous contaminates by gravity sedimentation (van Esch, 1991). Despite this researchers have attempted to apply centrifugal process for accelerating sedimentation or enzymatic process for purification (Radosavljevic et al., 1998), the costs of such operations greatly limit the industrial production of small-granule starch.

1.3.2 General properties of small-granule starch

Compared to commonly utilized starches, they showed unique potentials in many novel food, pharmaceutical and cosmetic applications, such as the microencapsulation (Crittenden et al., 2001; Mattila-Sandholm et al., 2002), fat replacement (Malinski et al., 2003), controlled release (Mills and Thurman, 1994) and high oil-load emulsification (Timgren et al., 2013). These applications are normally related to the small size and large specific surface area of small-granule starch that contribute to high capacity of surface interaction and special stimulation on oral perception of fat-like texture.

Besides the size-associated properties, small-granule starches also exhibit distinct physicochemical characteristics from large-granule starches:

(1) The ***granular composition*** of small-granule starch can be different from large-granule starch, even though they are sometimes isolated from the same genotype of plant. A well-known example is wheat starch, of which higher amylose and lower lipid contents are often observed for the large granules than the small granules (Peng et al., 1999; Soulaka and Morrison, 1985). Moreover, small-granule starch also shows good affinity to small molecule substances, so that may comprise considerable amount of minor compounds in the granules (Błaszczak et al., 2013).

(2) The ***granular morphology*** may also be different between large- and small-granule starches. In general, granular structures, such as channels, openings and central hilium, are less likely observed in small-granule starch (Huber and BeMiller, 2000; Jane et al., 1994).
(3) The ***structure transition*** in response to hydrothermal treatment is quite diverse for different small-granule starches. Some small-granule starches, such as amaranth starch, exhibit highly ordered granular structure as large-granule starches (Qian and Kuhn, 1999). Small-granule starches isolated from dasheen are reported to show high pasting temperature and granular stability but lower retrogradation (Goering and DeHaas, 1972).
(4) Small-granule starch may show very different behavior when subject to ***enzymatic hydrolysis***. Unlike the porous granule produced by the α-amylolysis of large-granule starch (e.g. corn starch), the hydrolysis of small-granule starch often occurs from the surface to inside yielding homogenous erosion towards the center of granules (Lindeboom et al., 2004).
The unique structure properties yield many potentials of small-granule starches in innovative high-value applications. Furthermore, the wide-spread healthy concern on artificial food additives renders a strong desire of food industry to find alternative ingredients for modified starch. These emerging demands and trends as well as the regulation hurdle of food encourage the starch industry to seek novel industrial starches. From the perspective of food industry, we are especially interested in the small-granule starches from food or animal feed sources. Based on this criterion, we focused on three kind of high-potential small-granule starches: sweet corn starch, amaranth starch and cow cockle starch.

1.3.3 Sweet corn starch

Sweet corn is widely planted for fresh consumption and canned food production (Coşkun et al., 2006). A series of different maize mutant types, the *shrunken-2* (*sh2*), *brittle-2* (*bt2*), *sugary1* (*su1*) and *sugary2* (*su2*), are considered as sweet corn due to their high sucrose contents in mature endosperms (Nelson and Pan, 1995). Among them, very unique starch biosynthesis occurs in the *su1* maize endosperms producing sweet corn starch and phytoglycogen as the primary carbohydrate polymers (James et al., 1995). The dry semi-transparent kernels of *su1* mutant are shown in **Fig. 1-3**.
In general, the deficiency in SU-1, an isoamylase-type starch debranching enzyme, significantly affects the composition and physicochemical properties of sweet corn starch. Sweet corn starch

is categorized as small-granule starch with higher amylose content compared to normal corn starch (Jane et al., 1994; Wang et al., 1993). Sweet corn starch granules were also reported to show low swelling and low melting enthalpy upon gelatinization (Singh et al., 2006; Tziotis et al., 2005). However, the unique properties of sweet corn starch and their relations to the granular and fine starch structure remain unclear to date.

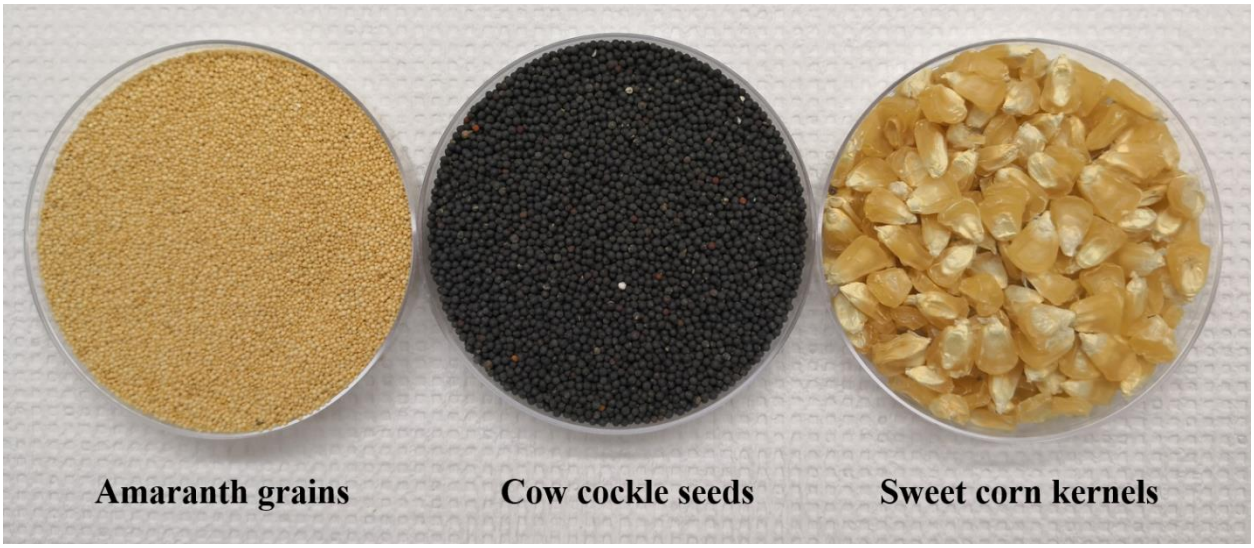

Figure 1-3. The image showing dried amaranth grains (left), cow cockle seeds (center) and sweet corn kernels (right).

1.3.4 Cow cockle starch

Cow cockle (*Saponaria vaccaria*) is an annual weed widely found in the United States and the western states of Canada (Goering et al., 1966). The current major use of cow cockle is as cow feed. In 1960s, cow cockle was firstly proposed as a potential source of oil-producing seeds, however, researchers soon realized the high starch content in mature cow cockle seeds (> 60% of the dry weight of seeds) (Mazza et al., 1992). Most recently, efforts have been made to cultivate cow cockle as an industrial crop in North America (Willenborg and Johnson, 2013). All these pioneering works highlight the possible industrial production of cow cockle starch in the future. Cow cockle seeds (**Fig. 1-3**) are in black with a thick hull outside the endosperm. The starch granules of cow cockle starch are extremely small (0.3-1.5 μm) and homogeneous (Biliaderis et al., 1993) Similar to other small starches, such as dasheen and pigweed starches, cow cockle starch was reported to show good granule stability and low pasting temperature as well as low setback upon gelatinization and pasting (Biliaderis et al., 1993; Goering and DeHaas, 1972).

Despite its high potential in future industrial production, the structural basis for its unique submicron granular size and physicochemical property are still not fully understood.

1.3.5 Amaranth starch

The leaves and grains of amaranth has long been consumed in America, Asia and Africa (Becker et al., 1981). Common types of cultivated amaranth (*Amaranthus* spp.) include *Amaranthus cruentus* L., *Amaranthus paniculatus* L., *Amaranthus hypochondriacus* L., *Amaranthus hybridus* L.. The grain of amaranth (in **Fig. 1-3**) is round shaped in yellowish color with high protein and lysine contents, which makes it stand out from common cereals (Caselato-Sousa and Amaya-Farfán, 2012). Amaranth grains also contain high amount of starch (~ 60% of dry weight) that show great potential as a novel source of industrial starch.

To date, both amylose-containing and waxy-type of amaranth starches have been isolated and studied in different studies. The small granules (0.5- 2 μm) of amaranth starch are quite homogenous (Hoover et al., 1998). Very diversified thermal, pasting and textural properties are observed for amaranth starches from different genotypes (Kong et al., 2009). Given the food source of amaranth starch, a few studies have been made recently to functionalize native amaranth starch by common food-grade chemical derivation methods targeting on novel uses of this starch in emulsification, aroma retention and food storage (Kshirsagar and Singhal, 2008; Pal et al., 2002; Timgren et al., 2013). Despite the fact that amaranth starch is free from food regulation hurdles, its unique structure, physicochemical property and food-related functions are far yet to be fully understood.

1.4. Interaction between starch and small molecules

Starch possesses various nanostructures permitting multiple non-covalent interactions with small molecules. The interaction between starch and small molecules can occur on the surface or inside the granules involving three mechanisms: the partition of small molecules inside and outside starch phase, the diffusion of small molecules through the starch matrix and the specific binding of small molecules to particular starch component or structure.

1.4.1 Native starch

1.4.1.1 Surface adsorption effect

For native starches, the granules from different botanical sources can be very different in specific surface area (Juszczak et al., 2002) and surface morphology (smooth, wrinkled or coarse) (Peng and Yao, 2018). These morphological features may permit the retention of small molecules on granular surface. This type of physical adsorption is usually driven by the hydrogen bonds between the hydrophilic surface of starch granules and small molecules (A Boutboul et al., 2002; Aurélia Boutboul et al., 2002; McGorrin and Leland, 1996). Thus, small-granule starches with large surface area can retain more small molecules than common starches. In addition, small-granule starches can form aggregated structures after spray drying with small molecules, which may further enhance the surface adsorption and the stability of small molecules (Tari et al., 2003; Zhao and Whistler, 1994).

1.4.1.2 Diffusion effect

As native starch granules are semi-crystalline, the densely packed intra-granular structures are less accessible to small molecules. Hence, the diffusion of small molecules into starch matrix is very difficult. An early study suggested that native potato granules were permeable to small molecules with the molecular weight smaller than 1000 Da (Lathe and Ruthven, 1956). However, some special granular features may facilitate the diffusion effects. Corn starches have been reported with submicron-sized surface pore and intra-granular channels (Huber and BeMiller, 1997). These structural features form the bypass routes for the diffusion of small molecules.

1.4.2 Swollen starch

1.4.2.1 Partition and diffusion effects

Gelatinized starch swells to a high extent in water, possessing diverse internal nanostructures for the accommodation of small molecules (Fannon and BeMiller, 1992; Jacobs and Delcour, 1998). Due to the dissociation of double helices, the hydroxyl group of starch molecules are more accessible to small molecules for hydrophilic interaction. With the melting of crystalline

structure and the volume expansion of starch, the whole matrix becomes much more permeable for small molecules (Lathe and Ruthven, 1956). Hence, small molecules are not only retained by surface starch molecules, but also retained by the internal starch molecules, which in sum enhances the partition of small molecules in starch phase.

Besides, the swelling of starch is also accompanied by entrapping large volume of water into the three-dimensional network of starch. Such microstructure is often described as a honeycomb-like or sponge-like network with abundant micro- or nano-scale interspaces (Zhang et al., 2002). Small molecules can either be absorbed into these interspaces with the swelling process or freely diffuse from the external water phase to the internal water phase that fills the interspaces.

1.4.2.2 Amylose inclusion

Small molecules as the ligand can be entrapped by the central cavity of V-type amylose (Putseys et al., 2010). V-type amylose is a single, left-handed helical structure with a hydrophobic central cavity (Whittam et al., 1989). Hence, this interaction is specific for hydrophobic small molecules. In the hydrated form, V-type amylose possesses well-defined conformation: a helix consisting of 6 glucose units per turn with an internal cavity (5.0-5.4 Å in diameter) (Hinkle and Zobel, 1968; Immel and Lichtenthaler, 2000). Owing to the limited size of central cavity, small molecules with long hydrocarbon groups are easier to reside in the cavity.

1.5. Molecular rotor

Molecular rotor (MR) is a group of special fluorophores that typically consists of an electron donor, an electron receptor and a π-conjugation system (denoted as the 'D-π-A' motif, **Fig. 1-4)** (Haidekker and Theodorakis, 2010). Molecular rotors exhibit unique fluorescent behavior that is exclusively dependent on the environmental spatial restrictions.

1.5.1 Structure and basic categories

Aniline nitriles, julolidine malononitriles, stilbenes and their derivatives are usually considered as MRs (Haidekker et al., 2010). Some selected commercially available MRs are summarized in **Table 1-2**. According to their physicochemical features, they are tentatively classified as: (1) hydrophobic MR (e.g. DMABN and DCVJ) (Ablinger et al., 2013; Haidekker et al., 2005), (2) hydrophilic MR (e.g. CCVJ, DMABOA and DCDHF) (Akers and Haidekker, 2004), and (3)

charged MR (e.g. CV and DASPMI) (Vogel and Rettig, 1985). In general, the commercially available MRs are with highly diversified hydrophobicity (-0.06-2.9), hydrogen-bonding capacity (2-5) and charges (-1-+1). Their molecular weights are ranging between 146 Da and 366 Da, which is equivalent to the size of a glucose or maltose molecule.

Table 1-2. Fundamental properties of commercially available molecular rotors

Molecular rotor[1]	Molecular weight (Da)	Hydrogen bonds[3]	Charge count[4]	Log [P][5]
CCVJ	268.3	1/4	-1	2.7
DCVJ	249.3	0/3	0	2.9
DMABN	146.2	0/2	0	2.2
DMABOA	162.2	1/3	-1	1.8
CV	408.0	0/3	+1	0.51
DCDHF	157.1	0/4	0	-0.06
DASPMI	366.2	0/2	+1	N.A.

[1]CCVJ, 9-(2-carboxy-2-cyanovinyl) julolidine; DCVJ, 9-(2,2-dicyanovinyl) julolidine; DMABN, 4-cyano-N,N-dimethylaniline; DMABOA, 4-(dimethylamino) benzoic acid; CA, crystal violet; DCDHF, 2-dicyano-methylene-3-cyano-2,5-dihydrofuran; DASPMI, 4-(4-(dimethylamino) styryl)-1-methylpyridinium iodide.

[2]Electron donor and receptor groups are in red and green colors, respectively.

[3]Number of hydrogen donor / acceptor groups

[4]Absolute number of charge groups

[5]Log [P], the partitioning coefficient, is the logarithm of the ratio of the concentrations of a solute between n-octenol and water, representing the hydrophobicity of molecules.

1.5.2 Fluorescent behaviors

The unique fluorescent behavior of MR is shown in **Fig. 1-4**. After being excited, a MR has two distinct states: (1) a planar conformation termed as locally exited state (LE) and (2) a twisted conformation termed as twisted intramolecular charge transfer state (TICT) (Rettig, 1986)Each excited MR can lose energy (to “relax”) through either the LE or TICT state. If the MR is in free

space, it relaxes through TICT state by releasing heat without emitting any photon (noted as "dark MR"). If the MR is in a local environment with spatial restriction (i.e. steric hindrance), the transition from LE to TICT state is retarded and the relaxation is completed through the photon emission from LE state (noted as "bright MR").

For a given microenvironment with spatial restriction (e.g. a polymeric solution), the overall spatial restriction governs the amount of MR molecules undergoing fluorescent emission. The quantum yield of MR, that is, the ratio of emitted photons to absorbed photons, precisely reflects the portion of "bright" MR and thus the extent of the spatial restriction to this MR. Therefore, the quantum yield of MR can be used to quantify the spatial restriction.

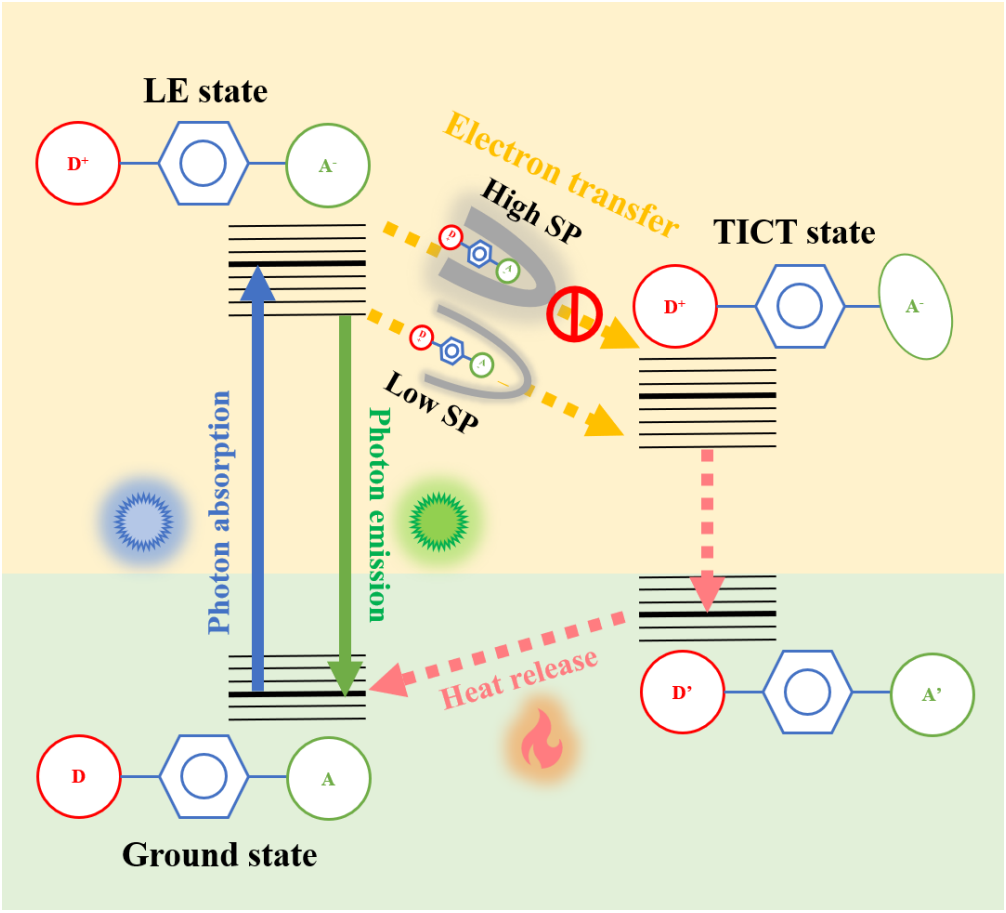

Figure 1-4. Schematics showing the structure (a 'D-π-A' motif) and fluorescent behavior of molecular rotor (MR). In the 'D-π-A' motif, D and A represent electron donor and acceptor, respectively; π represents a conjugation system connecting the electron donor and acceptor. LE (the locally excited state) and TICT (twisted intra-molecular charge transfer state) are two distinct excited state for a MR. Transition from LE to TICT state is strongly inhibited by spatial restriction (SP) exerted by polymeric matrix.

1.5.3 Current and future applications

1.5.3.1 Molecular rotor as the viscosity probe

The major application of MR is for viscosity probing. Viscosity is the resistance of a fluid against flow. It reflects the overall mobility of molecules in the fluid. The fluorescence emission of MR is associated with the viscosity through the *Förster-Hoffmann equation* (Förster and Hoffmann, 1971):

$$\Phi_F = C \cdot \eta^x \qquad \text{Eq. (1)}$$

where Φ_F, the quantum yield of MR, is the proportion of MR molecules that emits fluorescence. η is the fluid viscosity. C is a dye-dependent constant, and x is both dye and solvent dependent (Haidekker et al., 2010).

Based on both experimental and theoretical methods, x was found to be around 0.6 or 2/3 for different dyes in small molecule mixtures, such as water/ glycerol mixture and low-molecular-weight dextran solutions. For small molecule mixtures, solute and solvent molecules homogenously fill the bulk volume. In this scenario, the quantum yield of MR directly reflects the motion of MR that is predominantly constrained by the neighboring molecules.
The value of x is found to show deviations from the theoretical value (2/3) for macromolecule dispersions, such as gelatin, high-molecular-weight dextrans, native and modified starches (Akers and Haidekker, 2004; Gulnov et al., 2016). A possible explanation is that the micro- and nano-structures (or pockets) of macromolecules are the additional source of spatial restriction on the motion of MR. In this scenario, the quantum yield of MR reflects the overall spatial restriction induced by the neighboring molecules and the local structure of macromolecules.
In biology studies, MR permits the monitor of the physiological-induced viscosity change in biofluid or live cells. Intracellular viscosity change (especially on cell membrane) is crucial for many physiological process (Haidekker et al., 2010) and membrane receptors (Nadiv et al., 1994; Shiraishi et al., 1993). Hydrophobic MRs (e.g. DCVJ and CCVJ-derivatives) showed good affinity to cell membrane, liposomes and biological polymers in the cell (Haidekker et al., 2002, 2000). Subtle viscosity changes could thus be monitored or visualized by the fluorescence emission of MR (Iio et al., 1993; Kuimova, 2012; Kuimova et al., 2008).

1.5.3.2 Molecular rotor as the polymeric structure probe

MR is also capable of qualitatively probing different types of polymeric structures. First, MR is sensitive to the protein aggregation and conformational changes (Haidekker et al., 2010). Hydrophobic MRs, such as DCVJ, thioflavin T, and boron dipyrromethene derivatives, can specifically bind to the local hydrophobic regions of proteins (Hu et al., 2009; Lindgren et al., 2005; Thompson et al., 2015). Once the aggregation occurs among protein molecules, the TICT relaxation of attached MR is strongly inhibited as MR is entrapped within the aggregates. As a result, fluorescent emission or the fluorescence lifetime becomes the indicator of protein aggregation. A number of molecular rotors have been tested for their 'aggregation-induced emission' to date (Hong et al., 2011), and this unique fluorescent behavior is attracting growing attentions from different research areas.

Second, MR can be used for the characterization of polysaccharide structures, although very limited attempts have been made. Pelletier et al. (2000) applied a molecular rotor, 1,1-dicyano-(4'-N,N-dimethylaminophenyl)-1,3-butadiene (DMAC), to investigate the interactions among amphiphilic derivatives of sodium alginate. In this study, the fluorescence emission of DMAC was also correlated with the structure of the functional group used for derivatitation, thus suggesting the structural features of modified polysaccharides. Similar use of MR for the probing of the intramolecular interactions of modified polysaccharides was also reported by (Fischer et al., 1998). In sum, this type of application basically utilized the specific interaction between MR and the functional group. A more direct probing of polysaccharide structure occurs if the particular local structure of polysaccharides can accommodate and retain MR. MRs, such as DMABN and 6-Propionyl-2-(dimethylamino)naphthalene, were used for characterizing the polarity as well as the spatial restriction of the central cavity of cyclodextrin (Al-Hassan and Khanfer, 1998; Kim et al., 1996).

1.6. Experimental aims

Our overall goal is to carry out a comprehensive characterization of the selected small-granule starches from amaranth, cow cockle and sweet corn and to establish a novel fluorescent-based approach for the characterization of fine structure and fine structure-related properties of starch. It is hypothesized that the unique fine structure and granular characteristics of small-granule

granule contribute to unusual physicochemical property and distinct interaction behaviors with small molecules; and the fluorescent emission of molecular rotor can be used for representing the local structure and fine structure change of starch or other polysaccharides. To accomplish this objective, we proposed the following specific aims:

AIM #1: Evaluate the molecular structure and physicochemical property of small-granule starch, highlighting their unique fine structure compared to common cereal starches.

AIM #2: (1) Evaluate the retention of small molecules by small-granule or large granule starches and compare the different effects of native and swollen granules.

Our working hypotheses are: (1) compared to large-granule starches, small-granule starches are less permeable for small molecules; (2) Swollen granules are more permeable than native granules.

AIM #3: MR can work as polymeric structure probe and differentiate polysaccharide structures based on the dispersed density of whole molecule and the local conformation of polysaccharide.

Our working hypotheses are: (1) the fluorescent emission of MR is highly sensitive to the presence of polymer in dispersion; (2) the fluorescent emission of MR are highly sensitive to the dispersed molecular density and local conformation of polymeric structures.

AIM #4: A novel, sensitive, and MR-based fluorescent microscopic method can be applied to investigate starch retrogradation at very low starch concentrations.

Our working hypothesis is that the fluorescent emission of MR can be used for monitoring starch retrogradation as the reassociation of glucan chains can gradually alter the size of microvolumes in starch matrices and thus the spatial restriction exerting to MR.

It is anticipated that the results generated by this work will support the future utilization of small-granule starch and fundamental studies of starch. In particular, the studies on the fine structure of the selected small-granule starches will help our understanding on the biogenesis of the unique small granules. Furthermore, it is anticipated that the MR-based fluorescent characterization method will not only provide an innovative insight into the fine structure of starch, but also find broader applications in the research of biopolymeric micro- and nanostructures.

CHAPTER 2. PHYSICO-CHEMICAL PROPERTIES AND AMYLOPECTIN STRUCTURES OF SMALL-GRANULE STARCHES

(Part of this chapter has been published on Food Hydrocolloids, 74, 349-357)

2.1 Introduction

Starch is an important ingredient in the food industry due to its multiple functionalities in food systems. Starch functionalities are closely associated with the size, composition, and glucan structure of individual granules. In general, the granular size of starches from rice, amaranth, and cow cockle are much smaller than that of maize, potato, and wheat (Lindeboom et al., 2004). In recent years, small-granule starches (SGSs) have attracted growing attentions due to their potentials in providing smooth texture (Wani et al., 2012), fat replacement (Malinski et al., 2003), and controlled delivery (Gonzalez-Soto et al., 2011).

Cow cockle starch (CCS) exists in the seeds of cow cockle (*Saponaria vaccaria* L.), an annual weed found in United States and Canada (Goering et al., 1966). Recently, efforts have been made to cultivate cow cockle as an industrial crop in North America (Willenborg and Johnson, 2013). Starch isolated from cow cockle seeds showed homogeneously small granules (~ 0.3-1.5 microns) (Biliaderis et al., 1993), possibly the smallest granules that have been reported. However, only limited information is available for CCS, such as its granular stability, low pasting temperature, and low setback upon gelatinization and pasting (Biliaderis et al., 1993; Goering and DeHaas, 1972). Its unique property is likely associated with the submicron granules (Biliaderis et al., 1993). Furthermore, there is still a substantial lack of knowledge on the branching structure of CCS.

Phytoglycogen and starch are two primary carbohydrate polymers in *sugary-1* maize mutant (James et al., 1995), a traditional sweet corn. Previous studies have shown the small granular size of sweet corn starch (SCS) (Jane et al., 1994; Wang et al., 1993). Early studies on SCS revealed its high amylose content and several differences in the starch structure in comparison with normal corn starch (Wang et al., 1993). It was also revealed that SCS granules were hard to swell and low in melting enthalpy (Singh et al., 2006; Tziotis et al., 2005; Wang, 1993). In general, the SU-1 deficiency in sweet corn affects the structural and physicochemical properties of SCS, and

there is a need to better understand its granular and fine structure for potential industrial applications.

The leaves and grains of amaranth have long been consumed in America, Asia and Africa (Becker et al., 1981). The high nutrition value of amaranth grains has long been discussed in literatures (Caselato-Sousa and Amaya-Farfán, 2012). Amaranth grains also contain high amount of starch (~ 60% of dry weight) that show great potential as a novel source of starch. Similarly to CCS, the small granules (0.5- 2 μm) of amaranth starch (AS) are quite homogenous (Hoover et al., 1998). A few studies have been made recently to investigate the potential uses of AS in emulsification, aroma retention and food storage (Kshirsagar and Singhal, 2008; Pal et al., 2002; Timgren et al., 2013). Like other SGS, the unique structure, physicochemical property and food-related functions of AS are yet to be fully understood.

In this study, CCS, SCS, and AS were compared with normal and waxy rice starches and normal and waxy corn starches with regard to their morphological, thermal, pasting, and structural properties. The fine structures for all starches were determined to provide supporting information on their potential applications, such as fat replacement, encapsulation or delivery for active ingredients, and texture modification.

2.2 Materials and methods

2.2.1 Materials

Sweet corn (*sugary-1* variety) kernels were obtained commercially. Cow cockle seeds were purchased from Hangzhou Botanic Technology Co., Ltd., China. Amaranth grains were purchased from Woodland Foods Co., Ltd., IL. Waxy rice and normal rice were purchased from local grocery store. Waxy corn starch (WCS) and normal corn starch (NCS) were obtained from Cargill Inc. and National Starch and Chemical Company (now part of Ingredion), respectively. All chemical reagents used for the study were of analytical grade unless specified.

2.2.2 Methods

2.2.2.1 Extraction of crude starches

Sweet corn starch (SCS), waxy rice starch (WRS), and normal rice starch (NRS) were isolated using a modified alkaline extraction method. To start the extraction, 100 g of dry maize kernels

or milled rice grains were ground into grits using a blender (Waring Laboratory Science, Torrington, CT) to pass through a 16-mesh sieve. The grits were mixed with 350 mL of 0.1% (w/v) sodium hydroxide (NaOH) solution and kept at 50 °C in a water bath for 30 min with constant agitation. The mixture was then homogenized using a blender at high speed for 4 min and passed through a 270-mesh sieve. The retained solids (by the sieve) were extracted again using another 350 mL of NaOH solution. The fractions permeated through the sieve were combined and centrifuged at 3,000 × g for 15 min. The precipitate, as the crude starch material, was collected.

Amaranth starch (AS) was also isolated using a modified alkaline extraction method. To start the extraction, 100 g of dry grains were soaked in 350 mL of 0.1% (w/v) NaOH solution and kept at 50 °C in a water bath with slight agitation. Cow cockle starch (CCS) was isolated according to the methods of Goering et al. (1966) with modifications. Cow cockle seeds (100 g) were soaked in 350 mL 0.15 M lactic acid solution at 50 °C with slight agitation. After the 48 h steeping process, the steeping solution was decanted and wet amaranth grains or cow cockle seeds were homogenized with 350 mL of water using a blender at high speed for 4 min and passed through a 270-mesh sieve. The retained solids (by the sieve) were extracted again using additional 350 mL NaOH solution (for AS) or lactic acid solution (for CCS). The fractions permeated through the sieve were combined. For CCS, the permeated extracts were combined and allowed to stand for a short period of time (1-2 min) to decant hull pieces. The decanting process was repeated three times. After that, the combined permeated extracts were adjusted to pH 10 and centrifuged at 3,000 × g for 15 min. The precipitate, as the crude starch material, was collected.

2.2.2.1 Purification of starches

Each crude starch material (about 50 g) was resuspended in 300 mL of NaOH solution (pH 10), agitated for 30 min, and centrifuged again. The precipitate was repeatedly washed with NaOH solution four times, during which proteins on the top layer of the precipitate was scraped away using a spatula. Thereafter, the precipitate was resuspended in deionized water, neutralized to pH 7.0 using 1.0 M hydrogen chloride (HCl) solution, and centrifuged. The starch precipitate was further washed twice using deionized water (100 mL for each cycle) and finally using 100 mL of pure ethanol. The material collected was subjected to vacuum filtration and then dried overnight. All starch materials were stored in a desiccator at room temperature before use. In overall, the

starch yields were ~15% for sweet corn starch and 30-40% for amaranth starch and cow cockle starch.

2.2.2.3 Chemical compositions of starches

The moisture content of each starch material was determined using the AACCI Method 44-15.02. Starch content was determined as described by AACCI Method 76-13.01. Nitrogen content was determined using the combustion method with a LECO model FP-2000 Nitrogen Analyzer (LECO Co., St. Joseph, MI), with its value multiplied by 5.75 to obtain the protein content. Apparent amylose content was determined by colorimetric method according to Morrison and Laignelet, (1983).

2.2.2.4 Scanning Electron Microscopy

To image starch granules using scanning electron microscopy (SEM), each starch material was mounted on a circular metal stub with double-sided sticky tape and coated with platinum in a Cressington 208HR sputter coater. The specimens were observed using FEI NOVA nanoSEM Field Emmission SEM (FEI, OR) under the voltage of 5.0 kV. Images were taken at magnification of 5000 ×.

2.2.2.5 Wide-angle x-ray powder diffraction

The wide-angle X-ray crystallograms of starches were obtained using Philips PW3710 diffractometer equipped with Ni-filtered Cu-Kα (1.5418 Å) radiation, with the tube operated at 40 kV and 25 mA. Dried and purified starch material from **2.2.2.2** (0.5 g) was packed in an aluminum holder and mounted on the diffractometer. The intensity data were collected in the 2θ range 10-40°, and the scan rate was 1°/ min. The raw data was smoothed for further analysis by the Automated Powder Diffraction software (version 3.6). The crystalline peaks and crystallinity for each starch were determined according to Hickman et al., (2008) using the Origin Pro 2016 software. Crystallinity was calculated as: Crystallinity (%) = $(A_t - A_a) / A_t$, where A_a and A_t were the area for the amorphous background and the total area, respectively.

2.2.2.6 Differential Scanning Calorimetry

Gelatinization behavior of each starch was examined using differential scanning calorimetry (DSC Q-2000, TA instruments, US). Starch material (5.0 ± 0.1 mg) was mixed with deionized water in aluminum T-Zero pans (TA instruments, US) to prepare a 50% (w/w) mixture and then hermetically sealed. The samples were conditioned overnight at room temperature before scanning. The scanning temperature was 20 - 130 °C with a scanning rate of 5 °C/ min. An empty pan was used as the reference. The onset temperature (T_o), peak temperature (T_p), conclusion temperature (T_c), and melting enthalpy (ΔH) were recorded using the TA Universal Analysis software.

2.2.2.7 Rapid viscosity analyzer

Pasting behavior of each starch was evaluated using a rapid viscosity analyzer (RVA) (RVA-4, Newport Scientific Pty. Ltd., Narrabeen, Australia) using the method of Ragaee and Abdel-Aal, (2006) with modifications. Starch material 1.5 g was mixed with deionized water in an aluminum canister to make a 6% (w/w) starch slurry. The heating and cooling cycle included: 1) temperature held at 50 °C for 60 s, 2) temperature increased to 95 °C in 225 s and held at 95 °C for 150 s, and then 3) temperature reduced to 50 °C in 225 s and held at 50 °C for 120 s. Pasting parameters of each starch were determined from the pasting curve using Thermocline version 2.2 software.

2.2.2.8 Preparation of debranched starch

Starch material (5 mg) was dispersed in 125 μL of 90% dimethyl sulfoxide (DMSO) through heating in a boiling-water bath for 10 min. Sodium acetate (NaAc) buffer 875 μL (20 mM, pH 4.75, 50 °C) was added to the dispersion, and the mixture was heated again, cooled to ambient temperature (22 °C), and mixed with 50 μL isoamylase (Megazyme, 5 U/ mL in NaAc buffer). The mixture was incubated in a shaking water bath at 37 °C for 24 h and then heated in a boiling-water bath for 10 min to denature the enzyme. After cooling, 40 μL pullulanase solution (Megazyme, 7.2 U/ mL in NaAc buffer) was added and the mixture was incubated for another 24 h at 37 °C and then heated for 10 min. The moisture of each enzyme-treated mixture was removed using a nitrogen gas blower at ambient temperature and the volume of each sample was

adjusted to 1.0 mL using 90% DMSO. After vortexing and centrifugation to remove insoluble materials, a 20 μL aliquot was injected in a high performance size-exclusion chromatography (HPSEC) system. The HPSEC contained two connected Zorbax gel PSM 60-S columns (6.2 mm × 250 mm, Agilent Tech., Santa Clara, CA) equipped with a Waters 2414 refractive index (RI) detector (Waters, MA). The flow rate was 0.5 mL/min using DMSO as the mobile phase. Glucose, maltose, maltotriose, maltopentaose, maltoheptaose, and three pullulan standards (6 kDa, 50 kDa, 400 kDa) (Sigma, US) were used for column calibration. RI signal were collected using Millennium software (Waters, Milford, MA) and the raw data were exported to an Excel spreadsheet, loaded to the Origin Pro 2016 software, and normalized on the basis of the total area.

2.2.2.9 Preparation of debranched amylopectin

Amylopectin (AP) fraction was isolated from starch materials through differential alcohol precipitation using 1-butanol and isoamyl alcohol (Klucinec and Thompson, 1998). The debranched AP was prepared using the same procedure as described above.

2.2.2.10 Preparation of debranched β-limit dextrins

In order to prepare β-limit dextrin **(**BLD), AP was subjected to complete β-amylolysis at 50 °C for 48 h, and the resulting polysaccharide was precipitated and washed with ethanol and acetone as described by (Klucinec and Thompson, 2002). Dried BLD (~3 mg) was mixed with 50 μL of 90% DMSO and heated in a boiling water bath for 10 min, then mixed with 350 μL NaAc buffer (20 mM, pH 4.75) at 50 °C. The mixture was heated in a boiling-water bath again and cooled to ambient temperature. The debranching of BLD was performed using the same procedure as described above, except that 40 μL of an isoamylase solution (0.5 U/mL) and a pullulanase solution (0.43 U/mL) were used. After the reactions, moisture was removed using a nitrogen gas blower and the volume of each sample was adjusted to 0.2 mL with 90% DMSO. After vortexing and centrifugation to remove insoluble materials, a 20 μL aliquot was injected in the HPSEC system. The structural parameters that describe branching pattern of starch, amylopectin, and BLD were obtained according to previous publications (Klucinec and Thompson, 1998; Yao et al., 2004; Yuan et al., 1993). Models of BLD branching pattern were established using the method proposed by Yun and Matheson, (1993).

2.2.3 Statistical analysis

Measurements were conducted 3 times. ANOVA was conducted using SPSS 17.0 with all comparisons conducted at a significance level of 95%.

2.3 Results and discussion

2.3.1 Chemical composition of starch materials

Table 2-1. Chemical composition of starches

Starch type	Moisture content (%)[1]	Protein content (%)[1]	Starch content (%) [1]	Amylose content (%) [2]
Sweet corn	7.7 ± 0.0^{d}	7.7 ± 0.2^{a}	76.6 ± 4.9^{b}	31.1 ± 1.1^{a}
Cow cockle	8.5 ± 0.1^{c}	1.5 ± 0.1^{c}	95.8 ± 1.3^{a}	19.3 ± 0.1^{c}
Amaranth	10.2 ± 0.2^{a}	1.2 ± 0.1^{c}	94.8 ± 3.4^{a}	N.D.[3]
Waxy rice	8.0 ± 0.1^{d}	1.3 ± 0.2^{c}	91.3 ± 0.2^{a}	N.D.[3]
Normal Rice	8.0 ± 0.1^{d}	3.1 ± 0.0^{b}	92.7 ± 2.8^{a}	11.5 ± 0.0^{d}
Waxy corn	9.8 ± 0.0^{b}	1.4 ± 0.1^{c}	98.2 ± 2.6^{a}	N.D.[3]
Normal corn	10.2 ± 0.0^{a}	1.5 ± 0.2^{c}	98.4 ± 0.3^{a}	21.6 ± 0.4^{b}

Data expressed as means ± standard deviations (n = 3). The means in the same column with different letters are significantly different ($P < 0.05$).

[1] Data computed on dry basis.

[2] Data computed on starch basis.

[3] Non-detectable

Chemical compositions of different starches are shown in **Table 2-1**. Compared with WCS and NCS, the starch contents for the isolated CCS, AS, NRS, and WRS materials (ranging from 91-96%) were 3-6% lower without significant difference ($P < 0.05$). The starch content of SCS material (77%) was significantly ($P < 0.05$) lower than that of the other starch materials, with 7.7% of proteinous material and 12% of micron-sized hull pieces. The amylose contents for NCS and NRS were 21.6% and 11.5%, respectively, which were in accordance with previous studies (Morrison and Laignelet, 1983; Singh et al., 2003). Amylose was undetectable with AS, WCS

and WRS samples. In comparison, amylose content of CCS and SCS was 19.3% and 31.1%, respectively, which agreed with previous results (Biliaderis et al., 1993; Wang, 1993).

2.3.2 Granular characteristics of starches

2.3.2.1 Granular morphology

SEM images of starches are shown in **Figure 2-1**. Based on their size, starch granules were categorized into large granules (LG, > 10 μm), medium granules (MG, 2-10 μm), and small granules (SG, < 2 μm). In general, WCS and NCS contained primarily LG and minor amount of MG. WRS and NRS contained MG only. For CCS and AS, most granules were 0.5-1 μm in size. In contrast, SCS granules were highly heterogeneous in their sizes and appearance, containing not only MG and SG, but also aggregations of small granules (ASG, 2-10 μm). Individual MG and SG of SCS showed smooth and compact surfaces, whereas ASG showed rough, loose, or cracked surfaces. In an early study, three granular populations (small, 1-2 μm; intermediate, 5 μm; large, 10-20 μm) were found in immature sweet corn (Jane et al., 1994). Compounded granular structures were shown in their SEM image, which could be associated with the ASG we observed in this study.

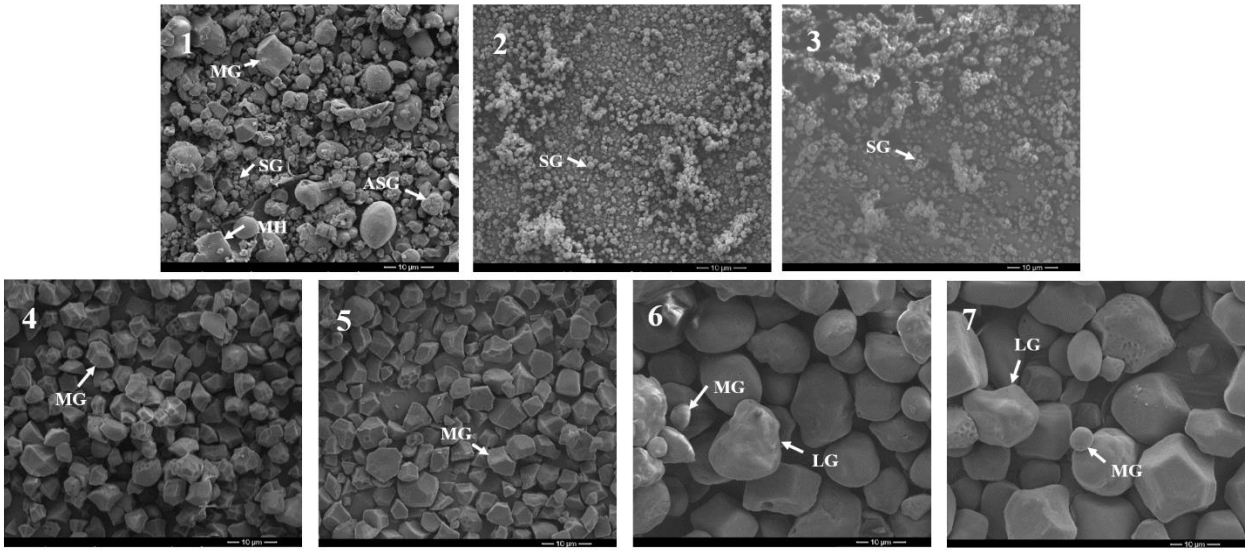

Figure 2-1. Scanning electron microscopy (SEM) images showing the morphology of starch granules of sweet corn (1), cow cockle (2), amaranth (3), waxy rice (4), normal rice (5), waxy corn (6), and normal corn (7). Starch granules were classified in large granules (LG, > 10 μm), medium granules (MG, 2–10 μm), small granules (SG, < 2 μm), and aggregated small granules (ASG). For sweet corn starch granules (1), maize hull pieces are indicated as MH.

2.3.2.2 Crystalline structure

The wide-angle x-ray crystallograms of starch materials are shown in **Figure 2-2.** Except for SCS, all starches showed A-type crystalline pattern with reflections at 2θ values of 15°, 17°, 18°, 23°. For SCS, A-type signals decreased and an additional response at 2θ value of 20° indicates the presence of V-type crystalline pattern (Singh et al., 2006; Zobel, 1988).

The crystallinities of starches are also labeled in **Fig. 2-2**. In general, WCS and WRS had higher crystallinity (50% and 51% respectively) than their normal starch counterparts (34% for NCS and 38% for NRS). The crystallinity of CCS (42%) fell between those of waxy and normal corn or rice starches. The crystallinity of AS was the highest (56%) suggesting the well-ordered granular structure despite the extremely small size of granules. Among all starches, SCS showed the lowest crystallinity (28%).

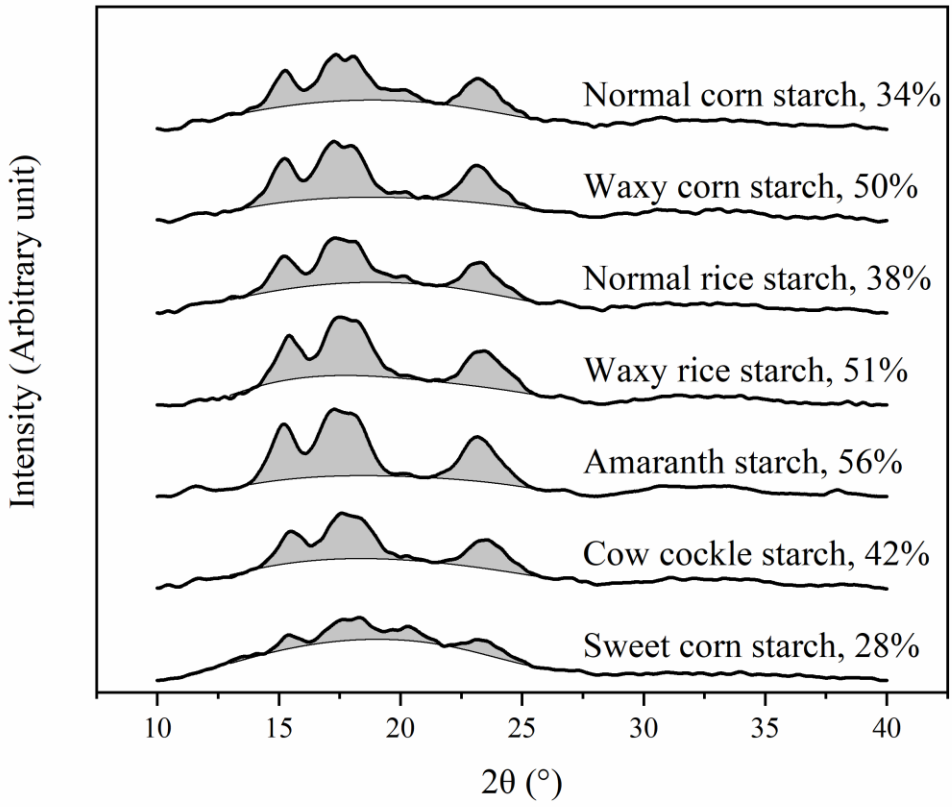

Figure 2-2. Wide-angle X-ray powder diffraction crystallograms of starches. The shaded areas show the crystalline regions. The crystallinity (%) of each starch is labeled.

2.3.3 Starch gelatinization

Starch gelatinization was evaluated using differential scanning calorimetry (DSC). As shown in **Figure 2-3**, NCS, WCS, NRS, and WRS showed the endothermic peak temperature (T_p) of 69.4, 71.2, 65.9, and 66.5 °C, respectively. Among these starches, NCS displayed a most defined endothermic peak. In contrast, CCS also showed a well-defined endothermic peak, however, with a relatively low T_p (64.1 °C). This shows that the ordered structure of CCS was rather homogenous but less robust than those of NCS, WCS, NRS, and WRS. In contrary, AS exhibited the highest T_p (74.1 °C) and the largest enthalpy change (ΔH, 19.4 J/ g), which again confirmed that the small granules of AS had highly thermostable crystalline structure.

The DSC thermogram of SCS was flat and broad, with T_p at about 70.9 °C. The value of ΔH was 5.6 J/ g, much lower than that of other starches (11.7 -19.4 J/ g). The low ΔH value correlated with the low crystallinity of SCS (**Fig. 2-2**), and the broad range of enthalpy signal showed that the ordered structure was quite heterogeneous.

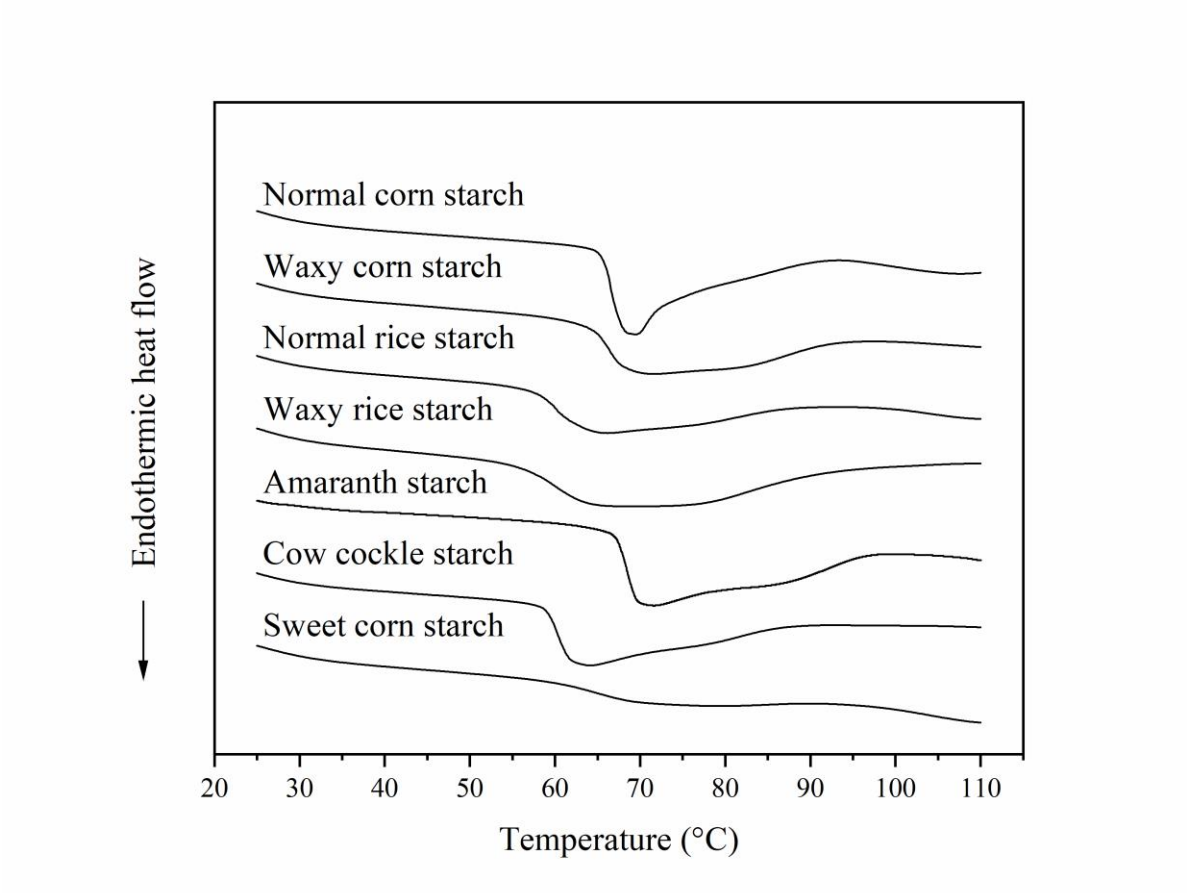

Figure 2-3. Differential scanning calorimetry (DSC) endothermic thermogram of starches.

2.3.4 Starch pasting behavior

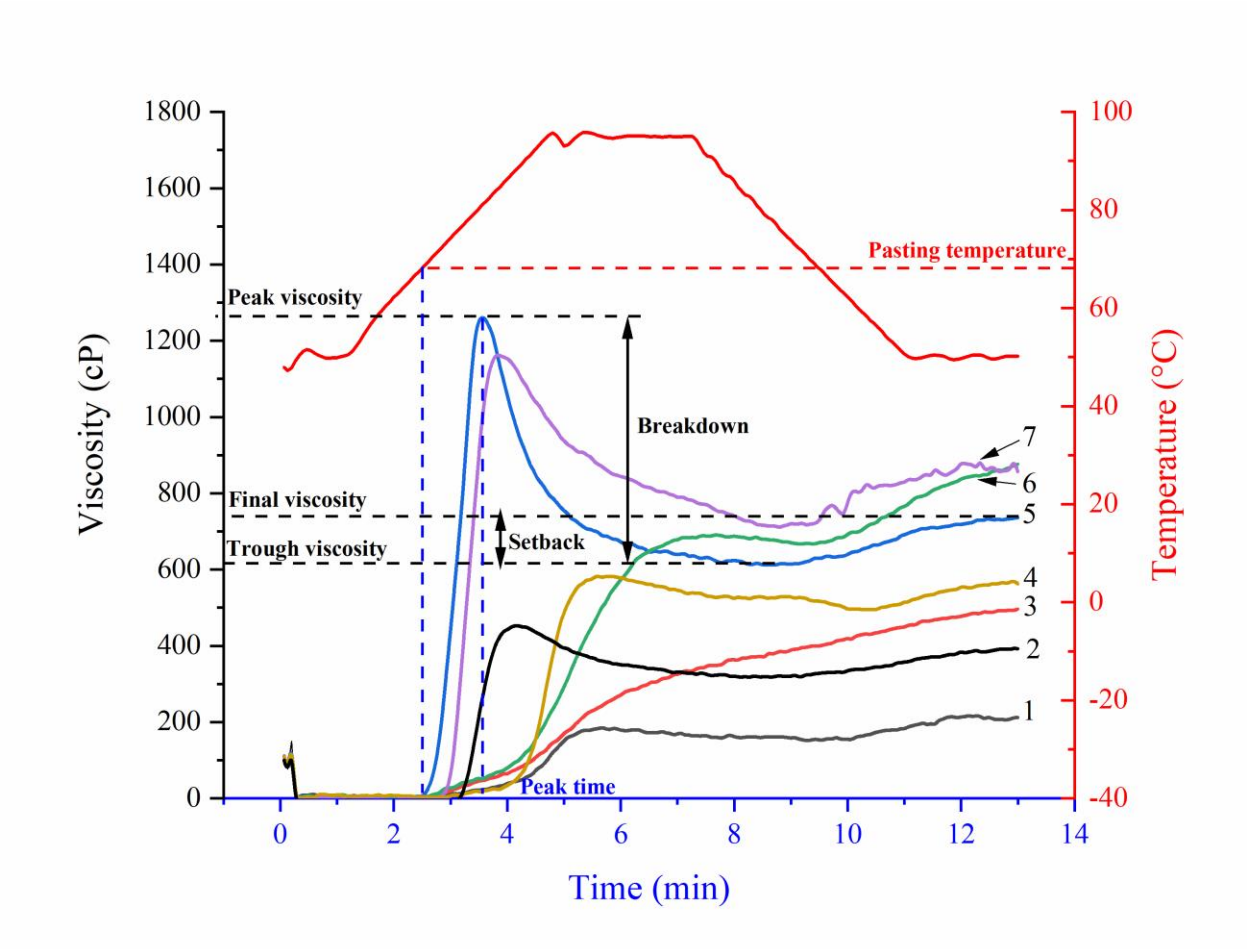

Figure 2-4. Rapid Viscosity Analyzer (RVA) viscograph of: (1) sweet corn starch, (2) amaranth starch, (3) cow cockle starch, (4) normal corn starch, (5) waxy rice starch, (6) normal rice starch, (7) waxy corn starch. RVA parameters are depicted using waxy rice starch as an example, including peak viscosity (the maximum hot paste viscosity), trough viscosity (the minimum hot paste viscosity); final viscosity (the viscosity at the end of test), breakdown (the difference between peak viscosity and trough viscosity), setback (the difference between final viscosity and trough viscosity), pasting temperature (the temperature where viscosity first increases by > 25 cP over a 20-s period), and peak time (the time needed to reach peak viscosity).

As shown in **Figure 2-4**, the RVA viscograph of CCS displayed a large deviation from that of all other starches, that is, the viscosity undergoing a steady increase to 473 cP with no defined breakdown and setback. Similar RVA behaviors were found with other submicron-granule starches, such as the *Mirabilis jalapa* starch (Pumacahua-Ramos et al., 2015), small pigweed / dasheen starch (Goering and DeHaas, 1972), and quinoa starch (Lindeboom et al., 2005). In general, the rate of particle breakage is proportional to the mass-equivalent diameter (Barthelmes

et al., 2003), suggesting that large particles are more susceptible to disruption under steady shearing. Conceivably, the unique pasting behavior of CCS was associated with its submicron granular size that effectively protected the integrity of swollen granules.

A low peak viscosity (449 cP) together with limited level of breakdown (138 cP) are observed on the RVA viscograph of AS (**Fig. 2-4**), which significantly differs from other waxy-type starches (WRS and WCS) but is analogous to NCS. The swelling power of AS was reported to be much lower than that of WCS, but in similar to that of NCS (Bhosale and Singhal, 2007; Paredes-López et al., 1989). The results suggest that the limited swelling of AS contributes to low peak viscosity during gelatinization. Coupled with the small size of granules, the limited swelling granules of AS exhibit an extent of resistance to shear and therefore show low breakdown.

The viscograph of SCS shows typical peak, breakdown, and setback viscosities. However, the values of these parameters were much lower than those of NCS, WCS, NRS, and WRS (**Fig. 2-4**). For example, in the temperature range of 50-90 °C, SCS and NCS performed similarly in initial viscosity increase, but the viscosity increase was limited with SCS. Very low peak viscosity (177 cP) was found for SCS in comparison with that of NCS (584 cP). For SCS, slight breakdown (about 30 cP) and setback (about 60 cP) were followed with a rather low final viscosity (about 207 cP).

2.3.5 Chain length distribution of starches

Figure 2-5A shows the normalized mass-based chain length distribution of starches. Based on previous studies (Klucinec and Thompson, 1998; Yao et al., 2004), characteristic populations representing amylose (AM) and amylopectin (AP) were identified at the retention time of 11-13.5 min and 13.5-21.5 min, respectively. Based on the chromatogram of each starch, the percentage of AM population was determined as the fraction of AM population area within the total area. The percentage of AM population for SCS, NCS, CCS, NRS, WCS, WRS and AS was 32.5%, 24.9%, 18.4%, 16.2%, 1.4%, and non-detectable, respectively. It should be noted that, due to the presence of lightly branched intermediate molecules (LBIM) in the AM population, the percentage of AM population determined was not equivalent to the amylose content determined using blue value (**Table 2-1**).

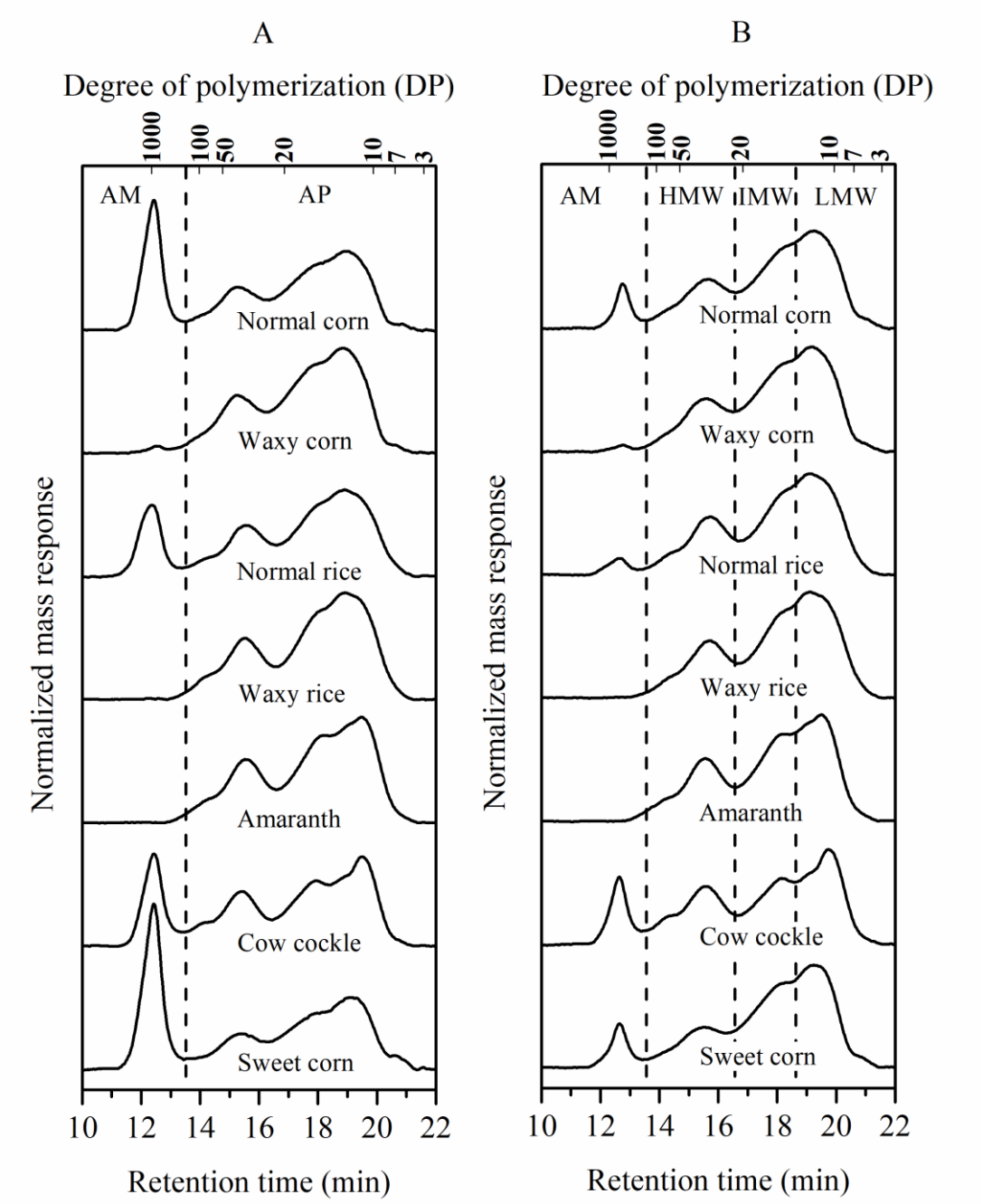

Figure 2-5. High performance-size exclusion chromatograms showing the chain length distribution of: **A**, debranched starch, and **B**, debranched amylopectin fraction obtained after alcohol precipitation of amylose. AM: amylose population defined by molecular weight >170 DP. AP: amylopectin population defined by molecular weight <170 DP. Within the amylopectin population, the high molecular weight (HMW), intermediate molecular weight (IMW), and low molecular weight (LMW) sub-populations are defined by local minimums indicated by dash lines.

Figure 2-5B shows the chain length (CL) distribution of debranched amylopectin fraction obtained after the alcohol precipitation of amylose. Amylose molecules form inclusion complexes with 1-butanol and isoamyl alcohol and precipitate (Liu et al., 1997). In contrast, LBIM do not effectively bind and precipitate with alcohols (Klucinec & Thompson, 1998). Therefore, by comparing the percentage of AM population before and after alcohol complexation (**Fig 2-5A and B)**, the amount of LBIM can be assessed. In this study, less than 25% of AM population was retained for NCS, NRS, and SCS, whereas about 62% of AM population was retained for CCS after alcohol precipitation, suggesting a much higher LBIM amount with CCS than with other amylose-containing starches.

As shown in **Figure 2-5B,** AP population can be divided into three segments based on the local minimum responses at about DP 22 and 15. These segments represented the high (HMW, DP > 22), intermediate (IMW, DP = 15-22), and low (LMW, DP < 15) molecular weight chain constituents of amylopectin. In comparison with corn and rice starches, amylopectin of SCS contained lower amount of HMW fraction (19% v.s. 25-27%), higher amount of IMW fraction (34% v.s. 19 - 27%), and slightly lower amount of LMW fraction (47% v.s. 46 - 54%). Compared with corn and rice starches, amylopectin of AS contained higher amount of HMW fraction (29% v.s. 25 - 27%), lower amount of LMW fraction (45% v.s. 46 - 54%), and slightly higher amount of IMW fraction (26% v.s. 19 - 27%). Compared with corn and rice starches, amylopectin of CCS contained higher amount of HMW fraction (31% v.s. 25 - 27%), lower amount of LMW fraction (42% v.s. 46 - 54%), and slightly higher amount of IMW fraction (27% v.s. 19 - 27%). For CCS, the peak value of LMW fraction (DP10.7) was lower than that of other starches (DP12.4 - 13.7). This observation was in agreement with the study of Biliaderis et al. (1993) who showed that the peak position of the shortest population of debranched CCS was 2 DPs shorter than that of waxy corn starch.

2.3.6 Branching pattern of amylopectin

The branching patterns of SCS and CCS amylopectin were studied using their β-limit dextrins (BLDs). The normalized mass- and molar-based CL distributions of BLDs are shown in **Figure 2-6 A and B**, respectively. Based on Hizukuri's amylopectin cluster model (1986), five populations were defined in the chromatograms: A chains, intra-cluster B chains (B1a and B1b), and inter-cluster B chains (B2 and B3) (Hizukuri, 1986; Yao et al., 2004).

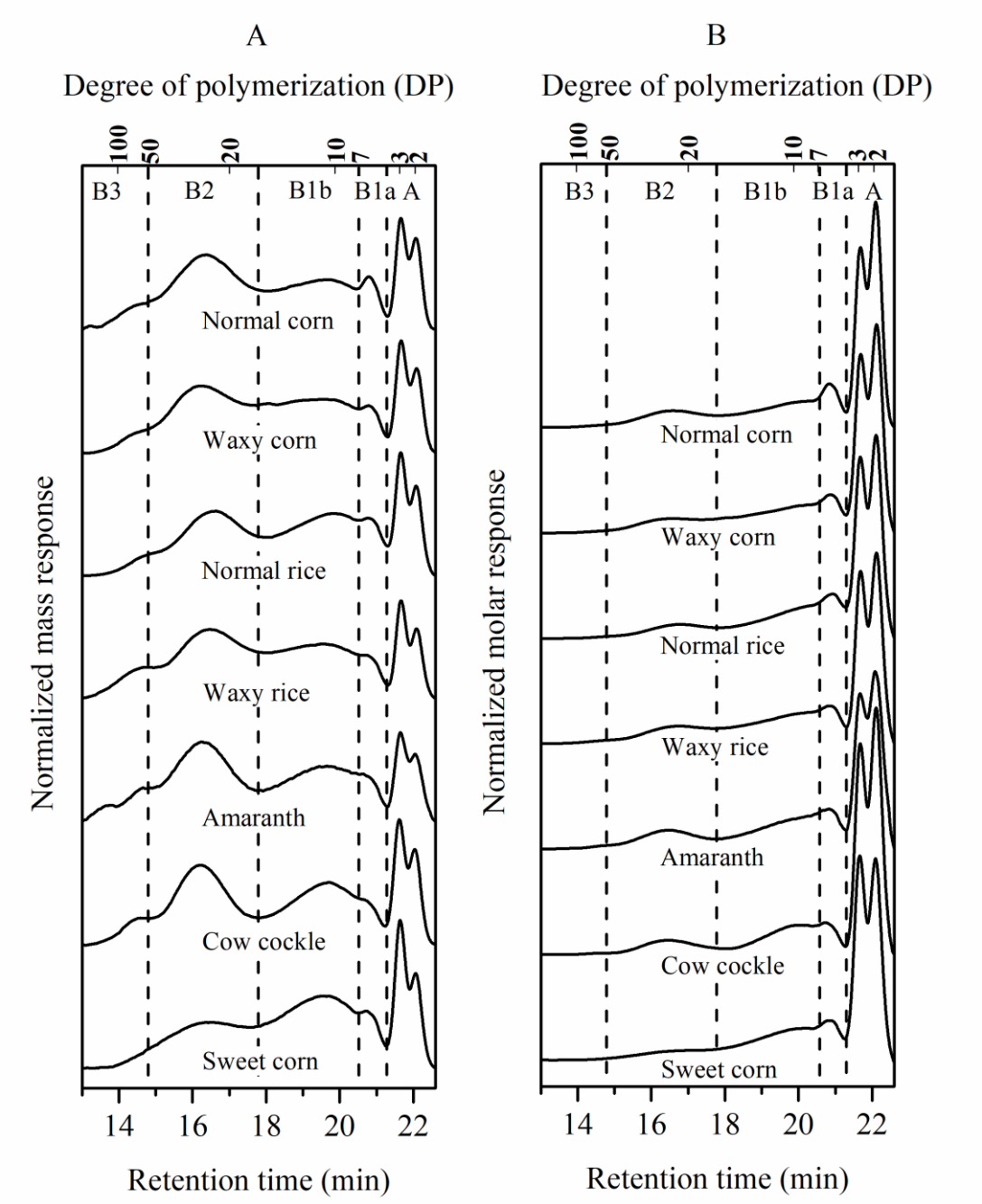

Figure 2-6. High performance-size exclusion chromatograms showing **A**, weight-based, and **B**, molar-based chain length distribution of β-limit dextrins. Dash lines are used to divide the chromatograms into A chains (i.e. external chains attaching to other chains) and several types of B chains (i.e. chains with other chains attaching to them). B chains include B1a and B1b chains (short and long intra-cluster B chains, respectively), B2 chains (inter-cluster chains connecting two clusters), and B3 chains (inter-cluster chains connecting three clusters).

BLDs of WCS and NCS were nearly identical, whereas BLDs of WRS and NRS were slightly different in their percentage of B1b chains (**Fig. 2-6 A**). For BLD of CCS, well-defined peaks were found at the B3, B2 and B1b population whereas a shoulder separated B1a and B1b populations. BLD of SCS shows considerable differences from those of NCS and WCS, displaying a low and flat peak at B2 population, a negligible B3 population, and a large B1b population. The peak DP values for individual chain populations are shown in **Table 2-2**. The CL of intra-cluster chains were highly comparable among various starches, with B1a chain of about DP 6-7 and B1b chain of about DP 10-11. In contrast, the CL of inter-cluster chains varied, with B2 chains ranging at DP 22-25 and B3 chains ranging at DP 49-63.

To establish the branch model of BLDs, the molar-based CL distributions were obtained through dividing the RI responses by their corresponding molecular weights at each data point of mass-based chromatograms. The chromatograms were then normalized based on the total area (**Fig 2-6B**) and several parameters of branch structure were determined (**Table 2-2**). For the modeling of each BLD, the molar amount of B2 chains (i.e. chains that connect 2 clusters) was defined as 1.0 unit. Using the amount of B2 chains as reference, the molar amount of B3 chains (i.e. chains that connect 3 clusters) was very low (< 0.07) for all starches and undetectable specifically with SCS. The molar amounts of intra-cluster B chains (B1a and B1b) and external chains (A chains) are also shown in **Table 2-2**. Specifically, it was observed that: 1) SCS had the highest amount of intra-cluster chains, whereas AS and CCS has the lowest, and 2) SCS has the highest amount of A chains, whereas AS has the lowest.

2.3.7 Modeling of amylopectin clusters

To model and compare the branching pattern of individual starches, several BLD structural parameters (**Table 2-2**) were used. Among these parameters, the intra-cluster branch distance (IBD) was defined as the distance between two adjacent branches in a cluster. In the modeling of BLD, the average length of external stubs for both A and B chains was 2.5 DP (Yun and Matheson, 1993). Therefore, the value of IBD can be calculated as:

IBD = chain length of B1a chain in BLD – 2.5 DP (stub) – 1 DP (branching point)

In this study, the IBD value of about 3 DP was retained with all starches, suggesting a prevailing role of starch branching enzymes in positioning intra-cluster branches.

Table 2-2. Parameters describing the fine structural characteristics of debranched β-limit dextrins

Starch type	Length of chains in β-limit dextrin (DP[1])					Intra-cluster branch distance	Internal chain length of B2 chains	(Relative) number of chains (A : B1a : B1b : B2 : B3)	ANBPC[2]
	A	B1a	B1b	B2	B3				
Sweet corn	2, 3	6.4	10.2	23.3	N.D.[3]	2.9	20.8	8.4 : 1.8 : 3.5 : 1.0 : N.D.	14.7
Cow cockle	2, 3	6.6	10.6	24.5	60.2	3.1	22.0	5.7 : 0.8 : 1.7 : 1.0 : 0.04	8.6
Amaranth	2, 3	6.7	10.8	24.2	52.1	3.2	21.7	3.7 : 1.0 : 1.4 : 1.0 : 0.04	6.6
Waxy rice	2, 3	6.5	11.1	22.9	52.5	3.0	20.4	4.4 : 1.1 : 1.6 : 1.0 : 0.07	7.2
Normal rice	2, 3	6.3	10.0	22.1	49.0	2.8	19.6	6.1 : 1.6 : 1.8 : 1.0 : 0.05	9.6
Waxy corn	2, 3	6.2	10.8	24.6	62.8	2.7	22.1	5.1 : 1.0 : 1.9 : 1.0 : 0.05	8.2
Normal corn	2, 3	6.1	10.7	23.7	57.7	2.6	21.2	4.9 : 1.0 : 1.9 : 1.0 : 0.06	7.9

[1] Degree of polymerization.

[2] ANBPC: average number of branches per cluster.

[3] Non-detectable

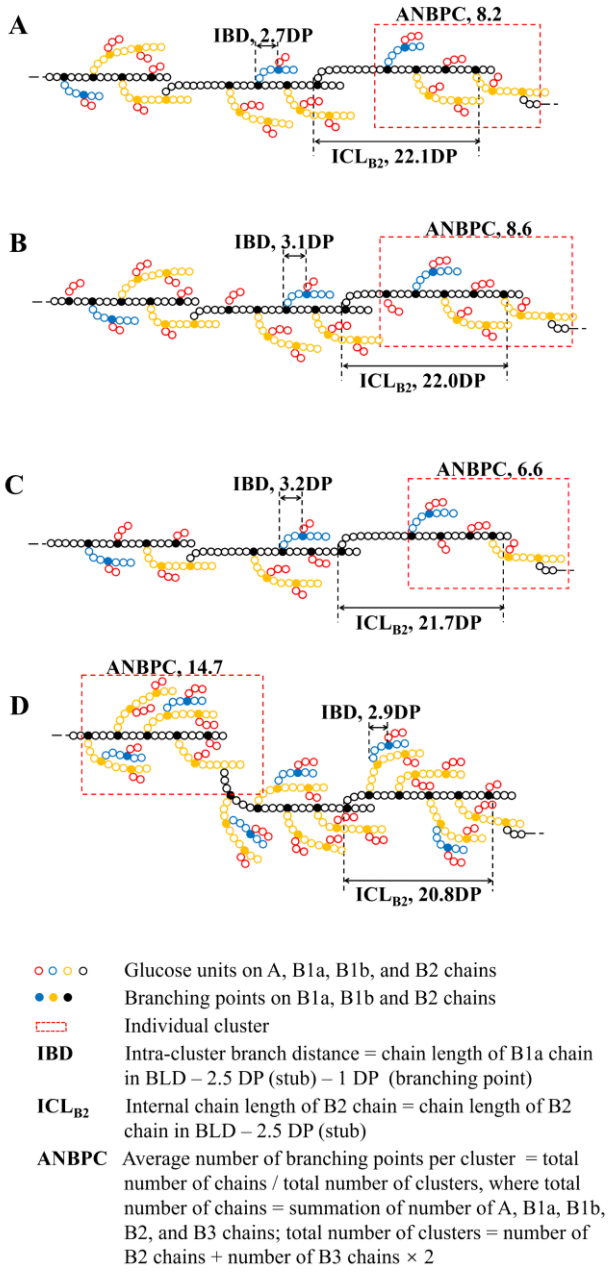

Figure 2-7. The schematics showing the cluster structure of amylopectin β-limit dextrins of **A**, waxy corn starch; **B**, cow cockle starch; **C**, amaranth starch, and **D**, sweet corn starch. Circles represent glucosyl units. Solid circles indicate branching points. The red, blue, orange, and black colored chains represent A, B1a, B1b, and B2 chains. Branching parameters labeled include the intra-cluster branch distance (IBD), the internal chain length of B2 chain (ICLB2), and the average number of branches per cluster (ANBPC).

As shown in **Figure 2-7**, the internal chain length of B2 chains (ICL_{B2}) can be used to represent the average distance between two connecting clusters (**Fig. 2-7**). Such a modeling approach is based on the following considerations: 1) the reducing end of a B2 chain initiates the formation of a cluster, 2) the outmost branch point of this B2 chain indicates a transfer from chain branching to chain elongation, and 3) one of the chains initiated at the point of this transfer would initiate the next cluster and thus becomes a B2 chain. For a BLD, the value of ICL_{B2} can be calculated as:

ICL_{B2} = chain length of B2 chain in BLD – 2.5 DP (stub)

In this study, the ICL_{B2} values ranged from 19.6 to 22.1 DP (Table 2), suggesting a highly regulated repeating of cluster initiation and growth among all starches. The mechanism of this regulation should be associated with coordinated actions of starch branching enzymes and starch synthases.

For structural model comparison among different starches, an effective parameter is the average number of branches per cluster (ANBPC) (Yao et al., 2004). In general, the ANBPC can be determined from the numbers of A, B1a, B2b, B2, and B3 chains:

ANBPC = total number of chains / total number of clusters

For calculation, only B2 and B3 chains were assumed to initiate new clusters in our model (each B2 initiating 1 cluster and each B3 chain initiating 2 clusters, respectively). Hence, we have the following equation:

The total number of clusters = number of B2 chains + number of B3 chains × 2.

And we have the following equation:

Total number of chains = summation of number of A, B1a, B1b, B2, and B3 chains.

As shown in **Table 2-2**, the ANBPC values range from 6.6 for AS to 14.7 for SCS, indicating a large variance of branch density among various starches. Compared with branch density (i.e. the percentage of 1,6-glucosidic linkages), ANBPC describes starch branching at the cluster level. For CCS, the ANBPC value was 8.6, suggesting that its cluster structure was similar to that of WCS (**Fig. 2-7A and B**). The ICL_{B2} for CCS was 22.0 DP, which was essentially the same as that for WCS.

For AS, however, the ANBPC value was much lower than that of WCS (6.6 v.s. 8.2), which should be associated with the relative less A chains in the cluster (**Fig. 2-7A and C**). The small size of amylopectin cluster may favor the parallel spatial arrangements of external chains both in

the native state and gelatinized state (Vamadevan et al., 2013). Therefore, the unique amylopectin structure of AS may contribute to the high crystalline granular structure and the lower volume expansion when ordered structure is disrupted after gelatinization.

The AP branching pattern of SCS (**Fig 2-7D**) is highly different from that of other starches. Due to the high amounts of B1a and B1b chains (1.8 and 3.5 per cluster), the ANBPC for SCS (14.7) was much higher than that for the other starches (6.6-9.6). The abundant and dispersed branches for SCS led to large branching and amorphous regions among repeating cluster units. Such a highly branched, low crystalline structure was originated from the deficiency of a starch debranching enzyme, SU1 (Ball et al., 1996; James et al., 1995). The regular assumption is that SU1 plays a crucial role in regulating the amount and distribution of branches generated by starch branching enzymes. The highly branched and amorphous nature of AP in SCS is closely associated with the low viscosity of SCS paste due to the low inter-granular chain entanglements.

2.4 Conclusion

Exploring new starch resources will benefit the fundamental research and technology advancement of food and food-related areas. In this study, several basic structural and physical properties of three small-granule starches, SCS, CCS and AS, were characterized. The results showed that SCS granules were rather heterogeneous, contained higher amylose content than normal corn starch, and showed highly branched structure. The high branching of SCS correlates with its low crystallinity and pasting viscosities. In contrast, CCS and AS showed submicron homogenous granules. Unlike SCS, amylopectin for CCS was less branched with smaller clusters. Largely due to its abnormally small granular size, CCS showed high shear-resistance during pasting. The amylopectin for AS was least branched with the smallest cluster among the starches that were investigated in this study. This unique amylopectin pattern was considered to account for the robust crystalline structure of the granules and low peak viscosity. In summary, SCS, CCS and AS showed highly unique properties that were associated with their granular sizes and/or branching patterns. Both SCS, CCS and AS may have potentials for new applications, such as fat replacement, encapsulation and delivery of active ingredients and food texture modification.

CHAPTER 3. RETENTION OF MALTODEXTRIN IN NATIVE AND SWOLLEN STARCH GRANULES FROM DIFFERENT SOURCES

3.1 Introduction

Starch is an important food ingredient for food industry. The major function of starch is to provide texturization and the bulking for foods (Eliasson, 2004). Common food products, such as bakery, noodle, and fried products, involve the mixing and processing of starch or starchy food ingredients (e.g. cereal flour) with fats, proteins and other minor food components (Crosbie, 1991; Lazarick et al., 2014; Patel et al., 2005). The retention of other food compounds (e.g. sugars, salts, maltodextrins, and polyphenols) by food starches affect food quality, shelf life, and health benefit, and has been studied in recent years (Baek et al., 2004; Barros et al., 2012). From broader perspectives, the incorporation of small-molecule food compounds in food starch may further contribute to the improvement of nutritional, eating, and safety qualities of food products (Bhatia and Bharti, 2015; Han et al., 2015; Schober et al., 2008; Wu et al., 2010). Simple sugars, maltodextrins and other non-starch oligo- and polysaccharides (e.g. inulin) are commonly formulated or processed with starch in bakery and frozen food products. These ingredients are often used at high content in food and may interact with starch granules. Thus, it is of high interests for the food industry to evaluate the interactions between these components and starch granules.

Maltodextrin is a mixture of starch hydrolysate mainly composed of glucose, maltose and a broad spectrum of polymeric glucans (Chronakis, 1998). The average degree of polymerization (DP) that is inversely proportional to the dextrose equivalent values (DE), dominates the application of maltodextrin as sweetener, texturizer and bulking agent (Avaltroni et al., 2004; Chronakis, 1998; Dokic-Baucal et al., 2004). Maltodextrin fractions with good solubility and relatively low DP may easily diffuse to the interspaces of food matrix leading to a change of the equilibrium composition of ‘bulk-phase’ maltodextrin and therefore affecting the functionality of maltodextrin. Such a change is more likely occur in starchy foods due to the hydrophilic nature and the abundant interspace-volumes of starch. A number of previous studies have reported great contribution of the DE of maltodextrin on the quality of starchy foods (Chronakis, 1998;

Galmarini et al., 2009; Witczak et al., 2010), suggesting the significance of the mechanistic study on the interactions between starch and maltodextrin.

The retention of soluble molecules in starch material is associated with the granular structure of starch. Native starches exist in the form of semi-crystalline granules with their sizes ranging from hundreds of nanometers to tens of micrometers (Jane et al., 1994). The native starch granules are not purely solid micro-beads. In contrast, abundant nano- or micro-scale structural features, such as the surface cavities, channels, and central hilium spaces as well as amorphous regions, are found in starch granules (Huber and BeMiller, 2000). Extraneous moisture and dispersed substances can be incorporated with starch granules. When starch granules lose original crystalline structure due to heating or chemical treatment, they swell to many times their original volume with water is entrapped in swollen granules (Biliaderis et al., 1980; Singh et al., 2003; Tester and Morrison, 1991). Meanwhile, extraneous substances may also be incorporated in swollen starch granules.

Swollen starch granules are mesh-like particles that contain two types of alpha-D glucan molecules: amylose (a mostly linear glucan) and amylopectin (a branched glucan). The ratio and the structure of amylose and amylopectin affect the integrity and swelling behavior of starch granules (Debet and Gidley, 2007; Fredriksson et al., 1998; Jane et al., 1999), which may further impact the mesh properties of swollen starch (Hickman et al., 2009; Jane et al., 1999). Given that common food starches are prepared from different plant sources, they may display different mesh structures.

The goal of this study was to compare the behaviors of selected starches in retaining soluble food component, using maltodextrin as model. The starches selected had different granular sizes, amylose contents, morphological properties, and swelling power. A commercial maltodextrin with the DE of 11 was used to include soluble glucan components of various molecular weights. The granular retentions of maltodextrin components were determined to evaluate the interactions between starch granules and soluble food components of various molecular weights.

3.2 Materials and methods

3.2.1 Material

Cow cockle seeds were purchased from Hangzhou Botanic Technology Co., Ltd., China. Amaranth grains were purchased from Woodland Foods Co., Ltd., IL. Waxy corn starch (WCS) and normal corn starch (NCS) were obtained from Cargill Inc. and Ingredion Inc., respectively. Maltodextrin (MALTRIN M100®) was obtained from Grain Processing Corporation. All chemical reagents used for the study were of analytical grade unless specified.

3.2.2 Methods

3.2.2.1 Isolation of starch

Amaranth starch (AS) was isolated using a modified alkaline extraction method. First, 1.5 kg of dry amaranth grains (1.5 kg) and 0.1% (w/v) sodium hydroxide (NaOH) solution (4 L) were slightly agitated at 50 °C in a water bath. Cow cockle starch (CCS) was isolated according to the methods of Peng and Yao (2018) with modifications. Cow cockle seeds (1.5 kg) were soaked in 4 L 0.15 M lactic acid solution at 50 °C in a water bath with slight agitation.

After the 48 h steeping process, the steeping solution was decanted and wet grains or seeds were homogenized with 3 L of water using a blender (Waring Laboratory Science, Torrington, CT) at high speed for 4 min and passed through a 270-mesh sieve. The solids retained by the sieve were extracted again using additional 3 L water. The extractions that permeated through the sieve were combined, adjusted to pH 10 and centrifuged (3,000 × g for 15 min). The precipitate, as the crude starch material, was collected.

Each crude starch material (about 700 g) was resuspended in 3 L of water and adjusted to pH 10, agitated for 30 min, and centrifuged again. The precipitate was dispersed again and then centrifuged. This dispersing-centrifuging cycle was repeated three times, during which the top layer of the precipitate containing proteinaceous material was scraped off using a spatula. Then, the precipitate was resuspended in deionized water, neutralized to pH 7.0 using 1.0 M hydrogen chloride (HCl) solution, and centrifuged. The starch precipitate was further washed twice using deionized water (1.5 L for each cycle). The material collected was resuspended in 500 mL 80% (v/v) ethanol, subjected to vacuum filtration, and then washed using 100 mL of pure ethanol. The

filter cake was collected and dried overnight. All starch materials were stored in glass jars at room temperature before use.

3.2.2.2 Preparation of granular cold-water swelling starch

Granular cold-water swelling starch (GCWS) was prepared according to the method of Chen and Jane (1994) with modifications. For each of WCS or AS, 20 g (dry basis) was suspended in 140 mL ethanol in a 400-mL beaker with constant stirring (200 rpm). To the starch-ethanol suspension, 35.7 mL NaOH solution (3M), 23 mL 80% alcohol and 9.8 mL NaOH solution (3M) was successively added at the rate of 2 mL/ min. The mixture was stirred for 15 min before an additional 23 mL 80% (v/v) ethanol was added slowly. The obtained mixture was allowed to stand for 10 min, subjected to vacuum filtration, and washed with 60 mL 80% (v/v) ethanol. The starch cake was re-dispersed in 200 mL 80% (v/v) ethanol and neutralized with hydrogen chloride solution (HCl, 3 M in ethanol). The starch fraction was obtained by vacuum filtration and washed with 60 mL 95% (v/v) ethanol and thereafter 60 mL 100% (v/v) ethanol. The filter cake obtained was dried at 80 °C for 3 h.

For each of NCS or CCS, 20 g (dry basis) was suspended in 140 mL 40% (v/v) ethanol in a 400-mL beaker with constant stirring (200 rpm). The beaker was kept in a water bath at 35 °C during the process. To the starch-ethanol suspension, 45.5 mL NaOH solution (3M) was gradually added at the rate of 2 mL/ min. The mixture was stirred for 15 min before an additional 25 mL 40% ethanol was slowly added. The starch-ethanol suspension was allowed to stand for 30 min. After decanting the supernatant, the starchy fraction was washed with 100 mL 40% (v/v) ethanol and re-dispersed with 100 mL 40% (v/v) ethanol. After being neutralized with HCl, the suspension was allowed to stand for 30 min. The starchy fraction was then successively dehydrated by a series of mixing and decanting process using 60%, 95% and 100% (v/v) ethanol. The obtained starch fraction was dried at 80 °C for 3 hr.

The GCWS materials obtained from the above process were sieved using a 50-mesh screen and stored in a screw-capped bottle at room temperature before use. In this study, swellable starch (SS) is used for the abbreviation of GCWS and GCWS prepared from AS, CCS, WCS and NCS were coded as S-AS, S-CCS, S-WCS, and S-NCS, respectively.

3.2.2.3 Chemical compositions of starches

The moisture content of each starch material was determined using the AACCI Method 44-15.02. Starch content was determined using the Megazyme Total Starch Assay Kit as described by AACCI Method 76-13.01. Nitrogen content was determined using the combustion method with a Nitrogen Analyzer (LECO model FP-2000, LECO Co., St. Joseph, MI), with its value multiplied by 5.75 to calculate the protein content. Apparent amylose content was determined by colorimetric method according to Morrison and Laignelet (1983).

3.2.2.4 Swelling power

Swelling power (SP) was determined according to the method of Li and Yeh (2001) with slight modification. Starch (~100 mg, dry basis) was precisely weighed into a capped centrifuge tube with 10 mL pre-added water. The tube was agitated at 25 °C in a water bath (120 rpm) for an hour and thereafter subjected to centrifugation (8,000 × g, 30 min). The supernatant was decanted. The materials adhered to the wall of centrifuge tube were considered as the sediment and the weight of the sediment was coded as W_S. The supernatant was dried to constant weight (W_1) in a ventilated oven at 100 °C. The water-soluble index (WSI) and SP were determined as the following:

$$\text{WSI (\%)} = \left(\frac{W_1}{dry\ mass\ of\ starch}\right) \times 100\% \qquad \textbf{Eq. (1)}$$

$$\text{SP (g/g)} = \frac{W_S}{[dry\ mass\ of\ starch \times (100\% - WSI)]} \qquad \textbf{Eq. (2)}$$

3.2.2.5 Wide-angle X-ray powder diffraction

The X-ray diffraction analysis was carried out using Philips PW3710 diffractometer equipped with Ni-filtered Cu-Kα (1.5418 Å) radiation. Starch material (~ 0.5 g) was packed in an aluminum holder and mounted on the diffractometer. The intensity data were collected through a scan operated at 40 kV and 25 mA with the 2θ range of 10-40° at the scan rate of 1°/ min. The raw data was smoothed for further analysis by the Automated Powder Diffraction software (version 3.6). The crystalline peaks and crystallinity for each starch were determined according to Peng and Yao (2018) using the Origin Pro 2016 software. Crystallinity was calculated as:

Crystallinity (%) = $(A_t - A_a) / A_t$, where A_a and A_t were the area for the amorphous background and the total area, respectively.

3.2.2.6 Preparation of maltodextrin stock solution

Maltodextrin solution was freshly prepared for each experiment. 5.0 g maltodextrin (MALTRIN M100) in dry powder form was dissolved in 30.0 mL water at 90 °C. The total volume of maltodextrin solution was subsequently made to 50.0 mL with water in a 50-mL volumetric flask at room temperature. The 10.0% (w/v) maltodextrin stock solution was stored at room temperature in capped glass bottles after filtered through 0.45-μm polyamide syringe filters (Thermo Scientific Nalgene, US). Preliminary tests have confirmed that the filtration with polyamide membrane did not alter the concentration and composition of the model maltodextrin solution.

3.2.2.7 Preparation of native and swellable starch suspensions

Except for S-AS, the homogenous suspension of native starch and SS materials were prepared (without the formation of lumps) through vortexing (2,500 rpm, 10 min) (Digital Vortex Genie® 2, Scientific Industries, NY) followed by mild agitation in a water bath (120 rpm, 4 h) (SHEL LAB Models WS27, VWR International, PA). In order to break the lumps, S-AS solid was first suspended in water through vortexing (3,000 rpm for 15 min followed with 2,500 rpm for 30 min); then the dispersion was subjected to mild agitation (120 rpm, 4 h). Before subsequent analysis, the suspensions were examined under the light microscopy to confirm the integrity of granules and the absence of lumps.

3.2.2.8 Particle size determination using light scattering

1% (w/v) native and SS suspensions were prepared as described above. The particle size distribution was measured using static multi-angle light scattering method using a Mastersizer Hydro 2000 system (Malvern Instrument, Malvern, UK). Average granular sizes were characterized in terms of the Sauter mean diameter (d_{32}) or volume mean diameter (d_{43}) defined by the following equations (Yusoff and Murray, 2011):

$$d_{32} = \frac{\Sigma_i n_i d_i^3}{\Sigma_i n_i d_i^2} \qquad \textbf{Eq. (3)}$$

$$d_{43} = \frac{\Sigma_i n_i d_i^4}{\Sigma_i n_i d_i^3}$$ **Eq. (4)**

where n_i is the number of the starch granules of diameter d_i. All measurements were made at room temperature on at least two freshly prepared samples. The refractive indices of water and starch were taken as 1.330 and 1.530, respectively.

3.2.2.9 Scanning electron microscopy

Scanning electron microscopy (SEM) was utilized to observe the morphological characteristics of native and swellable starch materials in the powder form. For SEM, the powder specimen was mounted on a circular metal stub with double-sided sticky tape and coated with platinum in a Cressington 208HR sputter coater. The specimens were observed using FEI NOVA nanoSEM Field Emission SEM (FEI, OR) under the voltage of 5.0 kV. Images were taken at magnification of 5,000 ×. Light microscopy (LM) was used to observe the morphological characteristics of swellable starch materials in dispersion. SS dispersions were prepared using the procedure described in **3.2.2.7**. The dispersions were diluted with water to appropriate concentrations, dyed with iodine, and observed under LM with a 40× objective lens.

3.2.2.10 Incubation of maltodextrin solution with starch materials

Each starch material (2.0 g for native starch and 0.5 g for GCWS) was suspended in 12.5 mL water in a 50-mL capped polypropylene centrifuge tube using the same procedure described in **3.2.2.7**. Subsequently, 12.5 mL 10% (w/v) maltodextrin stock solution was added. The time at which maltodextrin solution was added was defined as time zero. The aqueous starch-maltodextrin mixture was incubated in a shaking water bath (25 °C, 120 rpm) for 4 h. A 5% (w/v) maltodextrin control solution was prepared by adding 12.5 mL maltodextrin stock solution to 12.5 mL water.

Aliquot (1.5 mL) samples were drawn at 5 and 240 min of incubation. A mild centrifugation (1,000 × g, 10 min) was applied at first to precipitate the native or swollen starch fraction. Glucan molecules in the maltodextrin that were not retained by starch granules remained in the free water phase of supernatant. To purify the free water phase, about 400 μL supernatant from the first centrifugation was centrifuged again (8,000 × g, 10 min) and the supernatant obtained was filtered through a 0.45-μm polyamide syringe filter (CELLTREAT, the Lab Depot,

Dawsonville, GA). 50 µL filtrate, 50 µL water and 900 µL DMSO were mixed in a 1.5-mL centrifuge tube, heated at 100 °C for 10 min, and centrifuged (5,000 × g, 10 min). The molecular weight distribution of the maltodextrin component remaining in the free water phase was determined using high performance size exclusion chromatography.

3.2.2.11 High performance size exclusion chromatography (HPSEC)

The chromatographic equipment consists of a Waters 1515 isocratic pump, Waters 2717 autosampler (Waters, US), and a Waters 2414 refractive index detector (RID, Waters, US). The analytical column in use was two connected Zorbax gel PSM 60-S columns (6.2 mm × 250 mm, Agilent Tech., Santa Clara, CA). A 20 µL aliquot sample was injected for HPSEC analysis. The chromatographic separation was carried out in 30 min, with DMSO used as the mobile phase at the flow rate of 0.5 mL/ min and column temperature and detector temperature maintained at 35 and 40 °C, respectively. Peak areas were utilized for quantitative analysis. Calibration curves were prepared using maltose standards of 0 to 5.0 mg/ mL. Glucose, maltose, maltotriose, maltopentaose, maltoheptaose, and three pullulan standards (6 kDa, 50 kDa, 400 kDa) (Sigma, US) were used for column calibration. RI signal were collected using Millennium software (Waters, Milford, MA) and the raw data were exported to an Excel spreadsheet, loaded to the Origin Pro 2018 software to plot differential chromatograms.

3.2.2.12 Differential chromatogram

In the present study, each RI value at a certain retention time corresponded to the content of a maltodextrin component in the free water phase (MDC_f) with a particular DP. The RI value as a function of retention time (the chromatogram) described the content distribution of MDC_f. Hence, the variations in the content distribution of MDC_f could be characterized using differential chromatograms. The data points of differential chromatograms were obtained using the following equation:

$$\Delta RI = RI_{t=0} - RI_{t=t_i} \quad \textbf{Eq. (5)}$$

ΔRI is the differential mass response, $RI_{t=0}$ is the RI value corresponding to the content of MDC_f at time zero, and $RI_{t=t_i}$ is the RI value corresponding to the content of MDC_f after i minutes of incubation (i = 5 or 240).

$RI_{t=t_i}$ was experimentally obtained from the chromatograms of the injected samples taken by the 5 or 240 minutes of incubation. In contrast, $RI_{t=0}$ was obtained by theoretical calculation based on the chromatogram of the 5% (w/v) maltodextrin control solution. As no mass transfer from free water phase to starch granules occurred at time zero, the $RI_{t=0}$ for a sample system ($RI\text{-}s_{t=0}$) should be proportional to the $RI_{t=0}$ for the control system ($RI\text{-}c_{t=0}$) with a factor (x) of their concentration ratio. The equation is shown as follows:

$$RI\text{-}s_{t=0} = x \cdot RI\text{-}c_{t=0} = \frac{C\text{-}s_{f0}}{C\text{-}c_{f0}} \cdot RI\text{-}c_{t=0} \quad \textbf{Eq. (6)}$$

where $C\text{-}s_{f0}$ and $C\text{-}c_{f0}$ (g/mL) are the initial concentration of maltodextrin in free water phase for the sample system and the control system. For this study, $C\text{-}c_{f0} = 0.05 g/mL$, whereas $C\text{-}s_{f0}$ varied with sample systems.

For a sample system, 12.5 mL 10% (w/v) maltodextrin stock solution was mixed with 12.5 mL starch dispersions. Depending on the mass and swelling of starch, the volume of free water phase (V_f, mL) was calculated as follows:

$$V_f = V_t - M_{st} \cdot (SP - 1) \quad \textbf{Eq. (7)}$$

V_t is the total volume of sample systems (= 25.0 mL), M_{st} is the dry mass of starch (2.00 g for native starch, 0.500 g for SS and 0 for the control); and SP is the swelling power determined from **3.2.2.4**. At time zero, the added maltodextrin (1.25 g) in a sample system is assumed to be completely dissolved in the free water phase. Hence, combined with **Eq. (7)**, the $C\text{-}s_{f0}$ was calculated using the following equation:

$$C\text{-}s_{f0} = \frac{1.25}{V_f} = \frac{1.25}{V_t - M_{st} \cdot (SP-1)} \quad \textbf{Eq. (8)}$$

Now, in combination of **Eq. (5)**, **Eq. (6)** and **Eq. (8)**, the full equation for the calculation of differential mass response, which represented the variations in the content distribution of MDC_f is shown below:

$$\Delta RI = \frac{25}{25 - M_{st} \cdot (SP-1)} \cdot RI\text{-}c_{t=0} - RI_{t=t_i} \quad \textbf{Eq. (9)}$$

3.2.2.13 Retention capacity of starch materials

To permit the direct comparisons of different starch materials regarding their capacity of retaining maltodextrin, it is meaningful to estimate the mass of each maltodextrin component retained in unit mass of starch granules ($mMDC_{ums}$). As the differential mass response (ΔRI)

reflected the variations in the concentration of MDC_f, the variations in the mass of MDC_f ($\Delta mMDC_f$) was correlated with ΔRI and V_f through the following equation:

$$\Delta mMDC_f \propto V_f \cdot \Delta RI \quad \textbf{Eq. (10)}$$

For this study, $\Delta mMDC_f$ was equivalent to the mass of maltodextrin component that was retained by all starch granules for an incubation system. By dividing **Eq. (10)** with the mass of starch, we could estimate $mMDC_{ums}$ or the retention capacity of a particular starch material as below:

$$mMDC_{ums} = \frac{\Delta mMDC_f}{M_{st}} \propto \frac{V_f}{M_{st}} \cdot \Delta RI \quad \textbf{Eq. (11)}$$

3.2.2.14 Statistical analysis

Measurements were conducted for 3 times. ANOVA was conducted using SPSS 17.0 with all comparisons conducted at a significance level of 95%.

3.3 Results and Discussion

3.3.1 Chemical composition of starch materials

Table 3-1. Chemical composition of starch materials

Starch type	Moisture content[1] (%)	Protein content[1] (%)	Total starch content[1] (%)	Apparent amylose content[2] (%)
AS	10.2 ± 0.2 C	1.2 ± 0.1 A	94.8 ± 3.4 A	N.D.[3]
CCS	8.2 ± 0.1 D	1.2 ± 0.0 A	94.7 ± 1.8 A	17.6 ± 1.5 B
WCS	10.9 ± 0.1 A	1.1 ± 0.0 A	95.0 ± 2.4 A	N.D.
NCS	10.5 ± 0.0 B	1.3 ± 0.0 A	95.1 ± 3.5 A	23.5 ± 2.4 A

Data expressed as means ± standard deviations (n = 3). The means in the same column with different letters are significantly different ($P < 0.05$).

[1]Data computed on dry basis.

[2]Data computed on starch basis.

[3]Non-detectable.

Chemical compositions of different starches are shown in **Table 3-1**. There was no significant difference ($P < 0.05$) in the starch and protein contents for the isolated starches (AS and CCS)

and commercial starches (WCS and NCS). The amylose contents for NCS and CCS were 23.5 % and 17.6 %, respectively, which were in accordance with the previous studies (Biliaderis et al., 1993; Peng and Yao, 2018; Singh et al., 2003). The AS material used in this study was waxy-type starch, showing non-detectable amount of amylose. The preparation of SS did not alter the chemical compositions, yielding similar starch and protein contents to their native counterparts (Data not shown).

3.3.2 Granular characteristics of native and swellable starch

3.3.2.1 Crystalline structure

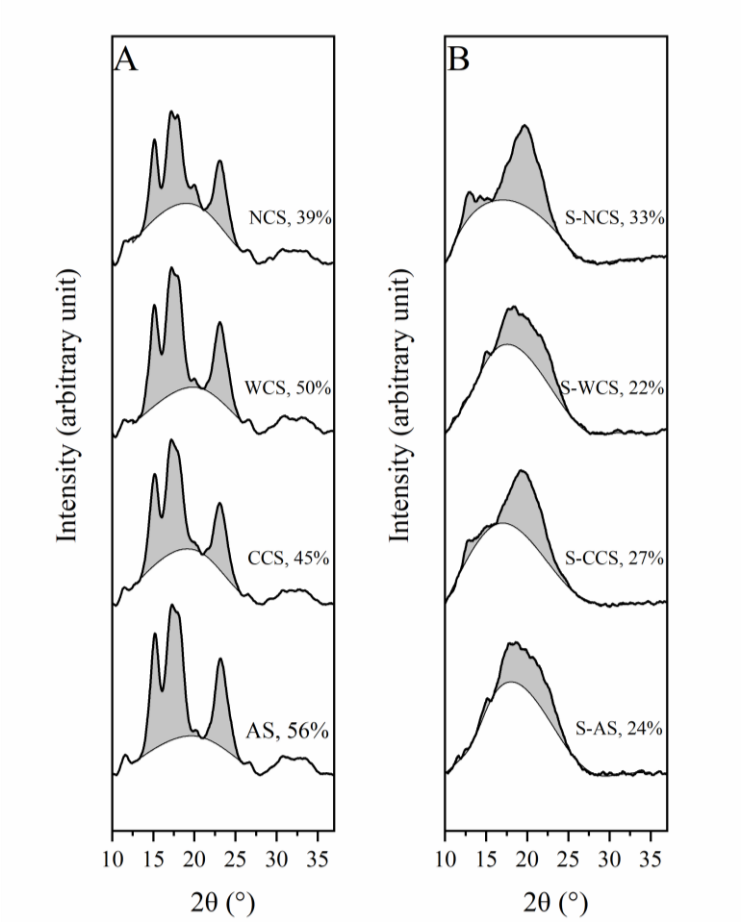

Figure 3-1. Wide-angle X-ray powder diffraction crystallograms of native starches **(A)** and swellable starches (SS)**(B)**. AS, CCS, WCS, and NCS represent native starches isolated from amaranth, cow cockle, waxy corn and normal corn. S-AS, S-CCS, S-WCS and S-NCS represent the SS prepared from AS, CCS and WCS, NCS. The shaded areas show the crystalline regions. The crystallinity (%) of each starch material is labeled.

The X-ray crystallograms of starch materials are shown in **Fig. 3-1**. All the native starches showed typical A-type crystalline pattern with reflections at 2θ values of 15°, 17°, 18°, 23°. In general, all the native starches possess high crystallinity (39-56%), which is in agreement with the previous studies (Peng and Yao, 2018; Stone and Lorenz, 1984). For SS, characteristic A-type crystalline response was almost lost except for some residual signals at 2θ value of 15° and 18°. A strong response was observed at 2θ value of 20° indicating the presence of V-type crystalline pattern (Zobel, 1988). Similar x-ray diffraction pattern has been reported since the ethanol used for the preparation of GCWS is a stabilizer to the V-type crystalline structure (Chen and Jane, 1994). The crystallinity of the SS materials for this study ranged from 22% to 27%.

3.3.2.2 Granular morphology

The granular morphology of native starches and SS in their dry powder forms are shown in **Fig. 3-2**. Typical small starch granules (< 2 μm) are observed for AS and CCS (**Fig. 3-2-1 and 3-2-3**), while large starch granules (2-20 μm) are observed for WCS and NCS (**Fig. 3-2-5 and 3-2-7)**. Similar to previous studies, surface pore and opening structures were visible for WCS and NCS granules (Huber and BeMiller, 2000).

The granular morphology for dry SS materials were apparently distinct from that of their native counterparts (Chen and Jane, 1994; Choi et al., 2017). SS exhibit wrinkled surfaces and irregular shapes, which was more evident with S-WCS and S-NCS (**Fig. 3-2-6 and 3-2-8**). While individual granules were mostly visible, the SS granules tended to agglomerate in large particles (10-50 μm), presumably related to ethanol precipitation and washing for the preparation procedure (Chen and Jane, 1994).

To observe SS granules in swelling state, SS dispersions at the concentration of 4% (w/v) were prepared using exactly the same procedure described in **3.2.2.7**. After the equilibrium dispersion, a series of dilution was done to make the SS concentration to 0.05% (w/v). The diluted SS dispersions dyed with iodine were subsequently observed under light microscopy (LM). The LM images of **Fig. 3-3** show the actual size and morphology of SS in water. It is observed that the majority granules of all SS materials are monodispersed in water, despite some agglomerates of SS granules present for S-AS and S-CCS. The images again confirm that the agglomerated particles of SS observed in **Fig. 3-2** are disintegrable after the dispersion procedure while preserving the integrity of SS granules. Compared to native starches, different level of swelling

was observed for SS materials: in general, the granules of S-AS and S-CCS maintained the spherical particulate shapes without visible change of granular size, whereas the granules of S-WCS and S-NCS were visually enlarged with irregular shapes. The result suggests that the contrasts of granular morphology between large-granule starch (NCS and WCS) and small-granule starch (AS and CCS) still exist even after swelling.

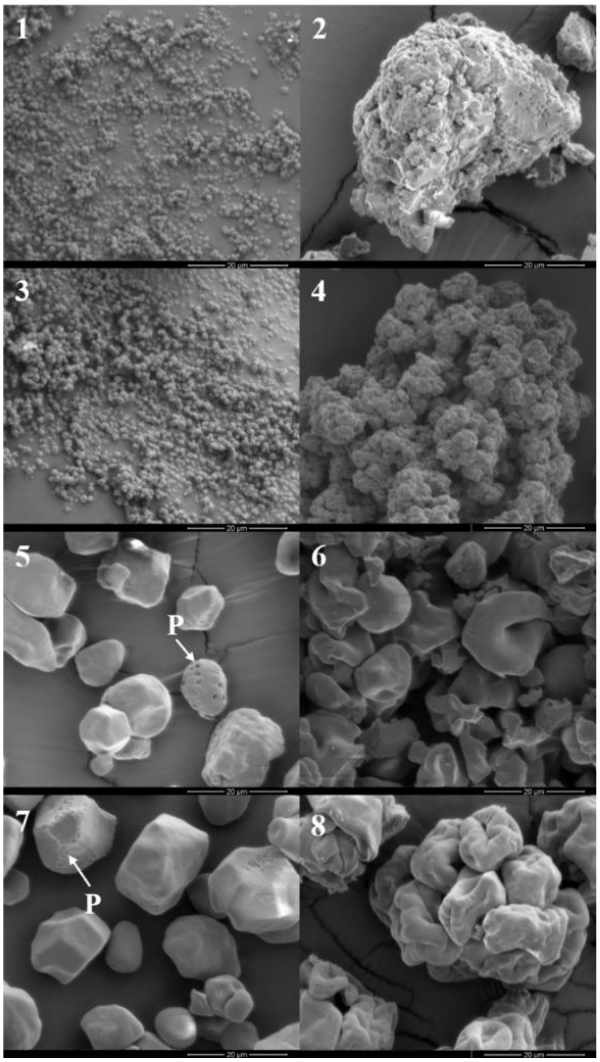

Figure 3-2. Scanning electron microscopy (SEM) images showing the morphology of native starch granules of amaranth **(1)**, cow cockle **(3)**, waxy corn **(5)**, normal corn **(7)**; and swellable starch granules of amaranth **(2)**, cow cockle **(4)**, waxy corn **(6)** and normal corn **(8)** in the dry powder forms. The surface pores and openings are labeled with arrows.

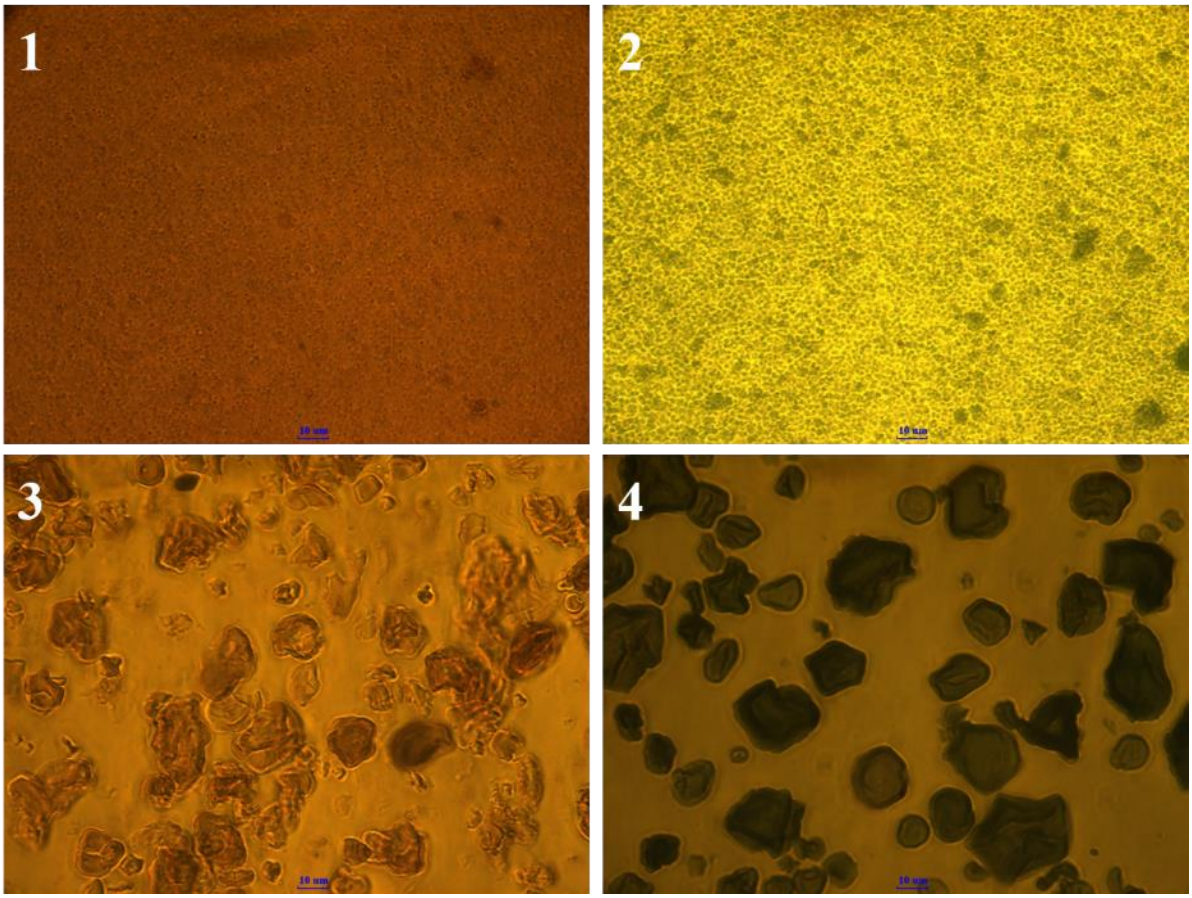

Figure 3-3. Light microscopy images showing the morphology of swellable starch granules of amaranth **(1)**, cow cockle **(2)**, waxy corn **(3)**, and normal corn **(4)** after equilibrium dispersion in water. The scale bar = 10 μm.

3.3.2.3 Swelling power and water-soluble index

Fig. 3-4 showed the SP and WSI values for different native and swellable starches. The SP values (**Figure 3-4A**) for native starches were low (2.7-3.3) and slightly varied with starch variety. In contrast, the SP for S-NCS, S-CCS, S-WCS and S-AS was 23.4, 16.7, 13.2 and 12.8, respectively. The WSI value is usually used to indicate the portion of starchy materials that leach from granules and are inseparable from the water phase through the centrifugation applied (Li and Yeh, 2001). The WSI values for different starch materials are shown in **Fig. 3-4B**. For native AS and CCS, the WSI values were not available as the sedimented starch granules, due to their very small sizes, were easily decanted with the supernatant. The WSI values for NCS and WCS were 1.2% and 1.6%, respectively. For SS materials, the WSI values of S-NCS, S-WCS, S-AS, and S-CCS were 17.8%, 12.9%, 16.0%, and 5.5%, respectively.

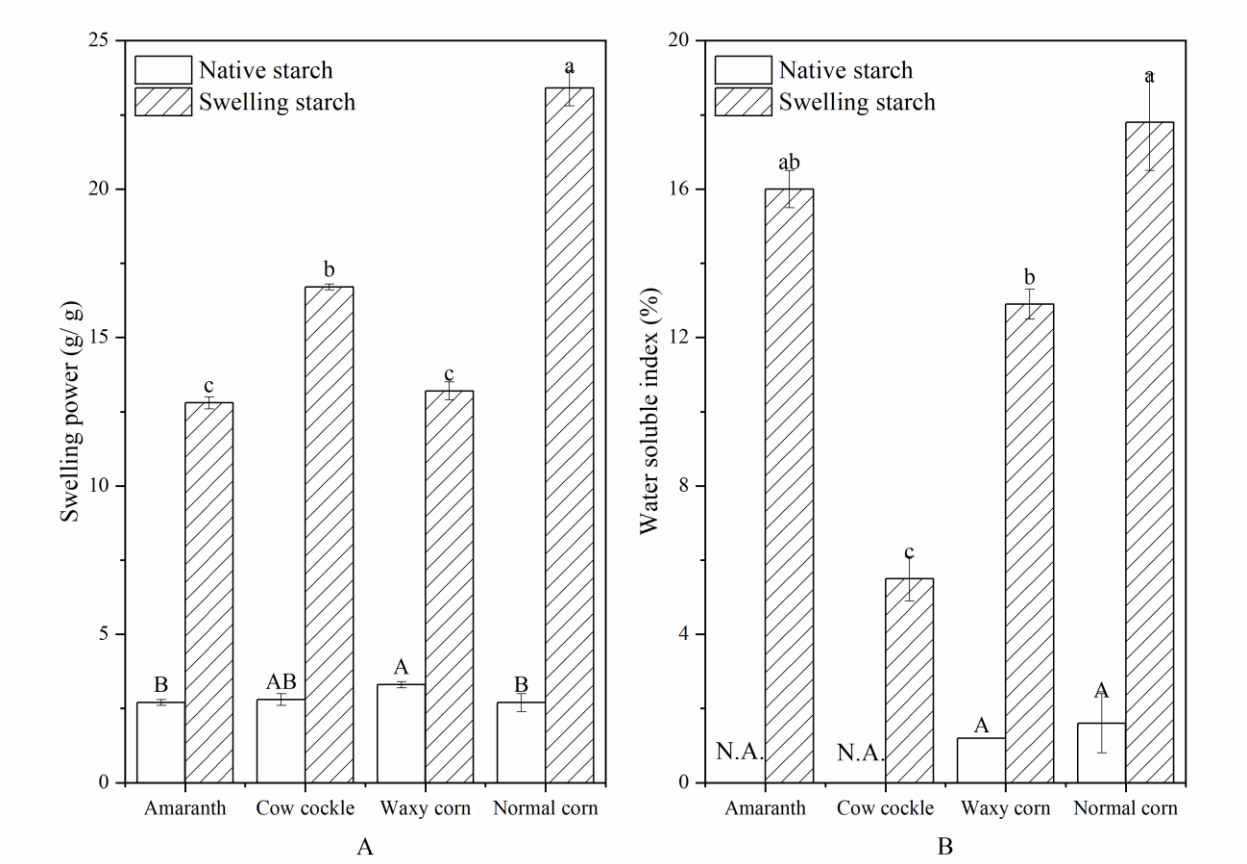

Figure 3-4. Swelling power **(A)** and water solubility index **(B)** of native and swellable starches. Bars indicate standard deviation. Columns in the same interior pattern that do not share a common superscript letter are significantly different ($P < 0.05$).

3.3.2.4 Particle size distribution

The particle size distributions of native and swellable starch materials in aqueous solution are shown in **Fig. 3-5**. The d_{43} and d_{32} values for AS were about 1.9 μm and 1.5 μm, respectively (**Fig. 3-5A**). The small difference between d_{43} and d_{32} values indicates the monomodal distribution of AS granules. In contrast, CCS exhibited smaller d_{43} value (1.8 μm) but similar d_{32} value (1.5 μm), also suggesting highly homogeneous distribution (**Fig. 3-5B**). Compared to d_{32}, d_{43} is more sensitive to large particles (Merkus, 2009). Therefore, the larger d_{43} value for AS is attributed to the higher proportion of large granules (>2 μm) that is observable in **Fig. 3-5A**. A big difference between d_{43} and d_{32} values were observed for WCS (18.1 μm v.s. 9.0 μm) and NCS (15.2 μm v.s. 7.8 μm). This result could suggest their bimodal distributions of starch granules (Jafari et al., 2006). The result is also confirmed with our observation in **Fig. 3-5C and**

3-5D, that is, two characteristic granule populations were identified with the size of 0.5-2.5 μm and 5-60 μm for WCS, and 0.45-2.5 μm and 5-35 μm for NCS.

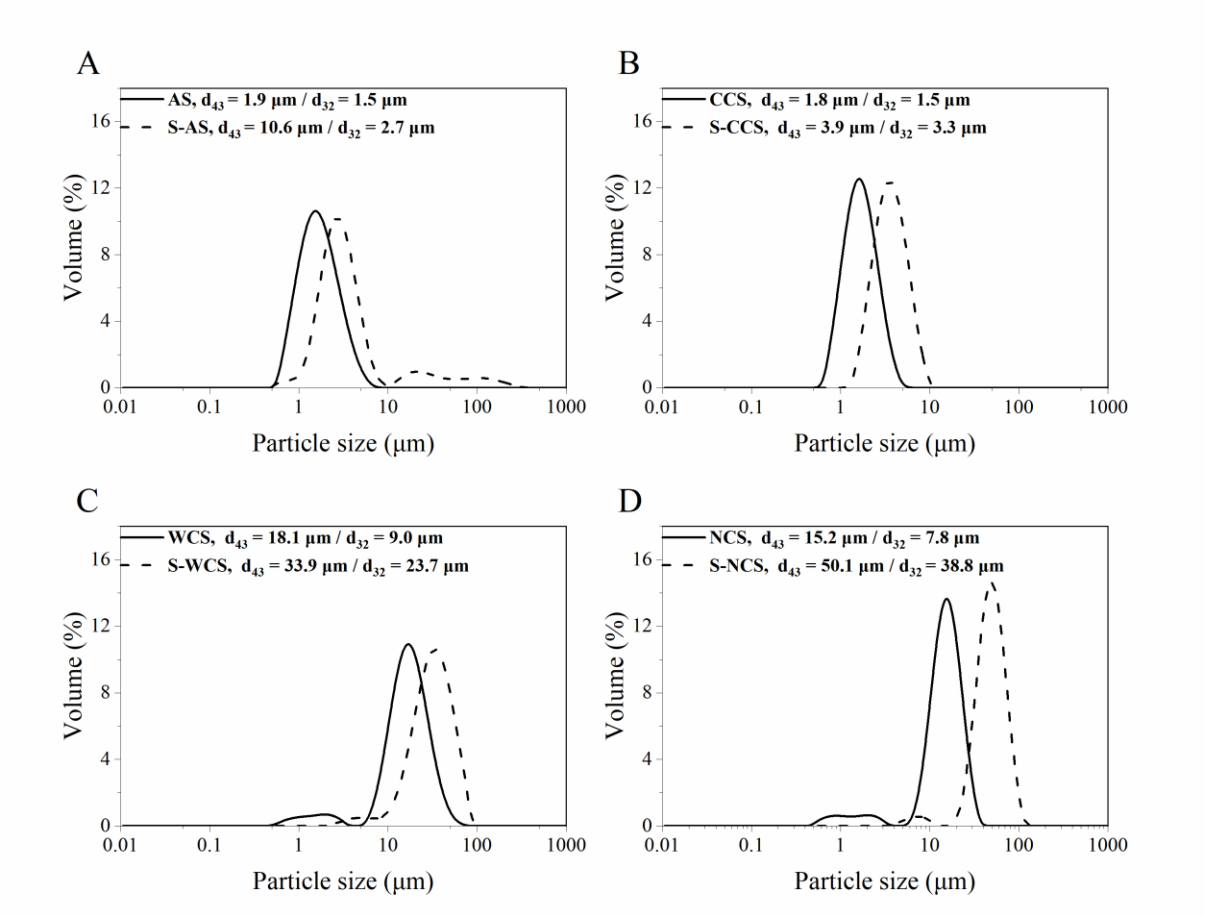

Figure 3-5. Volume-based particle size distribution of native and swellable starches (SS) in aqueous dispersion. AS, CCS, WCS, and NCS represent native starches isolated from amaranth, cow cockle, waxy corn and normal corn. S-AS, S-CCS, S-WCS and S-NCS represent the SS prepared from AS, CCS and WCS, NCS. The Sauter mean diameter (d_{32}) and volume mean diameter (d_{43}) for different samples are shown with the figure legends.

Except for S-AS, the d_{43} of S-CCS, S-WCS and S-NCS granules were 2.2, 1.8 and 3.3 times larger than their native counterparts indicating substantial swelling of SS in water after dispersion. The increase of granular size for different swellable starches can reasonably explain their various swelling power determined in **3.3.2.3**. Despite the monomodal size distribution of AS, multimodal particle size distribution was observed for S-AS yielding big deviation between d_{43} and d_{32} values (10.6 μm v.s. 2.7 μm). The granule population of S-AS with the size of ~10-200 μm should correspond to the presence of residual agglomerates. Moreover, the major granule

population of S-AS was ranging from 0.45 μm to10 μm with the d_{43} of 3.0 μm, essentially accounting for the lower SP of S-AS compared to other SS materials.

3.3.3 HPSEC profile of maltodextrin

Figure 3-6 shows the HPSEC profile of maltodextrin. Five peaks were identified at the retention time of 12.0, 19.3, 20.2, 20.7, and 21.2 min, corresponding to five glucan populations with modal degree of polymerization (DP) of 480, 7, 4, 2 and 1, respectively. The high DP population is believed to be the residual branching remnants survived from hydrolysis (Wang and Wang, 2000).

The chromatogram of maltodextrin can be arbitrarily divided into three regions: (1) the high DP region with the DP of 100 to 1225 DP, (2) the intermediate DP region of 12 to 100DP, and (3) the low DP region of 1 to 12 DP. The mass ratios of the three regions were 22%:43%:35%.

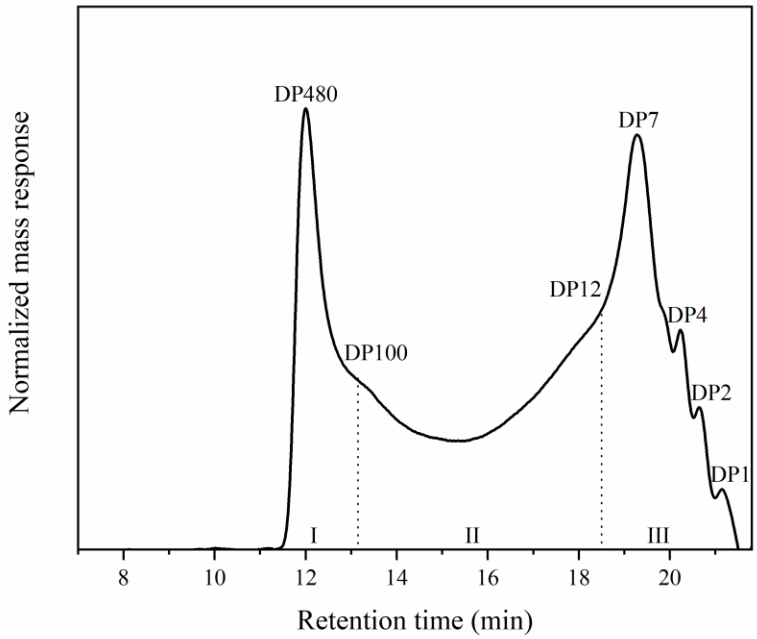

Figure 3-6. High performance-size exclusion chromatograms showing the chain length distribution of maltodextrin. Five characteristic composition of maltodextrin is identified from the chromatogram and labelled with their corresponding peak degree of polymerization (DP). The dashed lines separate the chromatogram to two sharp peak regions and a valley region, representing maltodextrin compositions with high (I, DP100-1225), intermediate (II, DP12-100) and low (III, DP 1-12) DPs.

3.3.4 Retention capacity of starch materials

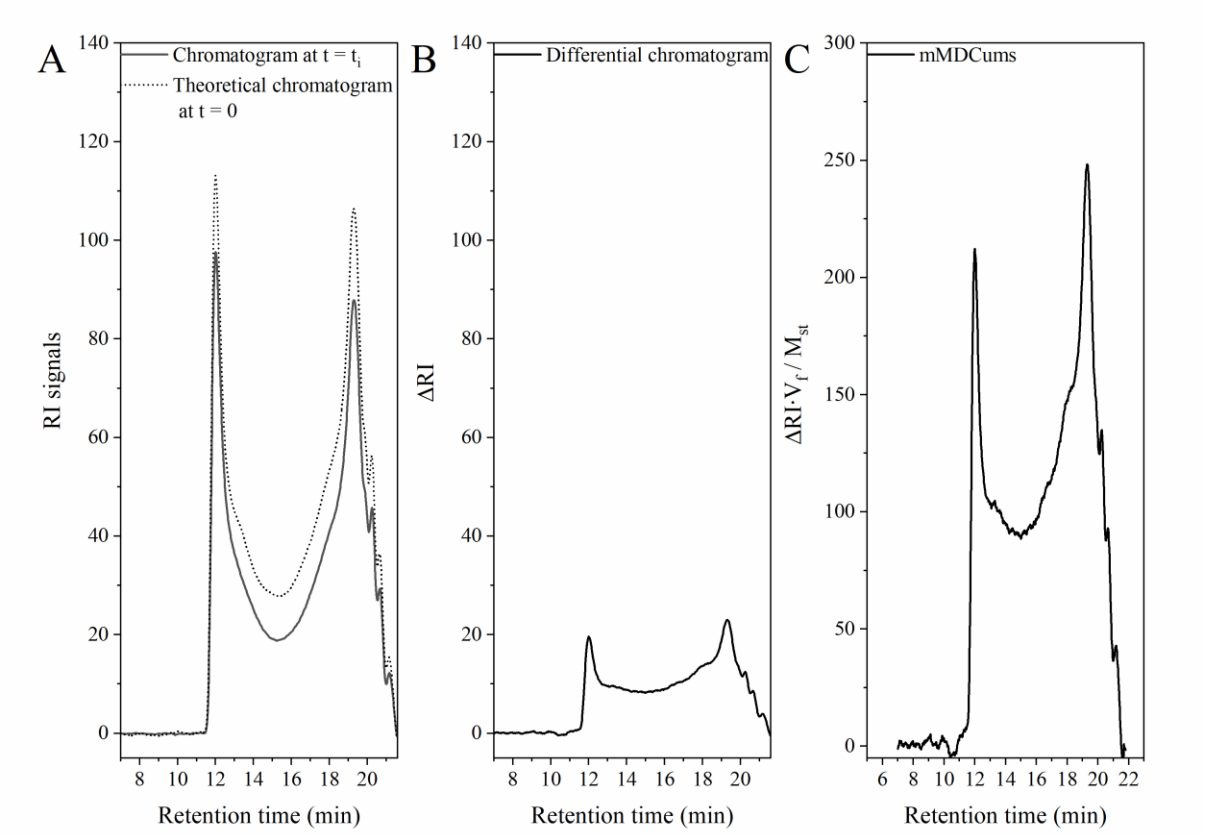

Figure 3-7. An example demonstrating the data processing procedures described in **3.2.2.12** and **3.2.2.13**. **A,** the dotted line represents the chromatogram corresponding to the theoretical concentration of maltodextrin components in the free water phase (MDC_f) at time zero; the solid line represents the chromatogram corresponding to the concentration of MDC_f at time I (t_i). **B**, the differential chromatogram is obtained by subtracting the chromatogram at $t = t_i$ (solid line in **A**) from the theoretical chromatogram at t = 0 (dotted line in **A**). **C**, the y-axis values of the plot is proportional to the mass of maltodextrin components retained in unit mass of starch.

Fig. 3-7 is to exemplify the actual data processing procedures given in **3.2.2.12** and **3.2.2.13**, through which the original chromatogram was transformed to represent the retention capacity of a unit mass of starch material. The chromatogram with dotted line of **Fig. 3-7A** corresponded to the theoretical RI response corresponding to the content of MDC_f at time zero. The chromatogram with solid line was experimentally obtained representing the content of MDC_f after a certain time of incubation. As is described in **Eq. (5)**, the differential chromatogram of **Fig. 3-7B** was obtained by subtracting the RI signals of the solid line from the RI signals of the dotted line. Based on **Eq. (11)**, every ΔRI signals in **Fig.3-7B** was multiplied with the volume of

free water (V_f), then divided by the mass of starch (M_{st}) to obtain the plot in **Fig 3-7C**, of which y-axis values ($\frac{V_f}{M_{st}} \cdot \Delta RI$) are proportional to the retention capacity of unit mass of starch. Accordingly, higher y-axis values mean stronger capacity of starch material in retaining maltodextrin components. In this study, we termed the plot in **Fig.3-7C** as 'retention plot' for convenience.

3.3.4.1 The effect of native starches

The retention plots for different native starches were compared in **Fig. 3-8.** It is observed that the retention plots are essentially analogous to the original HPSEC profile of maltodextrin (**Fig. 3-6**). The result suggests that all maltodextrin components with a broad range of DP values (1-1225 DP) can be retained by native starch granules. The retention plots with solid and dashed lines corresponded to the mass of maltodextrin retained in unit mass of starch after 5 min and 240 min of incubation, respectively. It is obvious that the retention capacity of native starch was enhanced with the incubation time, since the y-axis values for the dotted lines were in overall higher than those for the solid lines. Such time-dependent variations in y-axis values were more substantial in the intermediate and small DP regions (region II and region III, DP<100). A possible explanation is that intermediate and low DP maltodextrin components are able to diffuse from the free water phase to the internal volumes of starch granules, which takes time to reach equilibrium. This deduction was supported by our observation in **Fig.3-8** that the time-dependent variations in y-axis values was larger in region II than region III, as the diffusion of larger molecules (with higher DP) should be, to a higher extent, retarded by starch matrix. In contrast, the semi-crystalline granules of native starch appeared too dense to be permeable for high DP maltodextrin components (region I), since the maximum retention was almost instantly achieved after 5-min incubation possibly only through surface interaction.

The retention capacity also showed strong dependence with the variety of starch. First, the y-axis values of retention plots for amylose containing starches (CCS and NCS) were higher than those for waxy-type starches (AS and WCS), indicating higher retention capacity of amylose-containing starches. This can be attributed to the less ordered granular structure of amylose-containing starches (crystallinity = 39%-45%) compared to waxy-type starches (crystallinity = 50%-56%) (**Fig. 3-1A**). Second, granular morphology was also considered to contribute to the difference in retention plots. Larger difference in retention capacity was observed between the

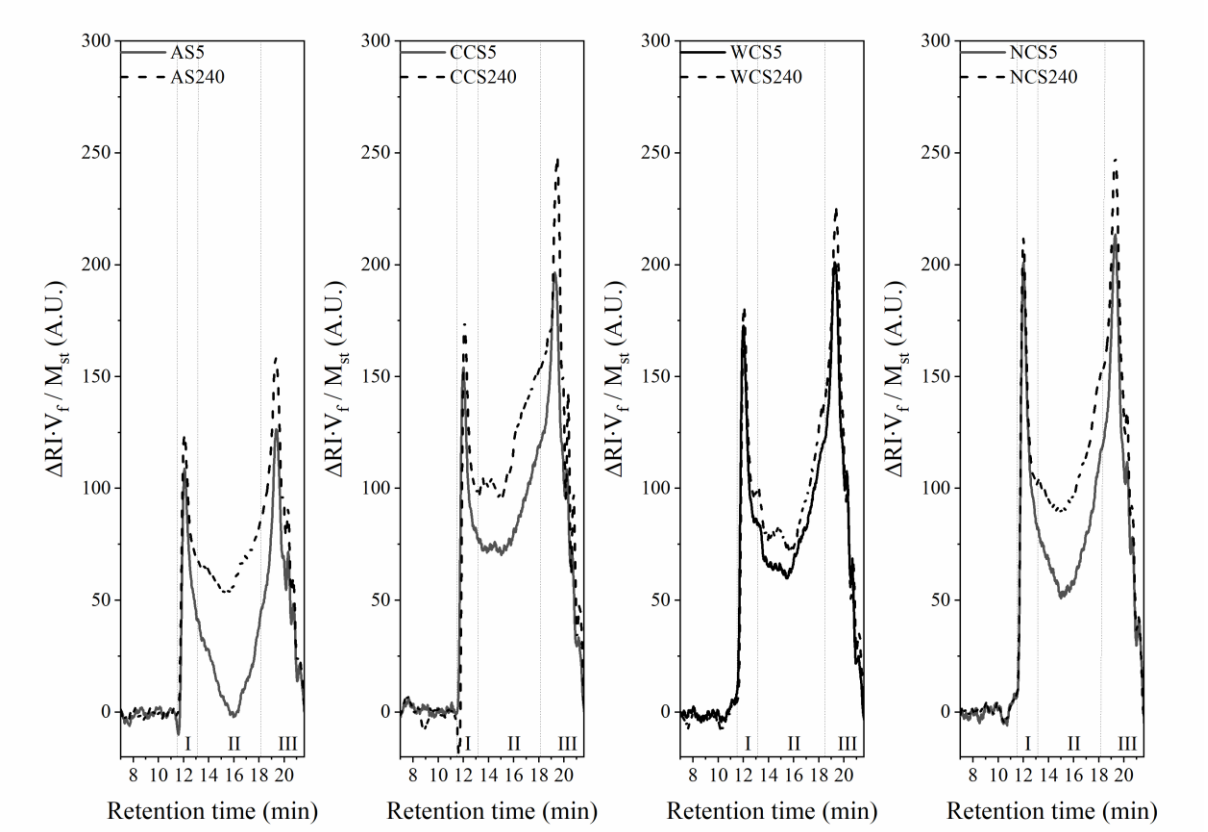

Figure 3-8. Retention capacity of native starches after 5-min incubation (solid lines) and after 240-min incubation (dashed lines). AS, amaranth starch; CCS, cow cockle starch; WCS, waxy corn starch; NCS, normal corn starch. The y-axis values are proportional to the mass of maltodextrin retained in unit mass of starch granules. The dotted lines are divided the retention plots to three regions (I, II and III), corresponding to the maltodextrin components with high (100-1225 DP), intermediate (12-100 DP) and low (1-12 DP) degree of polymerization.

pair of AS and CCS than the pair of WCS and NCS, despite the similar variation of crystallinity (~5%) in each pair. This is largely due to the presence of opening microstructures in WCS and NCS (**Fig. 3-2-5 and 3-2-7**), which may provide the by-pass route for the diffusion of maltodextrin. Third, the retention capacity of small-granule starches (AS and CCS) exhibited stronger dependence with the incubation time. This phenomenon is more substantial when comparing the retention plots between AS and WCS. For AS, the intermediate DP components were retained in AS granules at a very low level in the first 5-min incubation, but the retention increased substantially in the subsequent incubation. In contrast, the retention of intermediate DP components in WCS granules only increased a little after 5 minutes.

The total area under the retention plot could be integrated for the calculation of retention capacity of each starch. After 5-min incubation, the retention capacity (expressed as ‘mg

maltodextrin/g starch') for AS, CCS, WCS and NCS were 61, 150, 144, and 146. After 240-min incubation, the retention capacity (in mg maltodextrin/g starch) for AS, CCS, WCS, and NCS were 117, 192, 161 and 189. In sum, our results clearly suggest that (1) the retention of maltodextrin in native starch granules easily occur within several minutes of mixing which should not be overlooked in food processing, (2) the interaction between small molecules and starch granules is seriously affected by starch variety due to the diversified granular morphology of different starch.

3.3.4.2 The effect of swellable starches

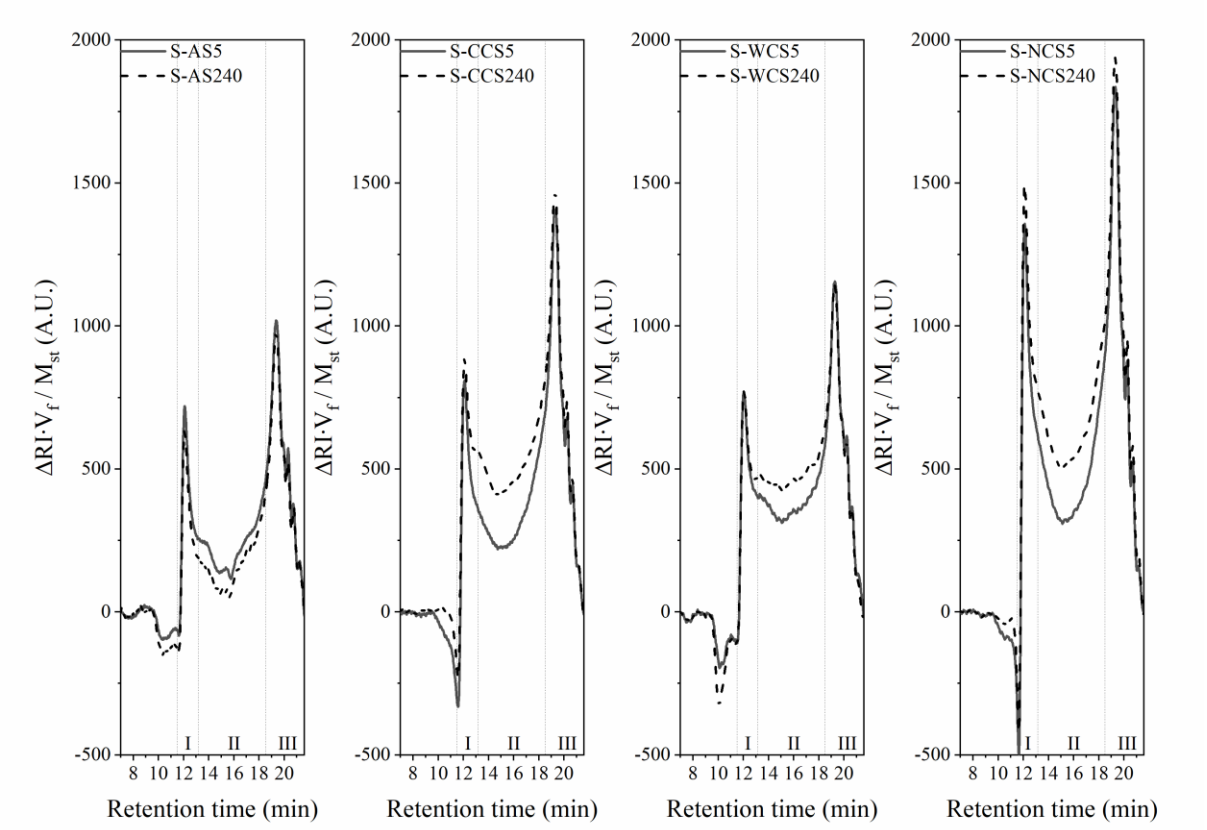

Figure 3-9. Retention capacity of swellable starches after 5-min incubation (solid lines) and after 240-min incubation (dashed lines). S-AS, S-CCS, S-WCS, and S-NCS represent swellable starches prepared from amaranth starch, cow cockle starch, waxy corn starch and normal corn starch. The y-axis values are proportional to the mass of maltodextrin retained in unit mass of starch granules. The dotted lines are divided the retention plots to three regions (I, II and III), corresponding to the maltodextrin components with high (100-1225 DP), intermediate (12-100 DP) and low (1-12 DP) degree of polymerization.

The retention plots of different swellable starches were compared in **Fig. 3-9.** The shape of the retention plots also indicated the substantial retention of maltodextrin components in high, intermediate and low DP regions. The y-axis values for the solid-lined and dash-lined plots were almost overlapping in the low DP and high DP regions (region I and III), indicating that the maximum retention achieved within the first 5-min incubation. As we have discussed earlier, SS granules were enlarged to 2-3 times their original sizes after dispersion yielding significantly swollen granules (~13-23 times their original volume). The swollen granular matrix may completely loss the retardation on the diffusion of low DP maltodextrin components and thus led to the maximum retention within 5 minutes. Conceivably, the interaction of the loose SS matrix and high DP maltodextrin components might not only be limited to the granular surfaces, but also expand towards the near-surface layers of the granules, which should give higher retentions. This is supported by the observation in **Fig. 3-9** that the y-axis values in the high DP region for SS materials (~700-1500) are ~ 6 times larger than those for native starches (~125-220). In contrast to the y-axis values in region I and III, time-dependent variations in y-axis values were preserved in region II, except for S-AS. This result indicates that the loose SS matrices of S-CCS, S-WCS and S-NCS still maintain the retardation on the diffusion of intermediate DP maltodextrin components.

Based on the y-axis values of retention plots, we were able to list SS materials in descending order of retention capacity as S-NCS>S-CCS>S-WCS>S-AS. Such order in the retention capacity is essentially in accordance with their SP values in **Fig. 3-4**. SS granules in dispersions can be treated as mesh-like particles with abundant interspaces filled with water. Maltodextrin components that are retained in SS granules, should mainly locate in these interspace volumes of mesh-like particulates. Hence, the retention capacity of SS granules should be presumably determined by the total volume of interspaces which is well measured by SP. More specifically, after 5-min incubation, the retention capacity (mg maltodextrin/g starch) for S-AS, S-CCS, S-WCS and S-NCS were 538, 719, 723 and 984. After 240-min incubation, the retention capacity (in mg maltodextrin/g starch) for S-AS, S-CCS, S-WCS, and S-NCS were 454, 926, 803 and 1206. In sum, SS materials exhibited considerably higher retention capacity compared to native starch granules due to swelling. In food production, native starch and maltodextrin were usually subject to heat treatments (e.g. baking, steaming, and sterilization) that may result in partial or complete swollen starch granules. The high retention capacity of swollen starch granules should

not be overlooked in practice, because such high extent of retention may seriously affect the sensory, physicochemical and processing quality of the products.

3.4 Conclusion

The retention of small molecules in native and swollen starch is a prevalent, fundamental and critical phenomenon that food industry may benefit from for the improvement of food quality. In this study, maltodextrin with broad DPs was used as the model. Native and swellable starches varying with amylose content, swelling power and granular morphology, were incubated with maltodextrin to simulate food formulation process involving the contact of raw and gelatinized starches with small molecules.

In summary, (1) both native and swollen starch matrices were active for the retention of small molecules, and different mechanisms (e.g. surface interaction or diffusion) were involved for small molecules with varying DP. (2) The instant (by 5 min of incubation) and equilibrium (by 240 min of incubation) retention capacity (mg maltodextrin/g starch) for native starch was ~ 60-150 and ~ 120-190, respectively. Granular morphology was the most impactful factor that dominated the retention capacity of native starches. (3) The instant and equilibrium retention capacity (mg maltodextrin/g starch) for SS starch was ~ 540-980 and ~ 450-1200, respectively. Swelling power was the most impactful factor that dominated the retention capacity of native starches. It is important and of high interest for food industry to elucidate the degree of interactions between starch and maltodextrin and the effects of starch variety on such interactions. Our study can support this area that facilitates selection of proper starches and processing conditions in the future targeting on the improvement of starchy food qualities.

CHAPTER 4. SUPRAMOLECULAR STRUCTURE OF PHYTOGLYCOGEN AND AMYLOPECTIN PROBED USING MOLECULAR ROTOR

4.1 Introduction

α-D-glucans are one of the most important kind of natural biomacromolecules that have broad applications in food, pharmaceutics and agriculture (Grossutti et al., 2017; Le Corre et al., 2010). Amylopectin (AP) and phytoglycogen (PG) are the major forms of branching α-D-glucans in nature and both are generated by the starch biosynthetic pathway (Hannah, 1997). Despite their similarities in chemical composition and biosysthesis, AP and PG exhibit quite distinct characteristics in crystallinity, stability, solubility and functionality. Such differences are solely associated with their unique molecular structures. For AP, the periodically clustering of branch points (the α-1,6-linkages) along with the elongation direction of AP renders repeating linear (crystallized) and branching (amorphous) regions (Tester et al., 2004; Thompson, 2000) . In contrast, branching occurs more regularly in PG than AP, leading to an amorphous and dendrimer-like structure of PG (Huang and Yao, 2011; Inouchi et al., 1987; Manners, 1989). More diversities in the glucan structure are found for APs from different botanic sources and mutants (Peng and Yao, 2018; Yao et al., 2004). Subtle structural difference in the size of branching clusters and the length and composition of unit branching chains may contribute to large variations in the physicochemical properties of AP (Jane et al., 1999). The primary functions of AP and PG, such as texturizing, encapsulation and controlled delivery, are relevant to the interactions among glucan chains (Tester et al., 2004) or among glucan chains and other components (Chen and Yao, 2017a, 2017b), which is also predominantly decided by their characteristic local branching nanostructures. From a broader perspective, the fundamental studies that can correlate the local nanostructure of AP and PG with their characteristic physicochemical properties are always welcome, because such scientific knowledge may not only highlight their unique functions, but also advance related research disciplines, such as the nanoengineering of biomacromolecules and the breeding of agricultural cultivars.

Current chromatographic and microscopic techniques often fail in the *in situ* measurement of local branching nanostructures of AP and PG through non-invasive approaches (Picton et al.,

2000; Szymońska and Krok, 2003; Tamjidi et al., 2013). This could be a significant technical hurdle in the utilization and innovation of AP and PG. Molecular rotor (MR) is a group of special fluorophores that is sensitive to the spatial restriction of local microenvironment (A. Haidekker and A. Theodorakis, 2007). In previous studies, MR has been used to monitor the viscosity changes in biofluid or live cells (Gulnov et al., 2016; Kuimova, 2012) and subtle structural changes of biopolymers (Hu et al., 2009). Thus, the fluorescent spectrometric methods based on MR might also be applicable to the measurement of local glucan structures.

MR generally consists of an electron donor (D), an electron acceptor (A), and a π-conjugation system (denoted as the D-π-A motif). After being excited, an MR has two distinct states: (1) a planar conformation termed as locally excited state (LE) and (2) a twisted conformation termed as twisted intramolecular charge transfer state (TICT) (Rettig, 1986). Each excited MR can lose energy (to "relax") through either the LE or TICT state depending on the level of local spatial restriction (Rettig, 1986). If the MR is in free space, it relaxes through TICT state by releasing heat without emitting any photon (noted as "dark MR"). If the MR is in a local environment with spatial restriction (i.e. steric hindrance), the transition from LE to TICT state is retarded and the relaxation is completed through the photon emission from LE state (noted as "bright MR"). For a given polymeric matrix, the overall spatial restriction governs the amount of MR molecules undergoing fluorescent emission. The quantum yield of MR, that is, the ratio of emitted photons to absorbed photons, precisely reflects the portion of "bright" MR (Haidekker et al., 2010) and thus the spatial restriction of certain polymeric matrix to this MR. Therefore, we hypothesized that MR can emit characteristic fluorescence in response to the unique spatial restriction exerted by the local glucan structures of AP and PG.

To test our hypothesis, we prepared four model glucans and characterized their structural attributes using well-established approaches. The fluorescent emission behaviors of MR in different model glucans were compared and discussed. More specifically, AP from waxy maize, PG from *sugary*-1 maize and their enzymatic derivatives were used to provide diversified local glucan structures with varying branching characteristics. 9-(2-carboxy-2-cyanovinyl)-julolidine (CCVJ), a hydrophilic molecular rotor, was used to probe the nanostructure of model glucans. This study may elucidate the interaction of MR and local glucan structure, which should support the development of novel, non-invasive and *in situ* measurement on AP and PG structure.

Results from this study may further benefit the utilization and innovation of natural α-D-glucans with superb functions in the future.

4.2 Materials and methods

4.2.1 Materials

Mutant maize *sugary-1* kernels were purchased from Burpee Co. (Warminster, PA). Waxy corn starch (WCS) was obtained from a commercial source. The molecular rotor, CCVJ with ≥ 97.0% purity, in the powdered form was purchased from Sigma. All chemical reagents used for the study were of analytical grade unless specified.

4.2.2 Methods

4.2.2.1 Preparation of phytoglycogen

500 g of *sugary-1* kernels were ground into grits and homogenized with a high-speed blender (Variable Speed Laboratory Blender, WARING Laboratory, CT) with 1.5 L deionized water. After passing through a 270-mesh sieve, the retentate was homogenized with another 1.5 L deionized water. All the permeates were combined and centrifuged at 10,000×g for 20 min. After removing the floating layer, the supernatant was collected and acidified (pH 4.6) with 0.1 M hydrogen chloride to allow protein precipitation, and centrifuged again (10,000 × g, 15 min). The supernatant fraction was then neutralized using 0.1 M sodium hydroxide, autoclaved (121°C, 50 min) and centrifuged (10,000 × g, 15 min) to remove residual proteins. PG component in the supernatant was precipitated using 3 volumes of ethanol. The PG solid obtained after centrifugation was resuspended in ethanol and centrifuged again. Purified PG solid (~150 g) was placed in a fume hood to remove residual ethanol and stored in a sealed glass jar before use.

4.2.2.2 Preparation of non-granular waxy corn starch

Non-granular (NG) waxy corn starch were prepared according to the method described by Huang and Yao (2011). Waxy corn starch (100 g, dry weight) was dispersed in 1.5 kg 90% (v/v) dimethyl sulfoxide (DMSO) and the mixture was heated in a boiling water bath with constant stirring until the suspension became clear. The suspension was then homogenized using a high-speed homogenizer (Waring Laboratory Science, Torrington, CT) for 4 min. Thereafter, 3

volumes of ethanol were added, and the mixture was then centrifuged at 6,500 × g for 15 min. The supernatants were discarded, and the pellets were washed by suspending them in 600 mL of 100% (v/v) ethanol followed by centrifugation (6,500 × g). The washing procedure was repeated three times with ethanol. The ethanol-washed precipitate was then dried in a ventilated air oven at 50°C for 24 h to remove residual ethanol. Dried NG starch was passed through a 50-mesh sieve and stored in a sealed glass jar. As the WCS was exclusively composed of amylopectin (≥ 98.6 wt%), the prepared material is used as AP in this study.

4.2.2.3 Preparation of β-limit dextrins

β-limit dextrins (BLD) of AP and PG were prepared according to Peng and Yao (2018). AP and PG (each about 40 g) were fully dispersed in 200 g of 90% (v/v) DMSO by heating in a boiling water bath for 10 min. The DMSO-dispersed sample was mixed with 1.4 kg sodium acetate (NaAc) buffer (20 mM, pH 6.0, preheated to 50°C), heated in a boiling-water bath for 20 min and cooled to 50°C. To each AP or PG dispersion, β-amylase (from Megazyme) was added at a dose of 710 U/ g glucan substrate. Thereafter, the reactants were incubated at 50°C with constant agitation. To reach the limit of β-amylolysis, the hydrolysate after 24 h β-amylolysis was heated in a boiling-water bath for 10 min and cooled to 50°C. To each hydrolysate, an additional dose of β-amylase was added. The β-amylolysis was carried out for another 24 h. To terminate β-amylolysis, the reactants were once again heated in a boiling-water bath for 10 min and cooled to room temperature. By the end of β-amylolysis, a 5 g aliquot of the hydrolysate was withdrawn for determining the degree of β-amylolysis. The rest of β-amylolysis hydrolysates were mixed with 3 volumes of 100% (v/v) ethanol, centrifuged (3000 × g, 10 min) and washed with ethanol for three times (300 mL each time). The precipitated BLDs were dried (50°C, 12 h) and passed through a 50-mesh sieve. The β-limit dextrin materials thus prepared were stored in sealed glass jars before use.

4.2.2.4 Degree of β-amylolysis

The net matter loss after the exhaustive β-amylolysis was used to indicate the degree of β-amylolysis. The hydrolysate aliquot (~5 g) withdrawn by the end of β-amylolysis was immediately added into 15 g 100% (v/v) ethanol and vortexed for 1 min. The mixtures were then centrifuged at 3000 × g for 10 min; the supernatants were separated and saved for maltose

quantification using high-performance size exclusion chromatography (HPSEC). A maltose standard curve was made using maltose standard solutions (0.1- 0.5 wt%). The degree of β-amylolysis was calculated using the following equation:

$$Degree\ of\ \beta\text{-}amylolysis\ (\%) = \frac{mass\ of\ free\ maltose\ in\ hydrolysate \times 0.9}{mass\ of\ PG\ or\ AP} \times\ 100\% \qquad \textbf{Eq. (1)}$$

4.2.2.5 Preparation of debranched AP, PG, and their BLDs

AP, PG and their BLDs (~5 mg each) were dispersed in 90% DMSO (125 μL) in a boiling-water bath for 10 min, then mixed with NaAc buffer 875 μL (20 mM, pH 4.75, 50°C). The mixture was heated again (95°C, 10 min), cooled to room temperature. To start the hydrolysis, 50 μL isoamylase (Megazyme, 5 U/ mL in NaAc buffer) was added to the mixture. The mixture was incubated in a shaking water bath at 37°C for 24 h and then heated in a boiling-water bath for 10 min to denature the enzyme. After cooling, 40 μL pullulanase solution (Megazyme, 7.2 U/ mL in NaAc buffer) was added and the mixture was incubated for another 24 h at 37°C and then heated for 10 min. The BLD was also debranched using the abovementioned procedure, except that 40 μL of an isoamylase solution (0.5 U/ mL) and a pullulanase solution (0.43 U/ mL) were used. Thereafter, a nitrogen gas blower (REACTI-THERM III, Thermo Scientific, US) was used to remove the moisture of each enzyme-treated mixture at room temperature and the volume of each sample was adjusted to 1.0 mL using 90% DMSO. After vortexing and centrifugation to remove insoluble materials, a 20 μL aliquot was injected in a HPSEC system.

4.2.2.6 High performance size exclusion chromatography

The HPSEC contained two connected Zorbax gel PSM 60-S columns (6.2 mm × 250 mm, Agilent Tech., Santa Clara, CA) equipped with a Waters 2414 refractive index (RI) detector (Waters, MA). DMSO was used as the mobile phase at the flow rate of 0.5 mL/min. Glucose, maltose, maltotriose, maltopentaose, maltoheptaose, and three pullulan standards (6 kDa, 50 kDa, 400 kDa) (Sigma, US) were used for column calibration. RI signals collected from the Millennium software (Waters, Milford, MA) were exported to an Excel spreadsheet, loaded to the Origin Pro 2018 software, and normalized on the basis of the total area. The structural parameters that describe branching pattern of starch, amylopectin, and BLD were obtained according to previous publications (Klucinec and Thompson, 1998; Yao et al., 2004; Yuan et al.,

1993). Models of BLD branching pattern were established using the method proposed by Yun and Matheson (1993).

4.2.2.7 Determination of weight-average molar mass, Z-average root mean square radius, and dispersed molecular density

HPSEC equipped with a multi-angle laser-light scattering detector and a reflective index detector (HPSEC-MALLS-RI) was used to determine the weight-average molar mass (M_W) and Z-average root mean square radius (R_Z) of AP, PG, and their BLDs. For the measurement, 1% (w/v) glucan dispersion was prepared using prefiltered deionized water (0.22-μm nylon syringe filters, Lab Depot, US). The dispersion was heated at 100 °C for 10 min to ensure the full solubilization of glucans. The HPSEC consists of an isocratic pump (515 HPLC, Waters), an injector (Model 7725i with a 20-μL sample loop, Rheodyne), a multi-angle laser-light scattering detector (MALLS, Dawn HELEOSII, Wyatt Technology) with a He-Ne Laser source (λ = 632.8 nm), and a refractive-index detector (RI, OptilabrEX, Wyatt Technology). Deionized water (pH 6.8, containing 0.02% sodium azide) was used as the mobile phase at a flow rate of 1.0 mL/min. Samples were filtered using 0.45-μm nylon syringe filters (Lab Depot, US) before injection. Each 50 μL filtrate was injected into the system and separated using two connected columns (PL Aquagel-OH 40 15 μm and 60 15 μm, Polymer Laboratories, Varian) with a guard column (PL Aquagel-OH Guard 10 μm, Polymer Laboratories, Varian). was used to determine The M_W and R_Z for the glucans were obtained from the first-order Berry model using the Astra software (Version 5.3.4.14, Wyatt Technology). The dn/ dc value of 0.146 was used for calculations. Dispersed molecular density (ρ) was calculated by:

$$\rho = \frac{M_w}{R_z^3} \qquad \textbf{Eq. (2)}$$

For each sample, triplicate injections were carried out.

4.2.2.8 Preparation of polysaccharide dispersions containing CCVJ

CCVJ powder (5 mg) was at first dissolved in 0.5 mL DMSO (HPLC grade, Fisher Chemical, US). 0.2 mL of the solution was further diluted with 3.8 mL phosphate buffer (5 mM, pH 7.0) to obtain the CCVJ stock solution (0.19 mM). The stock solution was stored in dark at room temperature before use.

AP, PG and their BLDs were accurately weighed to 15-mL capped polypropylene centrifuge tubes containing 9.9 mL phosphate buffer and 0.1 mL CCVJ stock solution. Polysaccharide dispersions in 5 mM phosphate buffer (pH 7.0, containing 1.9 μM CCVJ) were thus prepared at the diluted (0.1%-0.5%, w/v) and concentrated (2-10%, w/v) concentration ranges. The phosphate buffer with 1.9 μM CCVJ was used as the blank. To facilitate homogeneous dispersion, the mixtures in capped centrifuge tubes covered with aluminium foil were heated in a boiling water bath for 60 min with intermittent gentle converting in very 5 min. Our preliminary tests suggested that this heating treatment did not affect the stability of CCVJ, as the emission intensity for the blank solution was not significantly different before and after the heating ($P < 0.05$). After cooling to room temperature, the dispersions in tubes were spun at 200 rpm for 3 min to remove air bubbles. The liquid layer of polysaccharide dispersion was then subjected to viscosity and fluorescent spectra measurements.

4.2.2.9 Viscosity measurements

The viscosity of polysaccharide dispersion was conducted using a rheometer (ARG-2, TA Instruments, New Castle, DE). Dynamic viscosity tests were performed using the parallel plate geometry (4 cm diameter) at 25°C. Shear rate was increased logarithmically in a range of 1-1000 s^{-1}. The stress-shear rate plots corresponding to each sample was fitted with Newtonian and non-Newtonian (power law) fluid models ($\sigma = \eta_0 \cdot \dot{\gamma}^n$), where σ is shear stress, η_0 is flow consistency index, $\dot{\gamma}$ is shear rate, and n is flow behavior index). For this study, the flow behavior index (n) was used to determine the fluid type of glucan dispersions. To allow the comparison in glucan dispersions, the apparent viscosities at 50 s^{-1} were then calculated using the fitted shear stress (at 50 s^{-1}) divided by the shear rate (50 s^{-1}).

4.2.2.10 Fluorescent spectrometer

Fluorescence emission spectra and fluorescent intensity of CCVJ in polysaccharide or blank dispersions were measured using a Synergy H1 Hybrid Multi-mode Reader (BioTek, US) in the top-read mode (read height = 7 mm). Triplicate aliquots of dispersion (100-μL each) was pipetted to 96-well polypropylene microplates (Greiner Bio-one, Germany). The excitation wavelength and spectral bandwidth was set at 420 nm and 2 nm, respectively. The emission

spectra from 450 nm to 650 nm was measured with the spectra bandwidth of 2 nm. The system temperature throughout the tests was maintained at 25°C.

4.2.2.11 Statistical analysis

Measurements were conducted three times. ANOVA was conducted using SPSS Statistics 24.0 (IBM, US) with all comparisons conducted at a significance level of 95%.

4.3 Results and discussion

4.3.1 β-amylolysis of AP and PG

β-Amylase cleaves α-1,4-glycosidic linkages in every two glucopyranosyl units from the non-reducing end and yields maltose during β-amylolysis (Eglinton et al., 1998). At the limit of β-amylolysis, the hydrolysis stops close to the branching points (α-1,6-glycosydic linkage) leaving 2-3 residual glucopyranosyl units (the stubs) for individual hydrolyzed glucan chains (Yao et al., 2004). Hence, an exhaustive β-amylolysis results in the generation of BLDs composed of the internal chains, all branching points, and external stubs (**Figure 4-1**). In our study, the degree of β-amylolysis was 56% for AP and 42% for PG (**Table 4-1**). The result shows that PG was more resistant to β-amylolysis than AP ($P < 0.05$). Similar results were reported in previous studies, where the degree of beta-amylolysis for AP and PG were about 60% and 40%, respectively (Chen et al., 2015; Inouchi et al., 1987). The higher degree of beta-amylolysis for AP could be attributed to its high weight percentage of external chains in its cluster structure (Yun and Matheson, 1993), providing more abundant substrates for β-amylase.

4.3.2 Overall particulate features of AP, PG and their BLDs

AP, PG and their BLDs were used as the model glucan molecules for this study. Their basic structural parameters were shown in **Table 4-1**. Before β-amylolysis, the molecular weight (M_w) for AP (45.4 MDa) was nearly twice as that for PG (24.5 MDa), while the z-average size (R_z) for AP (83.6 nm) was ~3.4 times as that for PG (24.3 nm). The above M_w and R_z values for AP are smaller than the previously reported values of native (intact) AP moelcules (~650-8300 MDa and ~300-400 nm) (Yoo and Jane, 2002) but in accordance with the previous reports of our lab (~38-42 MDa and ~88-91 nm) (Chen et al., 2015; Huang and Yao, 2011). In this study, a shear

Table 4-1. Structural features of model polysaccharides[1]

Polysaccharide[2]	M_w (MDa)[3]	R_z (nm)[3]	ρ (g/mol·nm^3)[4]	Branch density (%)[5]	Maltose yield (%)
PG	24.5 ± 0.1^B	24.3 ± 0.2^C	1714.7 ± 41.5^A	8.2 ± 0.1^C	--
PG-BLD	13.4 ± 0.1^C	23.4 ± 1.2^C	1056.9 ± 150.3^B	13.0 ± 0.0^A	42.0 ± 0.1^B
AP	45.4 ± 0.8^A	83.6 ± 0.8^A	77.6 ± 1.5^C	5.4 ± 0.0^D	--
AP-BLD	24.8 ± 0.1^B	72.6 ± 0.6^B	65.0 ± 1.5^C	11.4 ± 0.1^B	56.1 ± 0.3^A

[1] Data expressed as means ± standard deviations (n = 3). The means in the same column with different letters are significantly different ($P < 0.05$)

[2] PG, phytoglycogen; PG-BLD, β-limit dextrin of PG; AP, amylopectin from waxy maize; AP-BLD, β-limit dextrin of amylopectin from waxy maize.

[3] M_w and R_z, weight-average molar mass and z-average root mean square radius obtained from first-order Berry model.

[4] ρ, dispersed molecular density using the following equation: $\rho = M_W / R_Z{}^3$.

[5] Branch density is calculated as the inverse number of number-average chain length ($\overline{CL_n}$). $\overline{CL_n} = \sum M_i \cdot N_i$, where M_i and N_i are the degree of polymerization at certain retention time and the corresponding molar response in the normalized molar-based chromatogram.

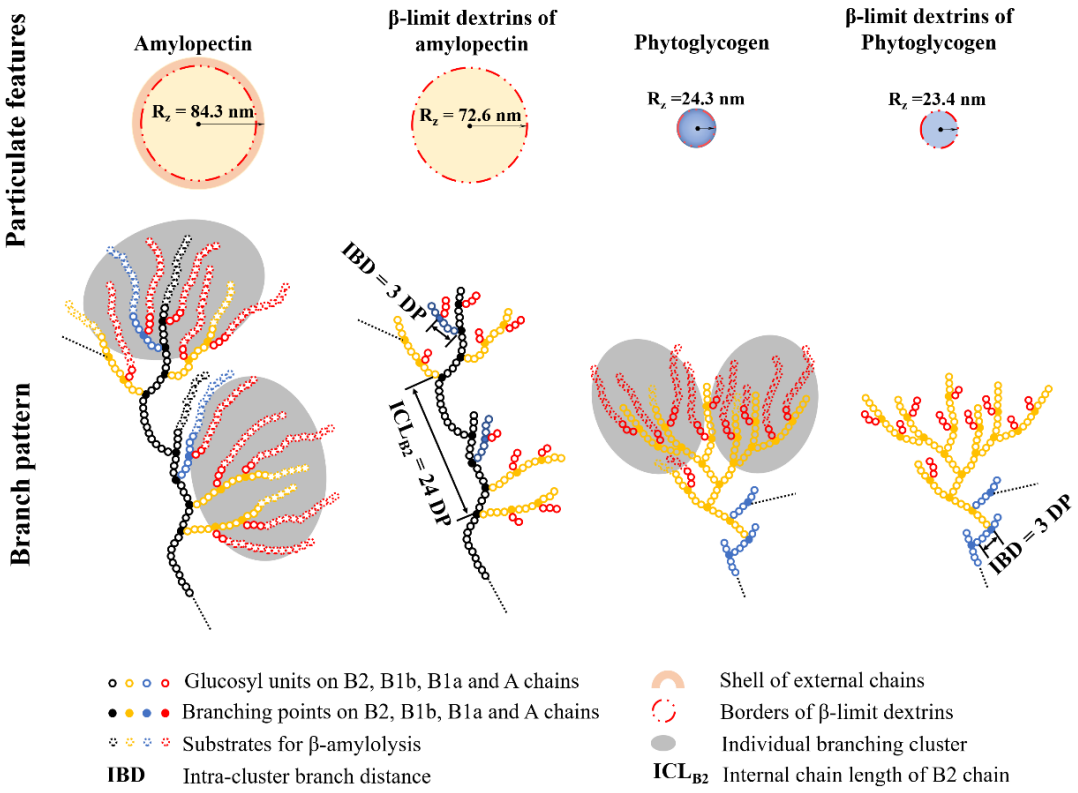

Figure 4-1. The schematics showing the particulate features and the cluster branching patterns of amylopectin, phytoglycogen and their β-limit dextrins.

treatment was applied to AP dispersion to increase the resistance of AP material to the shearing occurred in the HPSEC columns.

The dispersed molecular density (ρ) is a parameter that can reflect the compactness of glucan structure in hydration state (Wong et al., 2003). The molecular structure for hydrated PG was highly compact (ρ = 1714.7 g/mol·nm^3). Nevertheless, AP exhibited quite loose structure (ρ = 77.6 g/mol·nm^3) in aqueous solution, mainly due to the substantial swelling of AP after hydration (Li and Yeh, 2001). Our result suggests that hydrated AP is a uniformly swollen particulate (abundant in interspaces) whereas hydrated PG is a compact particulate.

After β-amylolysis, the M_w decreased by nearly 45% for both PG and AP This result is slightly different from the degree of β-amylolysis values determined in **4.3.1** (42% for PG and 56% for AP), possibly indicating that some shearing on AP in the HPSEC column might lead to an underestimating of the Mw for AP in **Table 4-1**. Meanwhile, the R_z for AP-BLD and PG-BLD decreased by ~11 nm and ~0.9 nm compared to AP and PG, respectively (**Fig. 4-1**). This result was in accordance with the previous observation (Chen et al., 2015). β-amylolysis only trimmed

external chains while preserving internal branches and chains. Our result indicates a layer of external chains with the thickness of ~ 11 nm exists at the outmost surface of AP particulate (**Fig. 4-1**). In contrast, such a thick layer of external chains was not found in PG. The ρ value for PG-BLD was 1056.9 g/mol·nm^3, showing significant reduction compared to that of native PG whereas still much greater than that for AP and AP-BLD (65-78 g/mol·nm^3) (**Table 4-1**). The result indicated that PG-BLD exhibits more open particulate nanostructures compared to PG, but AP-BLD maintained a loose and swollen particulate structure similar to AP.

4.3.3 Debranched AP and PG

Figure 4-2A and **4-2B** showed the normalized mass-based chain length distributions (CLD) of AP and PG, respectively. Two characteristic peaks are usually defined on the chromatogram according to previous studies: the peaks at the retention time of 11-13 min and 13-21.5 min correspond to the long linear chain population (i.e. amylose) and released linear segments from branched components, respectively (Chen et al., 2015; Klucinec and Thompson, 1998). As shown in **Figure 4-2A**, for either AP or PG, the branched components contributed about 99% of total mass.

The CL profile of AP and PG were highly different. Despite the similar large shoulder peak for AP and PG (peak at DP 12-15, and shoulder at DP 17-18), an additional peak at DP 35-36 existed for AP accounting for ~24% total mass. This observation supports the idea that the branching structure of PG is mainly built up by short glucan chains (Yun and Matheson, 1993), while AP molecules are composed of individual clusters connected with long, inter-cluster chains.

The molar-based CLDs for AP and PG were obtained through first dividing the RI responses (mass-based) by their corresponding molecular weights at each data point and then normalizing the chromatogram based on the total area (Peng and Yao, 2018) (**Fig. 4-2C** and **4-2D**). Based on the molar-based chromatograms, PG is comprised a greater number of short chains (< DP10) than AP (38% *v.s.* 5%).

The number-average chain length ($\overline{CL_n}$) of AP and PG were 12.2 and 18.5 DP, respectively. Branch density can be obtained as the inverse number of $\overline{CL_n}$ and shown in **Table 4-1** (Shin et al., 2008). The branch density for AP and PG was 5.4% and 8.2%, respectively, meaning that there were in average 5.4 and 8.2 branches per 100 DP in AP and PG.

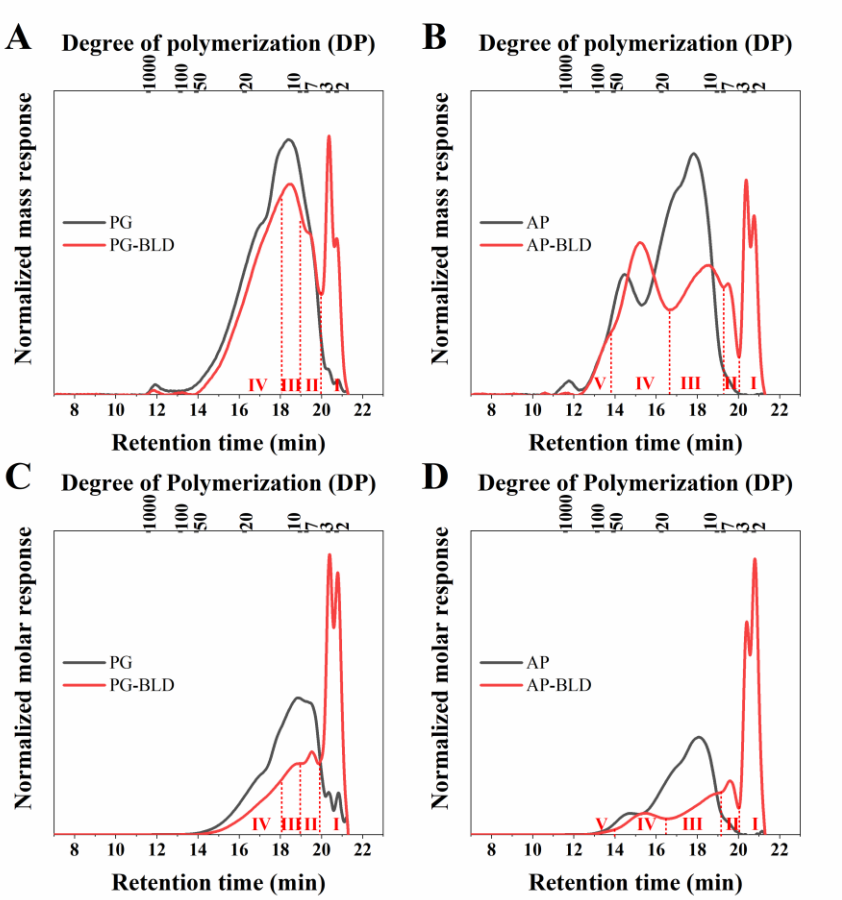

Figure 4-2. High performance-size exclusion chromatograms showing mass (**A** and **B**) and molar (**C** and **D**) based chain length distribution of phytoglycogen (PG), amylopectin (AP), β-limit dextrin of phytoglycogen (PG-BLD) and β-limit dextrin of amylopectin (AP-BLD), respectively. Red dotted lines classify the chromatograms of β-limit dextrins into characteristic regions. For the AP-BLD chromatogram: I, A chains (i.e. external chains attaching to other chains); II: B1a (short intra-cluster B chains), III: long intra-cluster B chains; IV: B2 chains (inter-cluster chains connecting two clusters), and V: B3 chains (inter-cluster chains connecting three clusters). For PG-BLD chromatogram: I, external chains without branching points; II, III and IV, internal chains containing 1, 2, and 3 or more branching points, respectively.

4.3.4 Branching pattern of AP and PG

The CL profiles of debranched BLDs were used to study the branching patterns of AP and PG. **Fig 4-2A** and **4-2B** (red lines) showed the normalized mass-based CL profiles of BLDs of AP and PG, respectively. The red dotted lines and Roman numerals defined the characteristic populations of chain constituents that formed the branching structures. For AP-BLD, the chains were differentiated and termed based on their primary role in constructing the clusters of AP: I,

Table 4-2. Parameters describing the structural characteristics β-limit dextrins

Polysaccharides[1]	Chain length of β-limit dextrins (DP[2])					IBD[3]	ICL_{B2}[4]	Relative number of chains (A: B1a: B1b: B2: B3)	ANBPC[5]
	I	II	III	IV	V				
AP-BLD	2/3	6	12	26	62	3	24	10 : 2.9 : 3.4 : 2.4 : 0.2	7
PG-BLD	2/3	6	10	14	N.D.[6]	3	N.D.[6]	10 : 3.3 : 6.2 : N.D.[6] : N.D.[6]	N.D.

[1] AP-BLD, β-limit dextrin of amylopectin from waxy maize; PG-BLD, β-limit dextrin of PG.

[2] Degree of polymerization.

[3] Intra-cluster branch distance.

[4] Internal chain length distance of B2 chains.

[5] Average number of branches per cluster.

[6] Non-determined.

the external A chains; II and III, intra-cluster B chains (B1a and B1b, respectively); and IV and V, inter-cluster B chains (B2 and B3, respectively) (Peng and Yao, 2018). The basic principles for defining these chains have been very well-established in previous studies (Peng and Yao, 2018; Yao et al., 2004; Yun and Matheson, 1993). It is evident that the branching cluster of AP comprises significant amount of inter-cluster B chains, accounting for 42% total mass of AP-BLD. The CL of inter-cluster chains for AP was DP 26 for B2 chain and DP 62 for B3 chains. In contrast, branches are not clustering but periodically presented in PG-BLD, which leads to the typical "branch-on-branch" pattern without the presence of 'cluster' (Nickels et al., 2016). Such structure allows us to differentiate the characteristic chains of PG-BLD based on the number of branching points they can carry, because all branches are homogeneously apart from each other in PG-BLD.

In the chromatogram of PG-BLD (**Fig. 4-2A**), the peak (DP6) nearest to the peaks of external chain stubs (DP2 and 3) should correspond to the internal chain containing only one branching point (IC_1). The average length of external stubs for both A and B chains was 2.5 DP (Yun and Matheson, 1993). Therefore, we obtained the average branch distance (~3 DP) for PG-BLD by subtracting the external stub (2.5 DP) and the branching point (1 DP) from the CL of the IC_1 chain (6 DP). Then we were able to calculate the CL of internal chains that carried 2, 3, 4, and 5 branching points, that is, DP 10, 14, 18, ad 22. Chains with the CL>DP22 only accounted for ~ 6% total mass of PG-BLD. On the other hand, the modal CL value for the chromatographic peak with the smallest retention time corresponded to DP 12 for PG-BLD. Hence, it is representative enough to define four chain populations in the chromatogram of BLD-PG: i, external chains without branching points; ii, iii and iv, internal chains containing 1, 2, and 3 or more branching points, respectively.

The molar-based CL profiles for AP-BLD and PG-BLD were shown in **Fig. 4-2C** and **4-2D**. The branch density for AP-BLD and PG-BLD was 11.4% and 13.0%, respectively (**Table 4-1**). The values were significantly greater than those of AP and PG due to the removal of linear segments through β-amylolysis. The CL and molar ratios of the characteristic chain populations defined above were determined in **Table 4-2**. These parameters were used to draw the schematic models showing the branch structure of AP, PG and their BLDs (**Fig. 4-1)**.

4.3.5 Concentration dependence of viscosity in AP, PG and their BLD dispersions

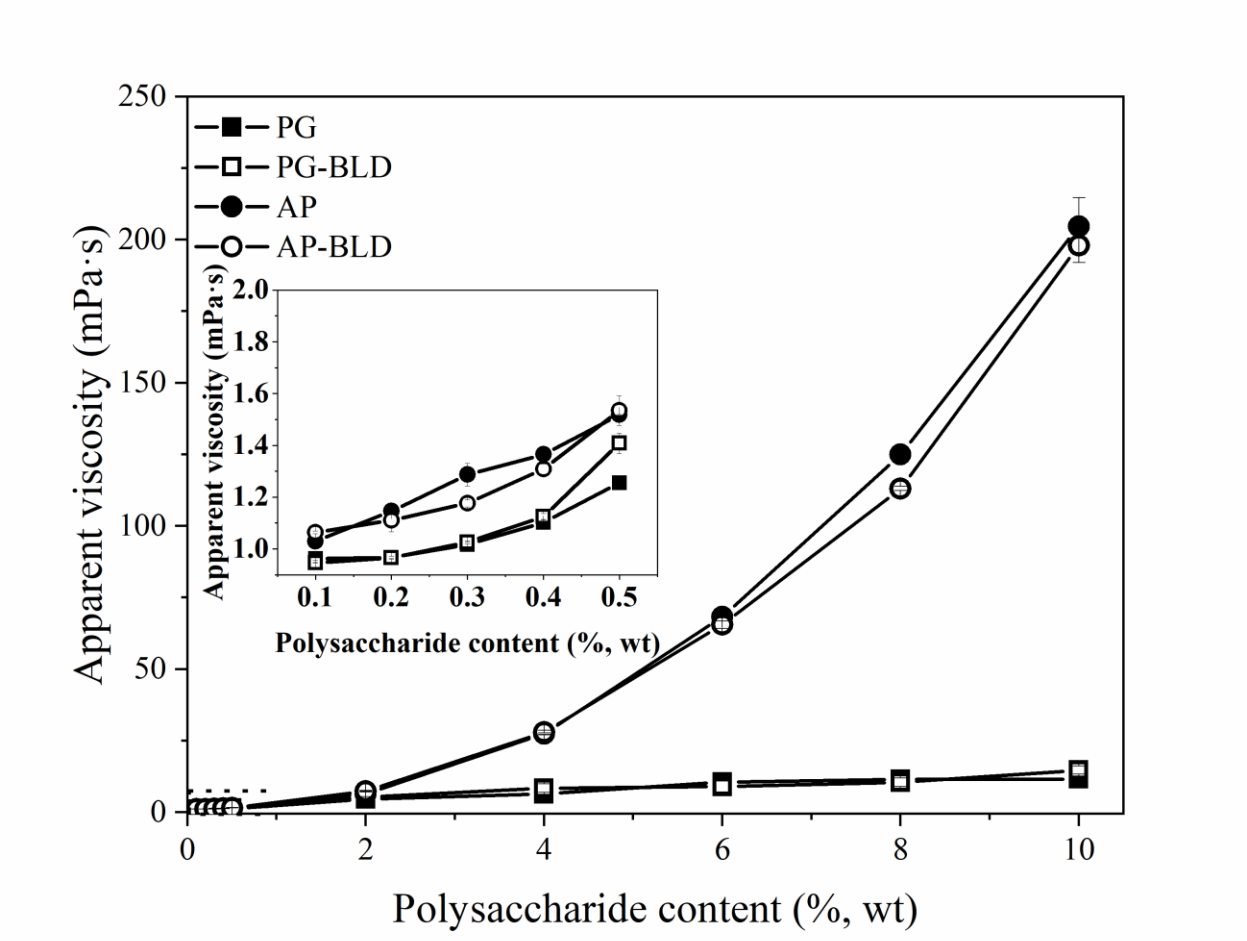

Figure 4-3. Apparent viscosity of polysaccharide dispersions as a function of glucan concentration. The Dynamic viscosity was measured at the shear rate of 1-1000 s^{-1}. The shear stress *v.s.* shear rate plot was fitted to the power law model ($R^2 = 0.99$) and the apparent viscosity at 50 s^{-1} was calculated based on fitted model. PG, phytoglycogen; PG-BLD, β-limit dextrins of phytoglycogen; AP, amylopectin; AP-BLD, β-limit dextrins of amylopectin. The embedded figure shows the apparent viscosities when polysaccharide content was 0.1- 0.5%.

The concentration dependence of viscosity reveals the interactions among dispered polymers (Morris et al., 1981). The apparent viscosities at 50 s^{-1} of model glucan dispersions in various concentrations (0.1-10 wt%) are shown in **Fig. 4-3**. All diluted glucan dispersions (0.1-0.5 wt%) exhibited Newtonian flow behavior with viscosities varying slightly in the range of 1.0-1.5 mPa·s. The viscosities are generally close to the viscosity of pure buffer (~1.0 mPa·s). The result suggests that the interactions among glucan particles are at the negligible level in the dilute concentration range, such that the flow behavior as well as viscosity are similar to pure water. In

general, the phyiscal entanglement of particles occur at 0.9 wt% for AP (Ring et al., 1987) and 25% for PG (Atkinson, 2015), which also indicates the absence of particle-particle interaction in 0.1-0.5 wt% glucan dispersions.

With the increase of mass content from 2 wt% to 10 wt%, dispersions showed different extents of shear-thining behavior ($n<1$) due to the presence of interactions among dispersed particles. Specifically, AP and AP-BLD dispersions showed the high flow behavior index of 0.84-0.98, sugguesting high resistance of inter-particulate interactions to shear. In this concentration range, interactions among individual AP and AP-BLD particles occurred due to their high swelling and chain flexibility. **Fig. 4-3** shows that, for AP and AP-BLD dispersions, the viscosity increased about 6 to 200 mPa·s with the increase of glucan concentration. In contrast, over this concentration range, PG and PG-BLD showed shear-thining flow behaviors but with much lower flow behavior index (0.3-0.6) and apparent viscosity (below 15 mPa·s), suggesting the high-density, low-swelling nature of phytoglycogen nanoparticles.

4.3.6 Fluorescent emission spectra

To test our hypothesis of using CCVJ to probe local glucan structure, the fluorescent emission of CCVJ in model glucan dispersions (0.1-10 wt% AP, PG and their BLDs) and glycerol solutions (0-80 wt%) were compared. The emission spectra of CCVJ in different dispersions or solutions are shown in **Figure 4-4**. The peak emission wavelength (λ_{max}) was labelled with dash lines.

As shown in **Fig. 4-4**, the emission spectra of AP, PG and their BLDs (λ_{max} = 492- 494 nm) are slightly blue-shifted compared to the spectra of glycerol and pure buffer (λ_{max} = 498- 500 nm). For starch, similar blue-shifting trend (495-500 nm for glycerol and pure buffer, and 490 nm for starch) was also reported by Gulnov et al. (2016a). CCVJ emits blue-shifted fluorescence in less polar microenvironment (Haidekker et al., 2005) and the microenvironment of amylopectin clusters is less polar than water and comparable to ethylene glycol (de Miranda et al., 2007). A previous study has shown that the λ_{max} of CCVJ in ethylene glycol was around 490 nm (A. Haidekker and A. Theodorakis, 2007). As no significant difference in λ_{max} is observed among model glucans, it is reasonable to consider that the model glucans used in this study provided similar and less polar microenvironment for CCVJ molecules.

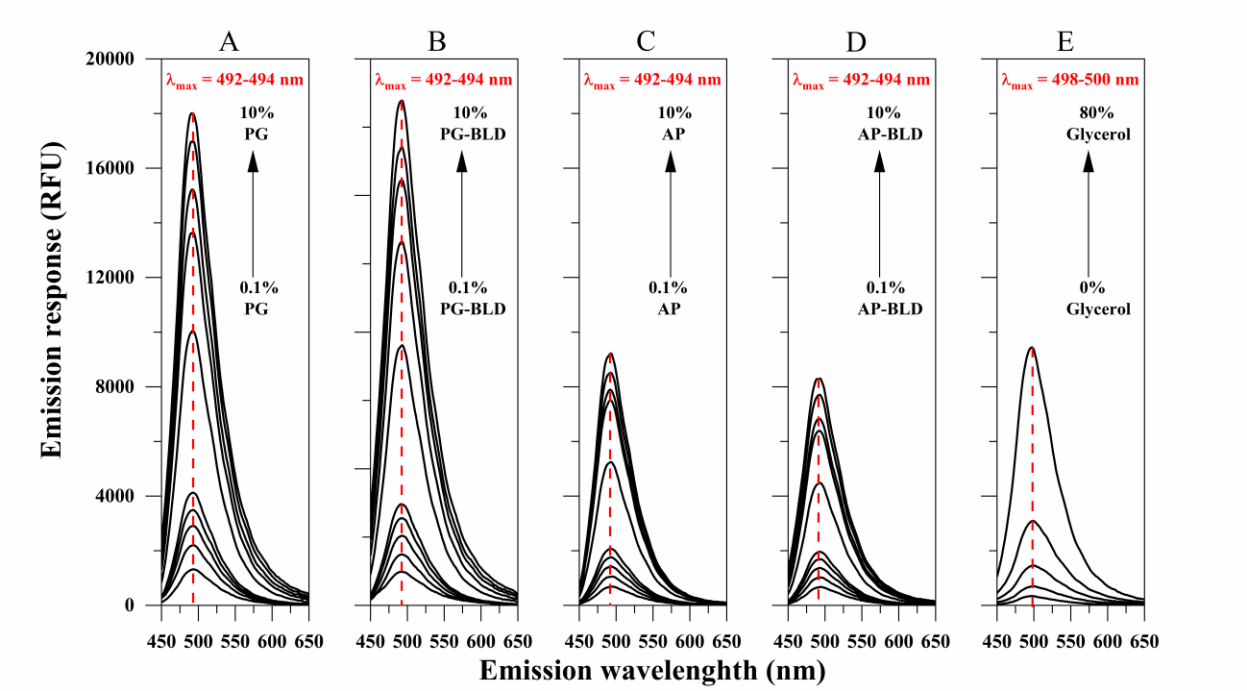

Figure 4-4. Fluorescent emission spectra of CCVJ in phytoglycogen (**A**), β-limit dextrins of phytoglycogen (**B**), amylopectin (**C**), β-limit dextrins of amylopectin (**D**) and glycerol (**E**) dispersions. The mass contents for polysaccharide dispersions and glycerol solutions are 0.1-10% and 0- 80%, respectively. Red dash lines indicate the peak emission wavelength (λ_{max}). The λ_{max} for each sample is shown on the top of the figure. RFU, relative fluorescence unit.

As is shown in **Fig. 4-4**, the emission intensity of CCVJ is affected by the concentration and structure of the glucan in the dispersion. In general, CCVJ emitted much stronger fluorescence in PG and PG-BLD dispersions (1200-18,000 RFU) than in AP and AP-BLD dispersions (850-10,000 RFU) at all concentration levels. Compared to glucans, CCVJ was less sensitive to the concentration of glycerol. The emission intensity was about 880 RFU for 20% glycerol that was comparable with 0.1% AP or AP-BLD. As the polarity does not affect the emission intensity of CCVJ, the fluorescent emission should be exclusively related to spatial restriction (Haidekker et al., 2005). In other words, 20% glycerol and 0.1% AP or AP-BLD yielded a similar level of spatial restriction.

4.3.7 Relations of CCVJ fluorescence and dispersion viscosity

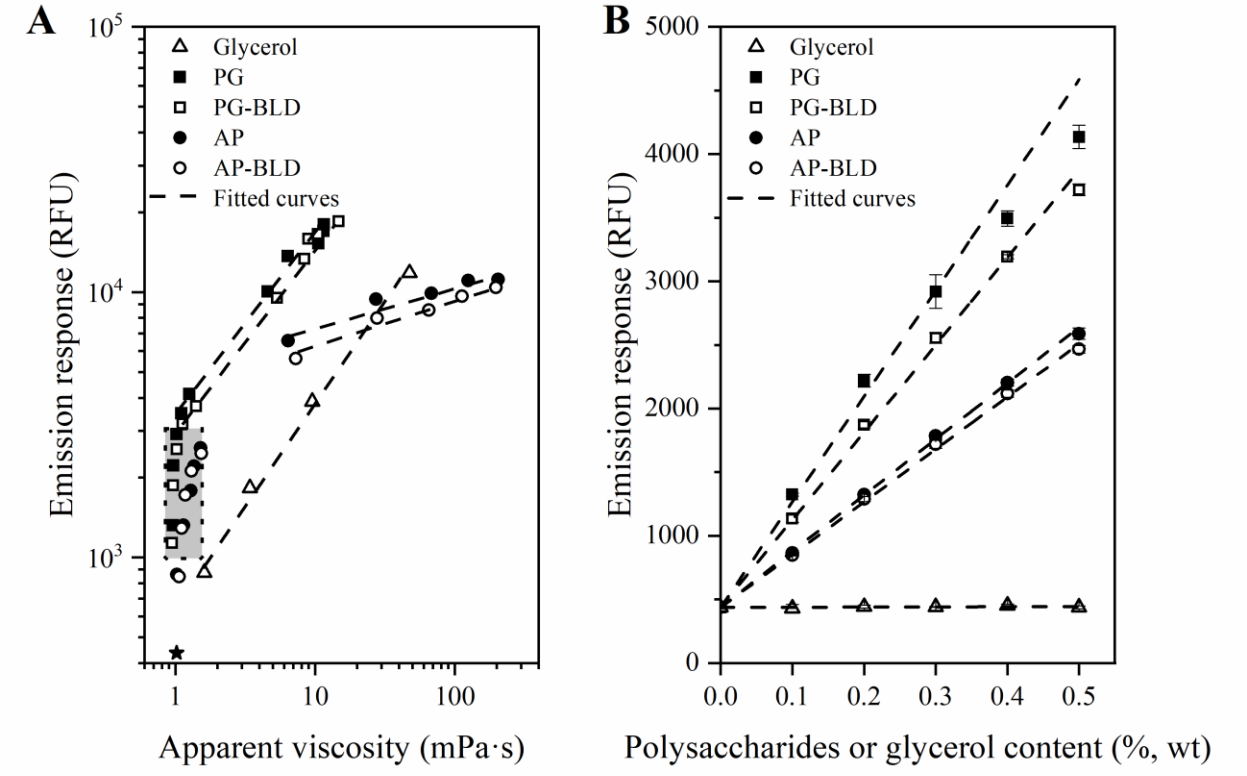

Figure 4-5. **A:** Emission intensity of CCVJ in glucan dispersions and glycerol solutions as a function of the apparent viscosity at 50 s^{-1} in a double-logarithmic scale. Data points in the linear region were fitted for the double-logarithmic linear model. The fitted curves were shown in dash lines. The shaded region highlighted the data points that deviated from the fitting model. **B**: Emission intensity of CCVJ in diluted glucan dispersions and glycerol solutions as a function of mass content. The dashed lines in **B** with the same intercept of 437 RFU (corresponding to the emission intensity of CCVJ in blank buffer) showed the linear relationship of emission intensity and mass content. PG, PG-BLD, AP and AP-BLD represents phytoglycogen, β-limit dextrins of phytoglycogen, amylopectin, and β-limit dextrins of amylopectin, respectively.

An early study indicated the double-logarithmic linear relationship between fluid viscosity and MR fluorescence response (Förster and Hoffmann, 1971). Based on this finding, MR such as CCVJ has been studied as a marker to determine fluid viscosity (Haidekker et al., 2010). In this study, the fluorescent emission response (I) and the apparent viscosity (η) for glucan dispersions and glycerol solutions were plotted in the double-logarithmic coordinate (**Figure 4-5A**).

As shown in **Fig. 4-5A**, β-amylolysis led to limited differences in the emission-viscosity (*I- η)* relationships, as the plots for the original glucan and its BLD counterpart are almost overlapping. Nevertheless, the type of dispersed particle or solute predominantly decides the mode of *I- η* relation. The *I- η* curve for glycerol kept good linearity in wide viscosity range (1- 40 mPa·s), whereas the curves for model glucans exhibited non-linear shape (labelled with shaded background in **Fig. 4-5A**) in the low viscosity region of 1- 1.5 mPa·s. Such observation is also reported by a previous study of using CCVJ to probe the viscosity of dextrins (Akers and Haidekker, 2004). The non-linear range is believed to be associated with the incorporation of MR in polymeric microstructure at diluted state resulting in strong mass-dependent instead of viscosity-dependent fluorescence.

For further comparison, data points within the linear regions of *I- η* plots were fitted to the double-logarithmic linear model developed by Förster and Hoffmann (R^2 = 0.93- 1.00) (Förster and Hoffmann, 1971):

$$Log\ I = A \cdot Log\ \eta + C \qquad \textbf{Eq. (5)}$$

The fitting parameters were shown in **Table 4-3**. The slope for the glycerol solution, PG and PG-BLD dispersions were similar ranging from 0.67 to 0.76, respectively. This result is in accordance with the reports of previous studies (0.67-0.75), as the slope is considered as a MR and solvent-dependent constant (Gulnov et al., 2016; Haidekker et al., 2010; Loutfy and Arnold, 1982). Despite the similar slope, the intercept for PG and PG-BLD dispersions (3.47-3.54) was higher than that for glycerol solution (2.82) resulting in stronger fluorescence at the same viscosity. This is because at the same bulk viscosity, bulk viscosity induces similar level of microfriction for the MR in bulk water phase, however, PG and PG-BLD possessing intra-particulate volumes should exert additional spatial restriction to the MR in particulate phase, which thus leads to stronger overall fluorescence compared to glycerol. In contrast, as the slopes for PG, PG-BLD and glycerol dispersions were highly comparable, suggesting that the increase of bulk viscosity enhances the microfriction for MR with a similar efficiency for PG, PG-BLD and glycerol dispersions. This phenomenon could be attributed to the rigid spherical nature of PG, PG-BLD and glycerol molecules, which fundamentally obeys the assumptions for the correlation between microfriction and bulk viscosity in the Förster and Hoffmann equation.

Table 4-3. Parameters for the fitted curves showing the double-logarithmic linear relationship of fluorescence emission and dispersion viscosity[1]

Sample[2]	Fitted viscosity range (mPa·s)	Slope (A)	Intercept (C)	r-square
Glycerol solution	1.6 - 47.4	0.76 ± 0.04	2.82 ± 0.04	0.995
PG	1.1 – 11.6	0.67 ± 0.03	3.54 ± 0.02	0.988
PG-BLD	1.1 – 14.7	0.72 ± 0.02	3.47 ± 0.02	0.993
AP	6.4 – 204.7	0.15 ± 0.02	3.72 ± 0.04	0.932
AP-BLD	7.3 – 198.0	0.18 ± 0.02	3.61 ± 0.03	0.969

[1] The double-logarithmic model: Log $I = A$ Log $\eta + C$, where I and η are the emission intensity and apparent viscosity at 50 $s^{-1,}$ respectively; A and C are the slope and intercept of the fitted curve.

The slope for the AP and AP-BLD curves was 0.15 and 0.18, which substantially deviated from the slopes for PG, PG-BLD and glycerol curves. The small slope values for AP and AP-BLD curves can be attributed to their high capacities of swelling. Completely hydrated AP or AP-BLD can uptake more than 20-fold mass of water in dispersions (Lei and Gao, 2014; Tester and Morrison, 1991). In the fitted concentration range (2-10 wt%), bulk viscosity was seriously affected by physical entanglements of dispersed AP and AP-BLD particles. However, such inter-particulate entanglements cannot be effectively probed in the form of microfriction for MR since major portion of MR should be entrapped in the intra-particulate volumes of swollen particles. As a result, the swelling of AP and AP-BLD may yield less available MR in the bulk buffer phase for the probing of microfriction altered by inter-particulate entanglements, which thus gives less sensitive fluorescence in response to the bulk viscosity change (the small slopes). This explanation is also supported by our data in **Table 4-3**, of which the slopes for BLDs (0.72 for PG-BLD and 0.18 for AP-BLD) were slightly larger than those for their native counterparts (0.67 for PG and 0.15 for AP), since BLDs usually exhibited reduced capacity of swelling. The intercept for AP and AP-BLD curves was 3.72 and 3.61, which was essentially comparable to that for PG and PG-BLD but larger than that for glycerol. The result again confirms that particulate structures can induce additional spatial restriction to MR.

4.3.8 Relation of CCVJ fluorescence and the intra-particulate structure of glucan

In diluted concentration range (0.1- 0.5 wt%), individual glucan particulates are spatially separated and surrounded by the solvent. In this circumstance, the fluorescence intensity of CCVJ was attributed to: (1) the viscosity-related restriction to the motions of molecules at the locations not occupied by individual particulates, and (2) the glucan structure-related restrictions at locations inside or closely associated with individual glucan particulates. For diluted glucan dispersions, comparable viscosities were observed at different glucan concentrations, and therefore the viscosity-related fluorescence would remain constant at different concentrations. As glucan concentration increased, the change of fluorescence intensity should correlate with the increase of spatial restriction associated with the glucan structure, and such an increase can be used to characterize glucan structure.

Table 4-4. Parameters for the fitted curves showing the linear relationship of fluorescence emission and mass content in the initial linear region[1]

Sample	Initial linear region for fitting (%, wt)	Initial slope (k)	r-square
Glycerol	0-0.5%	13.9 ± 4.6	0.999
PG	0-0.3%	8299.5 ± 292.7	0.996
PG-BLD	0-0.5%	6880.0 ± 67.5	1.000
AP	0-0.5%	4409.6 ± 29.7	0.999
AP-BLD	0-0.5%	4140.7 ± 35.8	1.000

[1] The linear model: $I = k\,W + C_0$, where I and W are the emission intensity and mass content, respectively; k is the slope of the initial linear region. C_0 is the intercept fixed to 437 corresponding to the emission intensity in blank buffer.

[2] PG, BLDPG, AP and BLDAP represents phytoglycogen, β-limit dextrins of phytoglycogen, amylopectin, and β-limit dextrins of amylopectin, respectively.

In **Figure 4-5B**, the fluorescence intensity of CCVJ *vs.* solute concentration was plotted for diluted glucan dispersions and glycerol solutions (0.1- 0.5 wt%). For glycerol solutions, the fluorescent emission of CCVJ remained essentially the same as that of the blank (437 RFU). However, substantial increases of fluorescence intensity with concentration were observed for

diluted model glucan dispersions. The linear regression results labeled on **Figure 4-5B** showed that for glucan dispersions at 0-0.5% range the fluorescence intensity-concentration relationship was essentially linear. Specifically, the trendline slopes of PG and PG-BLD were much greater than those of AP and AP-BLD (**Table 4-4**).

4.3.9. Impact of glucan supramolecular structure on CCVJ fluorescence intensity

Figure 4-6 shows the modeling of the three-dimensional branching structure comprising one B chain and two A chains (Chem3D 16.0, PerkinElmer, US). In a hydrated form, glucan chains display a single-helical conformation due to hydrogen bonding among individual glucopyranosyl units (Whistler and Daniel, 1984). As shown in the model, the external portion of an A chain forms a helix that contains a central cavity (indicated with orange circles in **Fig. 4-6**). The cavity of single-helical glucan chain, which has a diameter of 5.0-5.4 Å (Hinkle and Zobel, 1968; Immel and Lichtenthaler, 2000), is usually spacious enough to host small molecules with hydrocarbon chains (e.g. fatty acids) (Putseys et al., 2010). The diameter of a CCVJ molecule (with structure indicated in yellow) is 7 Å (Gulnov et al., 2016). Hence, such cavities can hardly accommodate CCVJ molecules.

A recent study reported that CCVJ can be retained by the cavity of β- and γ- rather than α-cyclodextrin, and the diameters of central cavity for α- , β-, and γ- cyclodextrins are 5.7, 7, and 9Å, respectively (Gavvala et al., 2015). Conceivably, the size of the nano-pockets needs to be 7Å or higher to accommodate CCVJ molecules.

The B chain and the stubs of A chains (labelled with green rectangles) exhibits more stretching helical conformations that surrounds a nanosized pockets (labelled with the yellow dotted line) around each branch point. A single glucosyl unit is about 8.6 Å (Lourvanij, 1995); formed with about 3 glucosyl units, the diameter of the nano-pockets should be around 2-3 nm, which is sufficient to host a CCVJ molecule. **Fig. 4-6-5 and 4-6-6** show a CCVJ molecule tightly fits in a nano-pocket with considerable spatial restriction.

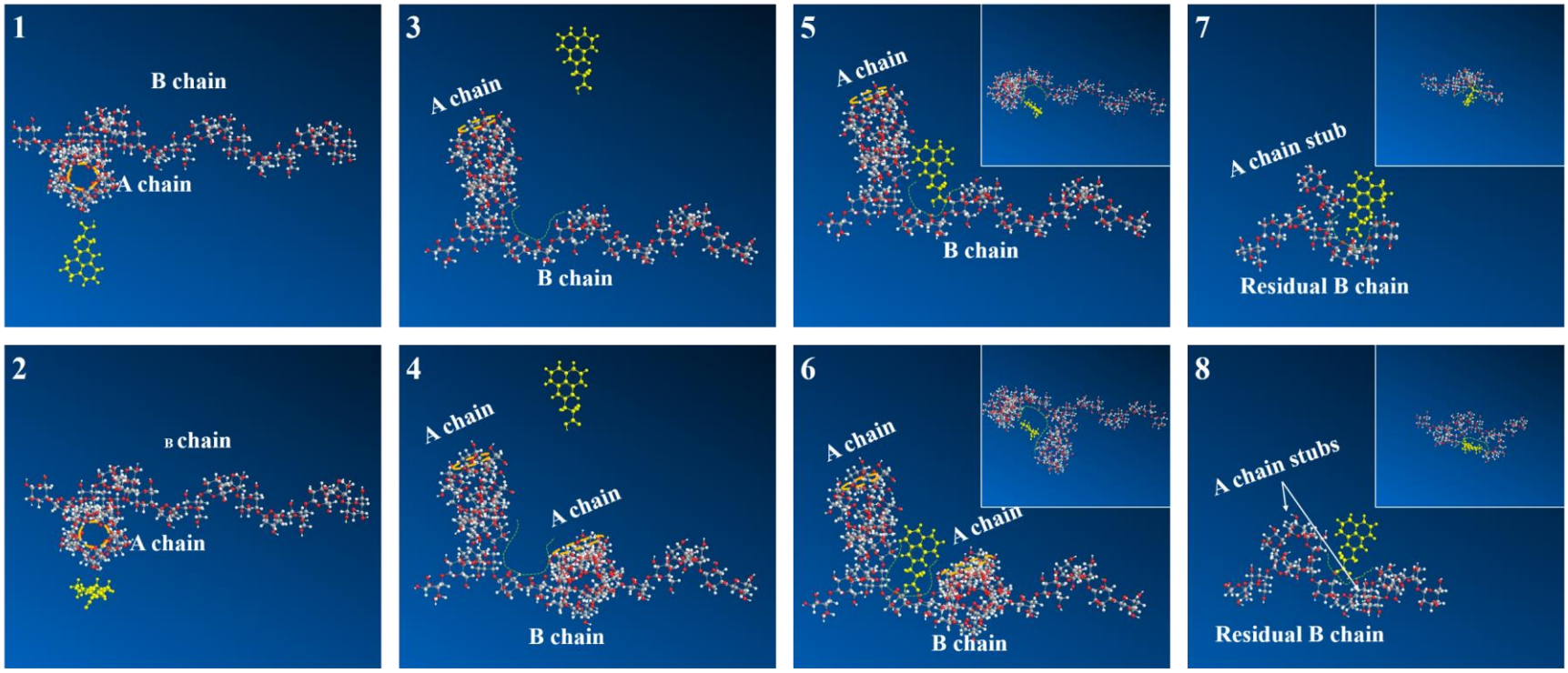

Figure 4-6. A three-dimensional model showing the interaction between CCVJ and the nano-pocket at the branching points of glucans. A segment of B chain (12 DP) and one (**1, 2, 3, 5** and **7**) or two (**4, 6** and **8**) full A chains (each12 DP) are included to show the local structure in the vicinity of branching points of amylopectin and phytoglycogen. The embedded images show the structures from the top view. Under room temperature, external linear segments of hydrated glucans form single-helical structure stabilized through hydrogen bonding. There are about 3 glucosyl units between two adjacent branching points. The CCVJ molecule is shown in yellow. **1-2**: the size comparison between the central cavity of external chain single-helix (orange circles) and CCVJ. **3-4**: a CCVJ molecule not associated with the glucan structure, thus subjected to negligible spatial restriction. **5-6**: a CCVJ molecule entrapped in the nano-pocket (defined using dotted border) formed at the branch point of native glucans. For **5**, the branching region of B chain and the A chain form a relative open nanopocket. For **6**, the branching region of B chain and the neighboring A chains form a relative complete nanopocket. **7-8**: a CCVJ molecule entrapped in the nano-pocket (defined using dotted border) formed at the branch point of β-limit dextrins. The branching region of B chain and the A chain stub form a more opening nanopocket in **7** than in **8**.

Based on the modeling, we consider that the concentration-related fluorescence intensity for glucan dispersions (**Fig. 4-5B**) is governed by the abundance of nano-pockets formed either at the branch point (**Fig. 4-6-5** and **4-6-7**) or among two neighboring external segments (**Fig. 4-6-6** and **4-6-8**).

In this study, the branch density is used to indicate the abundance of branch points. The branch density can be calculated using **Equation (6)**.

$$n_b = \left(\frac{m}{M_w}\right) \times \left(\frac{M_w}{16200}\right) \times Branch\ density = \left(\frac{m}{16200}\right) \times Branch\ density \qquad \textbf{Eq. (6)}$$

Where, n_b is the molar number of branch points per liter of glucan dispersion, and m (in g/L), M_w (in Da) and 16200 represent the mass content of glucan dispersion, molecular weight of glucan, and the total molecular weight of 100 glucosyl units, respectively.

The characteristic spatial restriction of nano-pocket is estimated using **Equation (7)**:

$$\mathrm{EG}_b = \frac{\mathrm{dEM}}{\mathrm{dn}_b} = \frac{dEM}{d\left(\left(\frac{m}{16200}\right) \times BD\right)} = \frac{16200}{BD} \cdot \frac{dEM}{dm} = \frac{16200}{BD} \cdot EG_m \qquad \textbf{Eq. (7)}$$

where EM and BD correspond to the emission intensity and branch density; EG_b and EG_m denote the emission strength gradients based on n_b and mass content of glucan, respectively. Overall, EG_b is used to estimate the emission strength with each molar unit branch points.

A new series of fluorescent gradient values with the unit of RFU/ mole branching points are thus developed to represent the characteristic spatial restriction of a single nano-pocket for different glucans.

In this study, the EG_b for model glucans were 1.68×10^6 for PG, 0.85×10^6 for PG-BLD, 1.31×10^6 for AP, 0.59×10^6 for AP-BLD. These values are well in accordance with our established models in **Fig. 4-1**. First, it is easy to conclude from **Fig. 4-6-5** and **4-6-6** that the nanopockets formed with the branching region of B chain and two neighboring A chains (denoted as '2A+1B' pocket) should exhibit higher spatial restrictions than those formed with the branching region of B chain and one A chain (denoted as '1A+1B' pocket). Owing to the 'branch-on-branch' pattern of PG, '2A+1B' pockets are more frequently found in PG than AP, which contributes to the high EG_b value for PG in overall. Second, β-amylolysis drastically reduces the local spatial restriction by forming more opening nanopockets compared to those in the native state (**Fig. 4-6-7** and 4-**6-8**). Compared to the native counterparts, the EG_b values decreased by 50-55% after β-amylolysis, suggesting the important role of A chains in forming the spatial boundaries of nanopocket. In β-limit dextrins, '2A+1B' pocket also appears to render higher spatial restriction than '1A+1B'

pockets (**Fig. 4-6-7** and **4-6-8**), thus contributing to the higher EG_b value in PG-BLD than in AP-BLD. Third, the EG_b values derived from MR fluorescence are essentially in accordance with the fine structure of model glucans we established by classic approaches, which may highlight the use of EG_b as a novel parameter in the characterization of glucan structure.

4.4 Conclusion

In this study, we assessed the structural features of AP, PG and their BLDs and tested our hypotheses that uses molecular rotor as a small molecule probe for the investigation of glucan particulate structure and glucan interactions in dispersion. The results indicated that the "branch-on-branch" structure of PG resulted in densely packed and highly branched structure with high spatial restriction to molecular rotor. Compared to phytoglycogen, amylopectin possesses swollen and less branched particulate structure due to the presence of long inter-cluster glucan chains, yielding less spatial restriction to small molecules. The study also established a novel fluorescent technique using molecular rotor to quantitatively characterize and differentiate glucan structures in terms of their spatial restriction to small molecules. In the future, this technique is believed to show great potential in advancing the utilization and innovation of carbohydrate polymers.

CHAPTER 5. IN SITU VISUALIZING SPATIAL RESTRICTION IN STARCH GRANULES DURING RETROGRADATION

5.1. Introduction

Starch is widely used as texturizer and stabilizer in food by providing characteristic texture, viscosity, and water holding capacity (Eliasson, 2004). However, cooked starch is unstable in structure. When cooked starch is subjected to low temperature or prolonged storage, glucan chains are readily re-associate and form crystalline structures (Wang et al., 2015). This process is known as starch retrogradation, which may show detrimental effects on food products, such as the staling (hardening) of bread and the syneresis of gelling foods during storage (Gray and Bemiller, 2003). In practical foods, starch is often formulated with other food ingredients in a complex system and some hydrophilic substances, such as simple sugars, salts, and polyphenols, and are able to interact with starch which can largely alter starch retrogradation (Baek et al., 2004; Baker and Rayas-Duarte, 1998; Barros et al., 2012). The accurate and convenient evaluation of starch retrogradation is therefore critical not only for the discovery of anti-retrogradation starch, but also for the optimization of food quality.

There are several routine approaches for the evaluation of starch retrogradation. Most of these approaches target on the measurements of characteristic physical transitions coinciding with starch retrogradation. The textural transition, such as the increase of hardness and elastic modulus, of retrograded starch is often evaluated by rheometer or textural profile analyzer (Klucinec and Thompson, 1999; Sandhu and Singh, 2007). The crystalline structure formed in starch retrogradation can be detected by differential scanning calorimetry (DSC) or X-ray diffraction (Karim et al., 2000; Kim et al., 1997). The reduction of mobility of starch molecules due to the reassociation of starch molecules during retrogradation is detectable by nuclear magnetic resonance (Chen et al., 1997). At the molecular level, Fourier transform infrared spectroscopy can follow the changes in the conformation of starch molecules during retrogradation (Flores-Morales et al., 2012). Turbidimetric methods are often applied to monitor starch retrogradation at low concentration (<2%) by means of measuring the reduction in transmitted light due to phase separation (Jacobson et al., 1997; Sandhu and Singh, 2007). However, these methods usually have their own limitations in the lack of sensitivity or the

applicability for probing *in situ* spatial arrangement of glucan chains and network. Although cryo-scanning electron microscopy may allow the direct observation of microstructure, the requisite procedure that immerses sample in liquid nitrogen followed by sublimation may be too invasive for the highly hydrated glucan networks and thus fails in providing *in situ* measurement. Molecular rotor (MR) is a kind of unique fluorophore that only emits fluorescence when its motion is retarded by the spatial restriction (Rettig, 1986). Based on this unique property, some previous studies have applied MR for the detection of polymeric aggregation (Hong et al., 2011) and cell membrane viscosity (Haidekker et al., 2002, 2000). In these applications, MR can locate at the places of interest and the microstructural changes due to the association or dissociation of molecules are reflected by MR fluorescence as the spatial restriction exerting to MR varying with the microstructures. Cooked starches, either in a fully dispersed form or a swollen granular state, form polymeric matrices that may exert spatial restriction to the small molecules locating at the interspaces of the matrices. If retrogradation of starch with molecular rotor occurs, the reassociation and recrystallization of starch molecules may alter the microstructure of starch matrices and further affect the spatial restriction exerted on molecular rotors as well. Hence, we hypothesized that the microstructural changes of starch matrices during retrogradation can be visually probed with the change of local fluorescent emission of molecular rotor. A most recent study evaluated the use of MR for the measurement of viscosity in starch pastes (Gulnov et al., 2016). However, there is no attempt to date in using MR for the *in situ* and visual observation of starch retrogradation.

The aim of this study is to develop a novel MR-based fluorescent microscopic method for the *in situ* and visual observation of starch retrogradation. A number of cereal and tuber starches from amaranth, cow cockle, waxy corn, normal corn and potato were used as the models. A hydrophilic molecular rotor, 9-(2-carboxy-2-cyanovinyl) julolidine (CCVJ), was used as the probe to monitor the microstructural changes of starch matrices induced by retrogradation. This work is expected to support the fundamental research on starch retrogradation as well as the quality control of starchy foods.

5.2 Materials and methods

5.2.1 Materials

Waxy corn starch (WCS), normal corn starch (NCS), and normal potato starch (PS) were obtained from Ingredion. Cow cockle starch (CCS) was extracted from cow cockle seeds purchased from Hangzhou Botanic Technology Co., Ltd., China. Amaranth starch (AS) was isolated from the amaranth grains purchased from Woodland Foods Co., Ltd., IL. All chemical reagents used for the study were of analytical grade unless specified.

5.2.2 Methods

5.2.2.1 Preparation of amaranth and cow cockle starch

Amaranth starch (AS) was isolated using a modified alkaline extraction method. To start the extraction, 1.5 kg of dry grains were soaked in 4 L of 0.1% (w/v) sodium hydroxide (NaOH) solution and kept at 50 °C in a water bath with slight agitation. Cow cockle starch (CCS) was isolated according to the methods of Peng and Yao (2018) with modifications. Cow cockle seeds (1.5 kg) were soaked in 4 L 0.15 M lactic acid solution at 50 °C in a water bath with slight agitation.

After the 48 h-steeping process and decanting the steeping solution, wet grains or seeds were homogenized with 3 L of water using a blender at high speed for 4 min and passed through a 270-mesh sieve. The retained solids (by the sieve) were extracted again using another 3 L of water. The fractions permeated through the sieve were combined, adjusted to pH 10 and centrifuged at 3000 g for 15 min. The precipitate, as the crude starch material, was collected. Each crude starch material (about 700 g) was resuspended in 3 L of water and adjusted to pH 10, agitated for 30 min, and centrifuged again. The precipitate was then repeatedly washed with water three times, during which the proteinaceous material on the top of the precipitate was scraped off using a spatula. Thereafter, the precipitate was resuspended in deionized water, neutralized to pH 7.0 using 1.0 M hydrogen chloride (HCl) solution, and centrifuged. The starch precipitate was further washed twice using deionized water (1.5 L for each cycle). The material collected was resuspended in 500 mL 80% (v/v) ethanol, subjected to vacuum filtration and finally washed using 100 mL of pure ethanol. Starch materials were collected and dried in an

oven at 40 °C overnight. All starch materials (~ 400-500 g for each) were stored in glass jars at room temperature before use.

5.2.2.2 Preparation of gelatinized and retrograded starch

80 mg starch was dispersed in 40 g phosphate buffer (5 mM, pH 7.0) pre-stained with 4.5 μM CCVJ. A blank solution without starch was used as the control. The starch dispersion in capped 50-mL centrifuge tube was heated in a water bath at 95 °C for 20 min and cooled to room temperature. To avoid clumps of gelatinized starch granules, the dispersion was first vigorously vortexed for 1 min before putting into the water bath. Thereafter, the tubes were gently inverted for 10 times in every two minutes of heating. The obtained dispersions were subsequently stored at 4 °C for 14 days. Samples were withdrawn from the tubes by the end of heating (as gelatinized starch samples) and 7 and 14 days after storage (as retrograded starch samples). The gelatinized and retrograded samples were evaluated by UV-Vis spectrophotometer and confocal fluorescent microscopy. All procedures were conducted in dark.

5.2.2.3 Differential scanning calorimetry (DSC)

The gelatinization property of each starch was evaluated using differential scanning calorimetry (DSC Q-2000, TA instruments, US). Starch material (~5.0 mg) and deionized water were precisely weighed into aluminum T-Zero pans (TA instruments, US) to prepare a 50% (w/w) mixture and then hermetically sealed. The starch slurry in the pans were conditioned at room temperature for 12 h. The scan was operated at 20-110 °C with the rate of 10 °C/ min. An empty pan was used as the reference. The peak temperature (T_p) and melting enthalpy (ΔH) were recorded using the TA instrument TRIOS software.

A second scan of DSC pans with freshly gelatinized starch were conducted right after the first scan for checking if starches were completely gelatinized. Then the pans were stored at 4 °C for 14 days. Pans with retrograded starch were scanned by DSC after 7 and 14 days of storage. The peak temperature (T_p) and melting enthalpy (ΔH) were recorded using the TA instrument TRIOS software. The extent of retrogradation was expressed as the ΔH for retrograded starch.

5.2.2.4 Spectrophotometric analysis

Aliquots (~1.5 mL) of starch dispersion obtained from **5.2.2.2** were placed in disposable cuvettes. The absorbance at 640 nm was measured using a UV-Vis spectrophotometer at room temperature.

5.2.2.5 Confocal fluorescent microscopy

Starch dispersion (50 μL) was withdrawn using a cut-end plastic tip and applied on the central cavity of a glass slide (VWR, US). A coverslip was gently placed on the slide and the four corners were attach to the slide using nail polish. The samples were observed using the Nikon-A1Rsi+ Confocal fluorescent microscopy with the 20× (Plan Apo 20× DIC M N2) lens. The excitation and emission wavelength were set at 448.3 nm and 482 nm, respectively.

5.2.2.6 Statistical analysis

Measurements were conducted three times. ANOVA was conducted using SPSS Statistics 24.0 (IBM, US) with all comparisons conducted at a significance level of 95%.

5.3 Results and discussion

5.3.1 Retrogradation behaviors evaluated by DSC

Retrogradation behaviors of different starches in the concentrated system (50 wt% starch) are shown in **Fig. 5-1**. In gelatinization, all starches show large endothermic peaks at ~ 65.3-71.6 °C with an enthalpy of 12.8-17.7 J/g (**Table 5-1.**), suggesting their highly ordered structures in the native state. It is worthy to note that amaranth starch as a small-granule starch exhibited the highest peak temperature (71.6 °C) and enthalpy (17.7 J/g) showing the robust crystalline structure of amaranth starch. These results are generally in agreement with previous studies (Paredes-López et al., 1989; Peng and Yao, 2018).

No endothermic peaks could be observed in the DSC thermograms for the freshly gelatinized starches suggesting that the crystalline structure had been fully melted after gelatinization. In contrast, substantial endothermic peaks were observed after 7 or 14 days of storage, clearly showing the starch retrogradation during storage. **Table 5-1**. compares the peak temperature and the enthalpy values for retrograded starches. In general, the peak temperature

Table 5-1. Gelatinization and retrogradation behaviors of starches in concentrated systems[1]

Sample	Native starch		Retrograded starch			
			7 days		14 days	
	T_p (°C)	ΔH (J/g)	T_p (°C)	ΔH (J/g)	T_p (°C)	ΔH (J/g)
Amaranth	71.6 ± 0.1 A	17.7 ± 0.1 A	53.9 ± 0.3 C	7.5 ± 0.4 AB	52.4 ± 0.4 C	8.6 ± 0.6 B
Cow cockle	66.9 ± 0.2 D	15.2 ± 0.5 B	53.7 ± 0.5 C	4.3 ± 0.4 C	52.7 ± 0.3 C	5.3 ± 0.1 D
Waxy corn	69.8 ± 0.1 C	12.8 ± 0.4 C	53.7 ± 1.0 C	8.7 ± 0.4 A	53.4 ± 0.8 C	10.4 ± 0.4 A
Normal corn	70.2 ± 0.1 B	13.8 ± 1.0 C	59.7 ± 0.9 B	7.0 ± 0.6 B	58.9 ± 0.6 B	6.9 ± 0.6 C
Potato	65.3 ± 0.2 E	16.5 ± 1.1A	67.6 ± 0.5 A	7.9 ± 1.1 AB	66.8 ± 1.0 A	8.0 ± 0.5 B

[1]The weight fraction of starch to water is 1:1. T_p, the peak temperature; ΔH, enthalpy corresponding to the melting of crystalline structures. Values were expressed by means ± standard deviations (n = 3). The means in the same column with different letters are significantly different ($P < 0.05$).

for retrograded AS and WCS were ~52-54 °C, which was significantly lower than that for retrograded NCS (59-60 °C) and PS (67-68 °C). The result may be possibly related to the presence of amylose in NCS and PS (Singh et al., 2003). Retrograded CCS as an amylose-containing starch, however, showed similar peak temperature as the waxy-type starches. This result indicates the molecular structure of CCS not favorable for retrogradation.

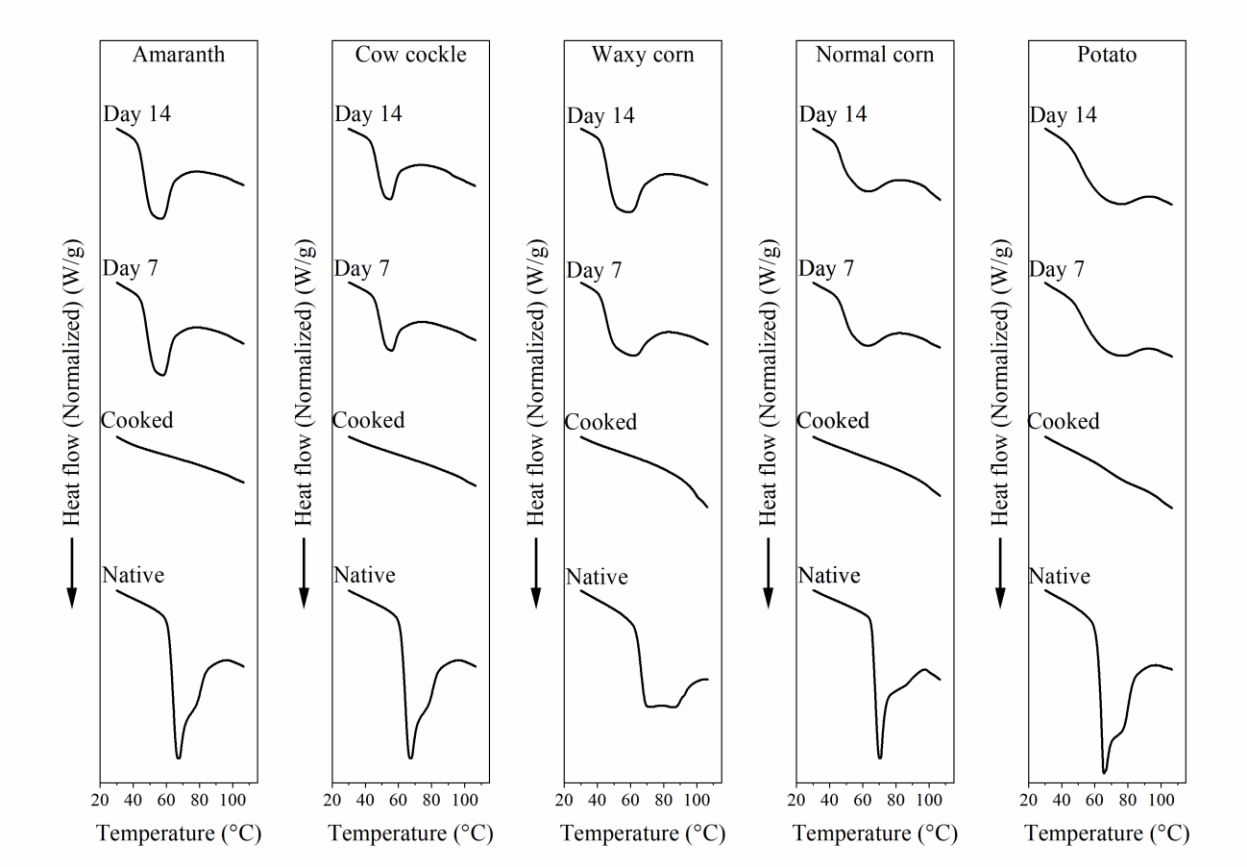

Figure 5-1. Differential scanning calorimetric (DSC) endothermic thermograms showing the gelatinization and retrogradation properties of different starches. From the bottom to the top, the thermograms represent the melting of native, freshly gelatinized (cooked) and retrograded (stored at 4 °C for 7 or 14 days) starches.

The enthalpy values for retrograded starches are usually considered to represent the degree of retrogradation. Our results showed that the retrogradation occurred in two different modes for various starches. For NCS and PS, starch retrogradation rapidly completed by 7 days of storage. For AS, CCS and WCS, starch retrogradation was on progress throughout the 14 days. By the end of the storage, the two waxy-type starches, AS and WCS, exhibited substantially higher degree of retrogradation (enthalpy values = 8.6-10.4 J/g) than the other amylose-containing

starches (enthalpy values = 5.3-8.0 J/g). In our study, a low degree of retrogradation was observed for CCS, highlighting its good storage stability in concentrated systems.

5.3.2 Retrogradation behaviors evaluated using turbidity change

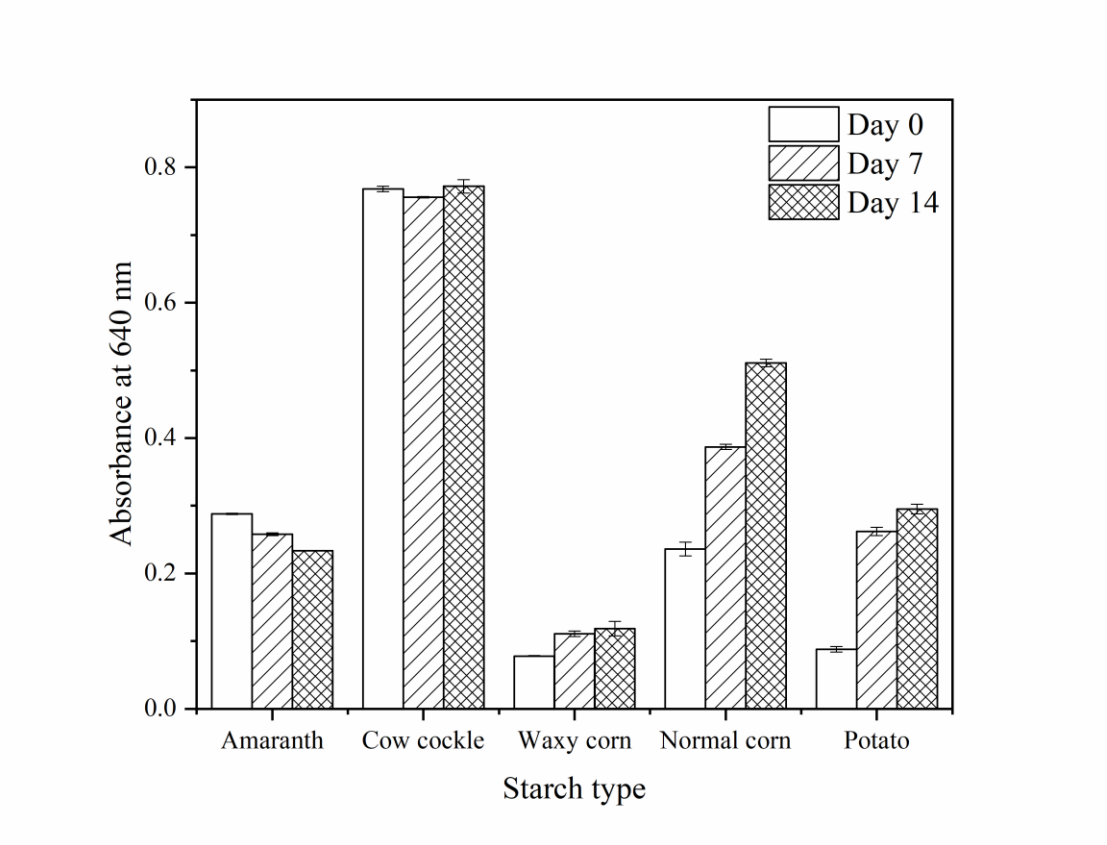

Figure 5-2. The change of absorbance for different starch dispersions (0.2%, w/v) stored at 4°C for 0, 7 and 14 days.

The retrogradation behaviors of different starches in the diluted system (0.2 wt% starch) is shown in **Fig. 5-2**. It is obvious that the initial absorbance values for fresh gelatinized samples vary greatly with starch varieties. Similar strong dependence on starch variety were also reported previously (Jacobson et al., 1997), mainly due to the various transmittance of starch dispersions affected by particle size, residual granular structure, and refractive index.

In general, the turbidity method is based on the idea that retrogradation may result in phase separation of starch matrices and lead to increasing absorbance (Karim et al., 2000; Sandhu and Singh, 2007). At the molecular level, the reassociation of glucan chains may repel water from the starch network and result in high-density starch networks that can seriously retard transmission

of light and increase the turbidity of whole starch dispersion. In our study, the absorbance for WCS, NCS and PS increased by ~52%, 117% and 235% during 14 days of storage, respectively. The result suggests that phase separation occurs more significantly in PS and NCS than WCS during storage. Our result is basically in agreement with the previous study (Jacobson et al., 1997).

The change of absorbance for small-granule starches (AS and CCS) is significantly different from that for the large-granule starches. After 14 days of storage, the absorbance for CCS kept stable while the absorbance for AS decreased by ~20%. The result may possibly indicate a limited level of phase separation for AS and CCS compared to the large-granule starches (WCS, NCS and PS).

5.3.3 Molecular rotor-based observation of starch retrogradation

In this study, we used a hydrophilic MR, CCVJ, to detect the granular structure change induced by starch retrogradation. As large variations in the intensity of fluorescence exist among the images, the high-contrast (HC) or low-contrast (LC) settings were applied by adjusting the saturation intensity values to 3500 (for HC) and 1500 (for LC), respectively, such that the confocal images were not too dark or too bright while preserving the true difference in fluorescent intensity. In this way, the intensity of each pixel (0.25 μm/ pixel) in a confocal image can represent the degree of local spatial restriction to MR, and any saturated pixels (the fluorescent intensity of the pixel > 3500 for HC and >1500 for LC) will be colored in orange.

5.3.3.1 Buffer solution

The fluorescent intensity of the blank buffer solution is too low to be visible under either HC or LC settings, showing a pure black background (data not shown). This is because negligible spatial restrictions exist when the MR molecules is completely dissolved in bulk water phase. After 7 and 14 days of storage, the confocal images for the blank solution kept showing pure black backgrounds under both HC and LC settings.

5.3.3.2 Visual observation of starch retrogradation

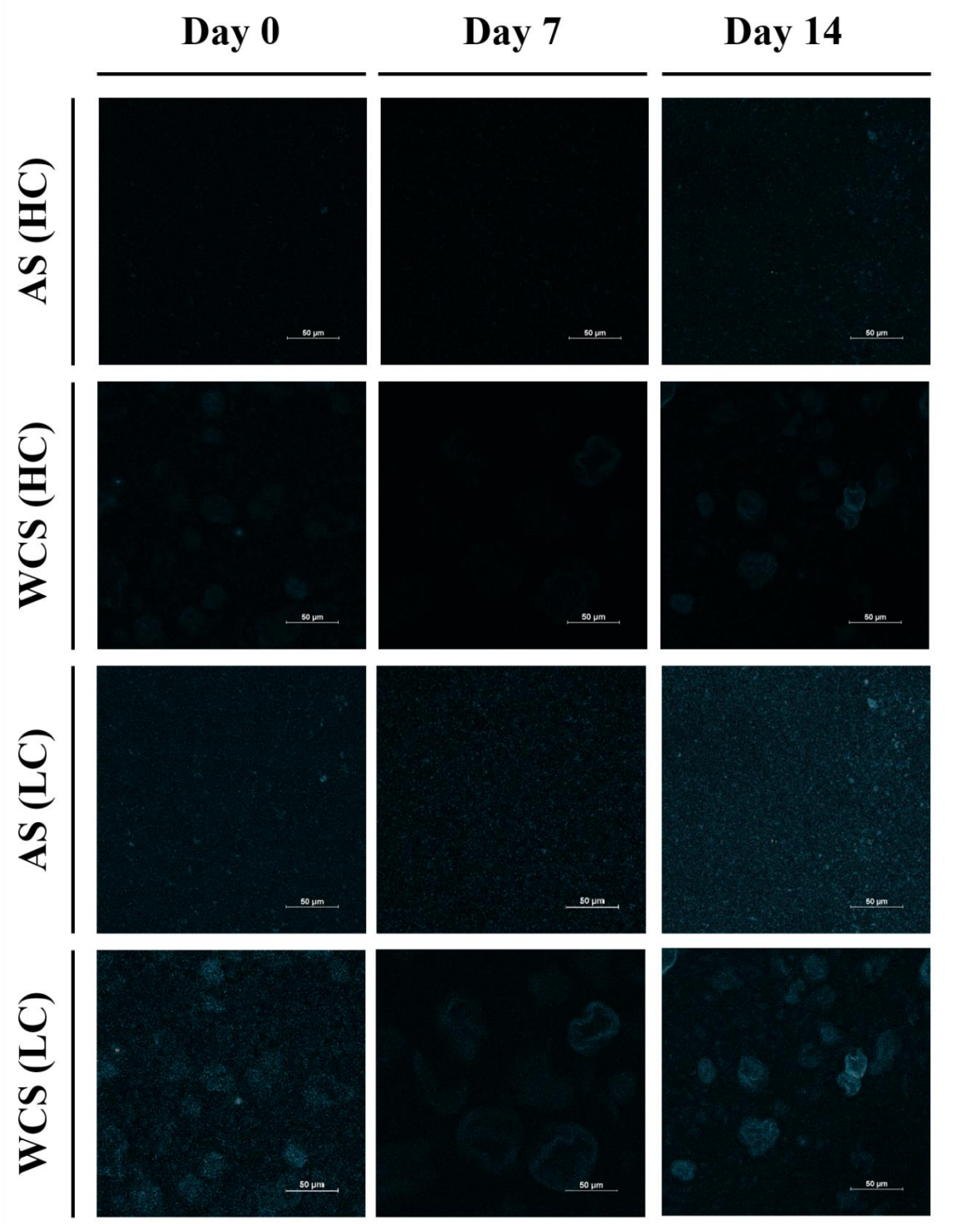

Figure 5-3. Confocal microscopic images of 0.2% (w/v) amaranth starch (AS) and waxy corn starch (WCS) dispersions dyed with 4.5 µM CCVJ. HC and LC represent the high contrast and low contrast settings, respectively. Images were taken after gelatinization (day 0) and on the 7 and 14 days of storage at 4°C. Bar = 50 µm.

The confocal images for waxy-type starches (AS and WCS) were too dark under HC setting, so we used the images under LC setting for analysis (**Fig. 5-3**). For freshly gelatinized AS (on Day 0), some irregular particulate structures (2-10 μm) were visible with blue fluorescence, while abundant dots with lower brightness were observed in the bulk phase. Similar result was observed for freshly gelatinized WCS, where larger (~20-50 μm), brighter and more particulate structures were visible. In overall, the pixels corresponding to dots were brighter than the pixels corresponding to the particulate structures. It is well known that waxy-type starches readily lose granular structure and form fully dispersed starch after cooking (Han and Hamaker, 2002). Thus, the blue dots in the bulk phase should correspond to fully dispersed starch molecules that yielded spatial restriction to CCVJ. In contrast, the particulate structures outlined by the blue fluorescence of CCVJ should correspond to the residual granule fractions survived in cooking. Previous studies have shown that the residual granule fractions found in cooked starch are composed of randomly crosslinked starch (i.e. amylopectin) (Zhang et al., 2014). In such residual granule fractions, amylopectin molecules should exhibit lower mobility compared to fully dispersed ones due to the presence of crosslinking. Thus, the local microstructure for the residual granule fractions should also exert higher spatial restriction to MR than the fully dispersed starch, which may explain the brighter pixels for the particulate structures in **Fig. 5-3**.

After the first 7-day storage, the particulate structures of both AS and WCS were less visible, whereas the brightness of the dots in the bulk phase increased for both images. After 14 days of storage, the pixels corresponding to both particulate structures and the dots became significantly brighter than the those shown in the images captured on day 0 and day 7. The results may indicate that (1) the residual starch fractions lose spatial restrictions to MR at first (0-7 days of storage), but restore spatial restrictions later (7-14 days of storage); (2) the retrogradation of amylopectin in bulk water phase continuously occurs yielding increasing spatial restriction to MR.

In contrary to waxy-type starches, the particulate structures were much better preserved after cooking and visible enough under the HC setting for amylose-containing starches (CCS, NCS and PS) images (**Fig 5-4**). In the confocal images for CCS, NCS and PS with LC setting (figures not shown), bright dots were only occasionally observed, suggesting that the majority of starchy materials remained in the particulate structures after cooking. Thus, we only used the images under HC setting for analysis. Compared to waxy-type starches, the stronger fluorescence

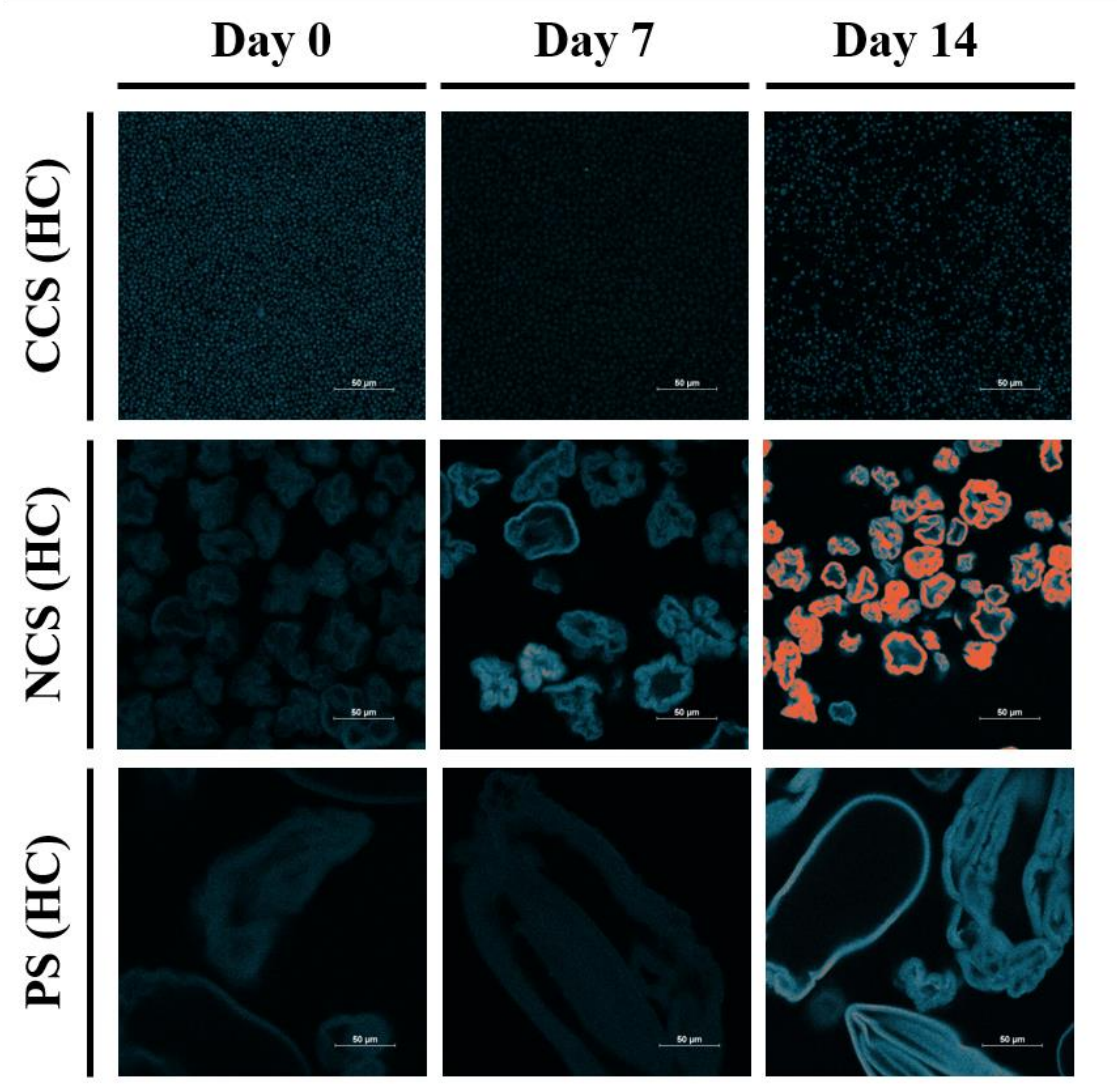

Figure 5-4. Confocal microscopic images of 0.2% (w/v) cow cockle starch (CCS), normal corn starch (NCS) and potato starch (PS) dispersions dyed with 4.5 μM CCVJ. HC represent the high contrast setting. Pixels with saturated fluorescent intensity were colored in orange. Images were taken after gelatinization (day 0) and on the 7 and 14 days of storage at 4°C. Bar = 50 μm.

for the particulate structures in **Fig. 5-4** suggests that the residual granule fractions for amylose-containing starches exert much stronger spatial restrictions to CCVJ than those for waxy-type starches. A possible explanation is that the presence of amylose can strengthen the crosslink among amylopectin molecules, immobilize starch networks as well as divide the matrices into finer microvolumes (Debet and Gidley, 2007).

Similarly to WCS and AS, the particulate structures for CCS and PS became less visible after the first 7 days but restore fluorescence after the second 7 days. However, NCS behaved differently

in storage, during which the fluorescence for the particulate structures did not decrease after 7 days of storage. A possible explanation is that the loss of fluorescence for NCS occurs faster than that for the other starches, such that was not captured on the 7th day of storage. It is worthy to note that the pixels corresponding to the particulate structure for NCS were saturated (intensity > 3500, shown in orange color) after 14 days of storage. This result indicates that the local microstructures in the residual granule fractions of NCS exert substantially stronger spatial restrictions to CCVJ than those for CCS or PS.

5.3.4 Interaction of molecular rotor with local starch microstructures

In our study, the variations in fluorescence for the particulate structures shared a similar trend, that is, the fluorescence decreases after 7 days and increases after 14 days. The results clearly indicated the common structural transition of starch network during retrogradation, which involved a 'decrease-and-increase' pattern of variation in the spatial restriction to CCVJ. Combined with the established theory on the structural transition during starch retrogradation (Wang et al., 2015), we proposed a possible mechanism to explain this critical phenomenon **(Fig. 5-5)**.

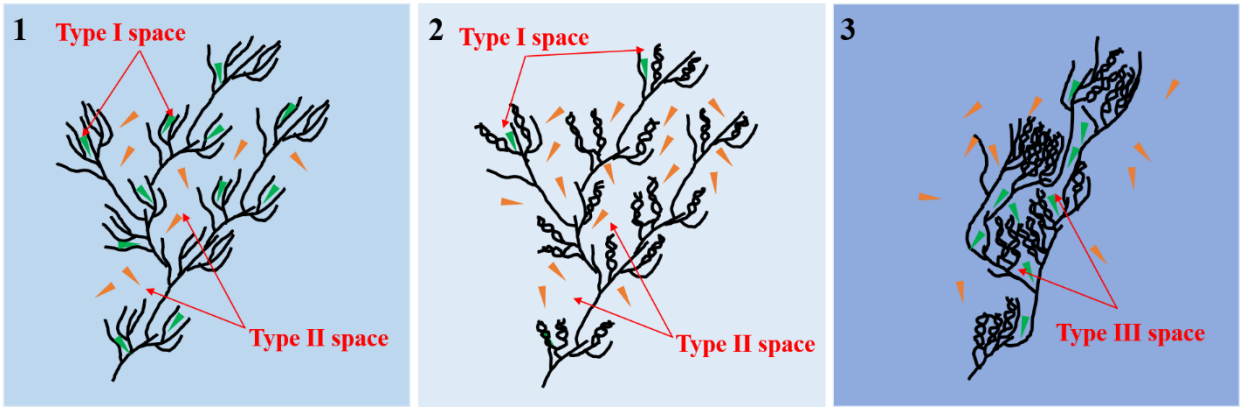

Figure 5-5. Schematics showing the interaction of molecular rotor with local starch microstructures. The blueness of background color shows the fluorescent intensity of CCVJ (green or orange triangles) in response to the different local structures. **1**, freshly cooked starch with glucan chains are separate from each other. CCVJ molecules can locate in the interspaces between single glucan chains (type I space) or in the interspaces among starch molecules (type II space). **2**, Glucan chains with double-helical associations in the early stage of retrogradation. CCVJ molecules are repelled out from type I space and enter to type II space. The dimensions for type II spaces are also increased due the reassociation of glucan chains. **3**, Spatial rearrangements of glucan chains with crystalline structure. CCVJ molecules can locate in the amorphous interspaces among starch network (type III space).

In freshly cooked starch, glucan chains are separated from each other yielding abundant interspaces between single glucan chains (labelled as ‘type I’) that can accommodate CCVJ molecules (**Fig. 5-5-1**). CCVJ can also dissolved in the intermolecular interspaces surrounded by starch molecules, which is labelled as ‘type II’ spaces. In the early stage of retrogradation, single helical or random coiled glucan chains can reassociate to double-helical chains (**Fig. 5-5-2**). In general, no central cavity is found in double-helical structures of starch (Immel and Lichtenthaler, 2000), which should repel CCVJ molecules out from the type I interspaces. For turbidimetric tests, the reassociation of glucan chains may conceivably yield higher absorbance due to the prevalent formation of double-helical chains. In contrast, such reassociation can substantially reduce CCVJ fluorescence, because (1) less CCVJ molecules are retained in the type I interspaces and (2) the repelled CCVJ molecules are relocated in type II spaces (micro to submicro scale) with much larger dimensions than the previous type I interspaces (nano to subnano scales).

In the subsequent stage of retrogradation, double-helical chains can further rearrange to ordered structures and eventually form local crystallites (**Fig. 5-5-3**). This process can further result in densely packed starch networks that again increase the absorbance for turbidimetric tests. In contrary to the early stage, CCVJ molecules can reside in the amorphous interspaces (labelled as ‘type III’) of rearranged local networks. Owing to crystallization, the overall flexibility of starch network should be substantially reduced, and the crystallized regions, as the junction zones may further divide the whole network into smaller microvolumes compared to the type II spaces or pull neighboring double-helical chains into contact and produce more intermolecular interspaces. Both of the factors can contribute to stronger spatial restriction to CCVJ. Therefore, the particulate structures restore strong fluorescence in the second 7 days of storage (**Fig. 5-3** and **5-4**).

5.4 Conclusion

In this study, the retrogradation of five model starches were evaluated by DSC, turbidimetric and the novel MR-based confocal microscopic methods. The DSC result showed the outstanding stability of cow cockle starch in concentrated state for prolonged storage time, highlighting its potential use as an anti-retrogradation native starch. The spectrophotometric result showed high storage stability of small-granule starches compared to large-granule starches. In contrast to the

conventional methods, the novel confocal microscopic method achieved *in situ* and visual observation on starch retrogradation. Two characteristic stages of structure transition during retrogradation were associated with the variations in MR fluorescence. Mechanistic studies are expected to be done in the future. To the best of our knowledge, this MR-based confocal microscopic method, for the first time, provides a direct visual observation on starch retrogradation. Owing to the quantitative nature of MR fluorescence, a quantitative method based on this confocal approach may also be established in the future.

REFERENCES

AACC International. Method 44-15.02. Moisture- Air-Oven Methods, in: Approved Methods of Analysis, 11th Ed. AACC International, St. Paul, MN.

AACC International. Method 76-13.01, Total Starch Assay Procedure (Megazyme Amyloglucosidase/alpha-Amylase Method), in: Approved Methods of Analysis, 11th Ed. AACC International, St. Paul, MN.

Ablinger, E., Leitgeb, S., Zimmer, A., 2013. Differential scanning fluorescence approach using a fluorescent molecular rotor to detect thermostability of proteins in surfactant-containing formulations. Int. J. Pharm. 441, 255–260.

A. Haidekker, M., A. Theodorakis, E., 2007. Molecular rotors—fluorescent biosensors for viscosity and flow. Org. Biomol. Chem. 5, 1669–1678.

Akers, W., Haidekker, M.A., 2004. A Molecular rotor as viscosity sensor in aqueous colloid solutions. J. Biomech. Eng. 126, 340–345.

Al-Hassan, K.A., Khanfer, M.F., 1998. Fluorescence probes for cyclodextrin interiors. J. Fluoresc. 8, 139–152.

Ao, Z., Jane, J., 2007. Characterization and modeling of the A- and B-granule starches of wheat, triticale, and barley. Carbohydr. Polym. 67, 46–55.

Atkinson, J., 2015. Structure and dynamics of aqueous dispersions of highly-branched monodisperse phytoglycogen nanoparticles (Ph.D. Thesis).

Avaltroni, F., Bouquerand, P.E., Normand, V., 2004. Maltodextrin molecular weight distribution influence on the glass transition temperature and viscosity in aqueous solutions. Carbohydr. Polym. 58, 323–334.

Azanza, F., Klein, B.P., Juvik, J.A., 1996. Sensory characterization of sweet corn lines differing in physical and chemical composition. J. Food Sci. 61, 253–257.

Baek, M.H., Yoo, B., Lim, S.-T., 2004. Effects of sugars and sugar alcohols on thermal transition and cold stability of corn starch gel. Food Hydrocoll. 18, 133–142.

Bahnassey, Y.A., Breene, W.M., 1994. Rapid visco-analyzer (RVA) pasting profiles of wheat, corn, waxy corn, tapioca and amaranth starches (A. *hypochondriacus* and A. *cruentus*) in the presence of konjac flour, gellan, guar, xanthan and locust bean gums. Starch–Stärke 46, 134–141.

Baker, L.A., Rayas-Duarte, P., 1998. Retrogradation of amaranth starch at different storage temperatures and the effects of salt and sugars. Cereal Chem. 75, 308–314.

Ball, S., Guan, H.P., James, M., Myers, A., Keeling, P., Mouille, G., Buléon, A., Colonna, P., Preiss, J., 1996. From glycogen to amylopectin: a model for the biogenesis of the plant starch granule. Cell 86, 349–352.

Barros, F., Awika, J.M., Rooney, L.W., 2012. Interaction of tannins and other sorghum phenolic compounds with starch and effects on *in vitro* starch digestibility. J. Agric. Food Chem. 60, 11609–11617.

Barthelmes, G., Pratsinis, S.E., Buggisch, H., 2003. Particle size distributions and viscosity of suspensions undergoing shear-induced coagulation and fragmentation. Chem. Eng. Sci. 58, 2893–2902.

Batey, I.L., Curtin, B.M., 2000. Effects on pasting viscosity of starch and flour from different operating conditions for the rapid visco analyser. Cereal Chem. J. 77, 754–760.

Becker, R., Wheeler, E.L., Lorenz, K., Stafford, A.E., Grosjean, O.K., Betschart, A.A., Saunders, R.M., 1981. A compositional study of amaranth grain. J. Food Sci. 46, 1175–1180.

Bello-Pérez, L.A., Paredes-López, O., Roger, P., Colonna, P., 1996. Amylopectin—properties and fine structure. Food Chem. 56, 171–176.

Bemiller, J.N., 1997. Starch modification: challenges and prospects. Starch–Stärke 49, 127–131.

Bhatia, S., Bharti, A., 2015. Evaluating the antimicrobial activity of Nisin, Lysozyme and Ethylenediaminetetraacetate incorporated in starch based active food packaging film. J. Food Sci. Technol. 52, 3504–3512.

Bhosale, R., Singhal, R., 2007. Effect of octenylsuccinylation on physicochemical and functional properties of waxy maize and amaranth starches. Carbohydr. Polym. 68, 447–456.

Biliaderis, C.G., Maurice, T.J., Vose, J.R., 1980. Starch gelatinization phenomena studied by differential scanning calorimetry. J. Food Sci. 45, 1669–1674.

Biliaderis, C.G., Mazza, G., Przybylski, R., 1993. Composition and physico-chemical properties of starch from cow cockle (*Saponaria vaccaria* L.) Seeds. Starch–Stärke 45, 121–127.

Błaszczak, W., Misharina, T.A., Fessas, D., Signorelli, M., Górecki, A.R., 2013. Retention of aroma compounds by corn, sorghum and amaranth starches. Food Res. Int. 54, 338–344.

Boutboul, A, Giampaoli, P., Feigenbaum, A., Ducruet, V., 2002. Influence of the nature and treatment of starch on aroma retention. Carbohydr. Polym. 47, 73–82.

Boutboul, Aurélia, Lenfant, F., Giampaoli, P., Feigenbaum, A., Ducruet, V., 2002. Use of inverse gas chromatography to determine thermodynamic parameters of aroma–starch interactions. J. Chromatogr. A, First International Conference on Inverse Gas Chromatography 969, 9–16.

Buléon, A., Colonna, P., Planchot, V., Ball, S., 1998. Starch granules: structure and biosynthesis. Int. J. Biol. Macromol. 23, 85–112.

Caselato-Sousa, V.M., Amaya-Farfán, J., 2012. State of knowledge on amaranth grain: A comprehensive review. J. Food Sci. 77, R93–R104.

Chen, H., Narsimhan, G., Yao, Y., 2015. Particulate structure of phytoglycogen studied using β-amylolysis. Carbohydr. Polym. 132, 582–588.

Chen, H., Yao, Y., 2017a. Phytoglycogen improves the water solubility and Caco-2 monolayer permeation of quercetin. Food Chem. 221, 248–257.

Chen, H., Yao, Y., 2017b. Phytoglycogen to increase lutein solubility and its permeation through Caco-2 monolayer. Food Res. Int. 97, 258–264.

Chen, J., Jane, J., 1994. Preparation of granular cold-water-soluble starches by alcoholic-alkaline treatment. Cereal Chem. 71, 618–622.

Chen, P.L., Long, Z., Ruan, R., Labuza, T.P., 1997. Nuclear magnetic resonance studies of water mobility in bread during storage. LWT - Food Sci. Technol. 30, 178–183.

Choi, Y.J., Baik, M.Y., Kim, B.Y., 2017. Characteristics of granular cold-water-soluble potato starch treated with alcohol and alkali. Food Sci. Biotechnol. 26, 1263–1270.

Chronakis, I.S., 1998. On the molecular characteristics, compositional properties, and structural-functional mechanisms of maltodextrins: A review. Crit. Rev. Food Sci. Nutr. 38, 599–637.

Coşkun, M.B., Yalçın, İ., Özarslan, C., 2006. Physical properties of sweet corn seed (Zea mays saccharata Sturt.). J. Food Eng. 74, 523–528.

Crittenden, R., Laitila, A., Forssell, P., Mättö, J., Saarela, M., Mattila-Sandholm, T., Myllärinen, P., 2001. Adhesion of bifidobacteria to granular starch and its implications in probiotic technologies. Appl Env. Microbiol 67, 3469–3475.

Crosbie, G.B., 1991. The relationship between starch swelling properties, paste viscosity and boiled noodle quality in wheat flours. J. Cereal Sci. 13, 145–150.

de Miranda, J.A., Cacita, N., Okano, L.T., 2007. Evaluation of amylopectin clusters and their interaction with nonionic surfactants. Colloids Surf. B Biointerfaces 60, 19–27.

Debet, M.R., Gidley, M.J., 2007. Why do gelatinized starch granules not dissolve completely? Roles for amylose, protein, and lipid in granule "ghost" integrity. J. Agric. Food Chem. 55, 4752–4760.

Ding, Y., Lin, Q., Kan, J., 2018. Development and characteristics nanoscale retrograded starch as an encapsulating agent for colon-specific drug delivery. Colloids Surf. B Biointerfaces 171, 656–667.

Dokic-Baucal, L., Dokic, P., Jakovljevic, J., 2004. Influence of different maltodextrins on properties of O/W emulsions. Food Hydrocoll. 18, 233–239.

Eglinton, J.K., Langridge, P., Evans, D.E., 1998. Thermostability variation in alleles of barley beta-amylase. J. Cereal Sci. 28, 301–309.

Eliasson, A., 2004. Starch in Food Structure, Function and Applications, Woodhead Publishing Series in Food Science, Technology and Nutrition. Burlington: Elsevier Science, Burlington.

Ellis, R.P., Cochrane, M.P., Dale, M.F.B., Duffus, C.M., Lynn, A., Morrison, I.M., Prentice, R.D.M., Swanston, J.S., Tiller, S.A., 1998. Starch production and industrial use. J. Sci. Food Agric. 77, 289–311.

Fannon, J.E., BeMiller, J.N., 1992. Structure of corn starch paste and granule remnants revealed by low-temperature scanning electron microscopy after cryopreparation. Cereal Chem 69, 456–460.

Fannon, J.E., Hauber, R.J., BeMILLER, J.N., 1992. Surface pores of starch granules. Cereal Chem 69, 284–288.

Fischer, A., Houzelle, M.C., Hubert, P., Axelos, M.A.V., Geoffroy-Chapotot, C., Carré, M.C., Viriot, M.L., Dellacherie, E., 1998. Detection of intramolecular associations in hydrophobically modified pectin derivatives using fluorescent probes. Langmuir 14, 4482–4488.

Flores-Morales, A., Jiménez-Estrada, M., Mora-Escobedo, R., 2012. Determination of the structural changes by FT-IR, Raman, and CP/MAS 13C NMR spectroscopy on retrograded starch of maize tortillas. Carbohydr. Polym. 87, 61–68.

Förster, T., Hoffmann, G., 1971. Die Viskositätsabhängigkeit der fluoreszenzquantenausbeuten einiger farbstoffsysteme. Z. Für Phys. Chem. 75, 63–76.

Fredriksson, H., Silverio, J., Andersson, R., Eliasson, A.C., Åman, P., 1998. The influence of amylose and amylopectin characteristics on gelatinization and retrogradation properties of different starches. Carbohydr. Polym. 35, 119–134.

French, D., 1972. Fine structure of starch and its relationship to the organization of starch granules. J. Jpn. Soc. Starch Sci. 19, 8–25.

Galmarini, M.V., Schebor, C., Zamora, M.C., Chirife, J., 2009. The effect of trehalose, sucrose and maltodextrin addition on physicochemical and sensory aspects of freeze-dried strawberry puree. Int. J. Food Sci. Technol. 44, 1869–1876.

Gavvala, K., Satpathi, S., Hazra, P., 2015. Ultrafast dynamics of a molecular rotor in chemical and biological nano-cavities. RSC Adv. 5, 72793–72800.

Goering, K.J., DeHaas, B., 1972. New starches. VIII. Properties of the small granule-starch from *Coloca. esculenta*. Cereal Chem 49, 712–719.

Goering, K.J., Eslick, R.F., Watson, C.A., Keng, J., 1966. Utilization and agronomic studies of cow cockle (*Saponaria vaccaria*). Econ. Bot. 20, 429–433.

Gonzalez-Soto, R.A., de la Vega, B., García-Suarez, F.J., Agama-Acevedo, E., Bello-Pérez, L.A., 2011. Preparation of spherical aggregates of taro starch granules. LWT–Food Sci. Technol. 44, 2064–2069.

Gray, J.A., Bemiller, J.N., 2003. Bread staling: Molecular basis and control. Compr. Rev. Food Sci. Food Saf. 2, 1–21.

Grossutti, M., Miki, C., John, D., 2017. Phytoglycogen nanoparticles:1. Key properties relevant to its use as a natural moisturizing ingredient. Househ. Pers. Care Today 12, 47–51.

Gulnov, D.V., Nemtseva, E.V., Kratasyuk, V.A., 2016. Contrasting relationship between macro- and microviscosity of the gelatin- and starch-based suspensions and gels. Polym. Bull. 73, 3421–3435.

Haidekker, M.A., Brady, T., Wen, K., Okada, C., Stevens, H.Y., Snell, J.M., Frangos, J.A., Theodorakis, E.A., 2002. Phospholipid-bound molecular rotors: synthesis and characterization. Bioorg. Med. Chem. 10, 3627–3636.

Haidekker, M.A., Brady, T.P., Lichlyter, D., Theodorakis, E.A., 2005. Effects of solvent polarity and solvent viscosity on the fluorescent properties of molecular rotors and related probes. Bioorganic Chem. 33, 415–425.

Haidekker, M.A., L'Heureux, N., Frangos, J.A., 2000. Fluid shear stress increases membrane fluidity in endothelial cells: a study with DCVJ fluorescence. Am. J. Physiol.-Heart Circ. Physiol. 278, H1401–H1406.

Haidekker, M.A., Nipper, M., Mustafic, A., Lichlyter, D., Dakanali, M., Theodorakis, E.A., 2010. Dyes with Segmental Mobility: Molecular Rotors, in: Advanced Fluorescence Reporters in Chemistry and Biology I, Springer Series on Fluorescence. Springer, Berlin, Heidelberg, pp. 267–308.

Haidekker, M.A., Theodorakis, E.A., 2010. Environment-sensitive behavior of fluorescent molecular rotors. J. Biol. Eng. 4, 11.

Han, S., Choi, S.H., Kim, W., Kim, B.Y., Baik, M.Y., 2015. Infusion of catechin into native corn starch granules for drug and nutrient delivery systems. Food Sci. Biotechnol. 24, 2035–2040.

Han, X.-Z., Hamaker, B.R., 2002. Association of starch granule proteins with starch ghosts and remnants revealed by confocal laser scanning microscopy. Cereal Chem. 79, 892–896.

Hannah, L.C., 1997. Starch Synthesis in the Maize Seed, in: Larkins, B.A., Vasil, I.K. (Eds.), Cellular and Molecular Biology of Plant Seed Development. Springer Netherlands, Dordrecht, pp. 375–405.

Hickman, B.E., Janaswamy, S., Yao, Y., 2009. Autoclave and β-amylolysis lead to reduced *in vitro* digestibility of starch. J. Agric. Food Chem. 57, 7005–7012.

Hickman, B.E., Janaswamy, S., Yao, Y., 2008. Properties of starch subjected to partial gelatinization and β-amylolysis. J. Agric. Food Chem. 57, 666–674.

Hinkle, M.E., Zobel, H.F., 1968. X-ray diffraction of oriented amylose fibers. III. The structure of amylose-*n*-butanol complexes. Biopolymers 6, 1119–1128.

Hizukuri, S., 1986. Polymodal distribution of the chain lengths of amylopectins, and its significance. Carbohydr. Res. 147, 342–347.

Hizukuri, S., Maehara, Y., 1990. Fine structure of wheat amylopectin: the mode of A to B chain binding. Carbohydr. Res. 206, 145–159.

Holm, J., Lundquist, I., Björck, I., Eliasson, A.C., Asp, N.G., 1988. Degree of starch gelatinization, digestion rate of starch in vitro, and metabolic response in rats. Am. J. Clin. Nutr. 47, 1010–1016.

Hong, Y., Y. Lam, J.W., Tang, B.Z., 2011. Aggregation-induced emission. Chem. Soc. Rev. 40, 5361–5388.

Hoover, R., 2001. Composition, molecular structure, and physicochemical properties of tuber and root starches: a review. Carbohydr. Polym. 45, 253–267.

Hoover, R., Sinnott, A.W., Perera, C., 1998. Physicochemical characterization of starches from *Amaranthus cruentus* grains. Starch–Stärke 50, 456–463.

Hsu, S., Lu, S., Huang, C., 2000. Viscoelastic changes of rice starch suspensions during gelatinization. J. Food Sci. 65, 215–220.

Hu, R., Lager, E., Aguilar-Aguilar, A., Liu, J., Lam, J.W.Y., Sung, H.H.Y., Williams, I.D., Zhong, Y., Wong, K.S., Peña-Cabrera, E., Tang, B.Z., 2009. Twisted intramolecular charge transfer and aggregation-induced emission of BODIPY derivatives. J. Phys. Chem. C 113, 15845–15853.

Huang, L., Yao, Y., 2011. Particulate structure of phytoglycogen nanoparticles probed using amyloglucosidase. Carbohydr. Polym. 83, 1665–1671.

Huber, K.C., BeMiller, J.N., 2000. Channels of maize and sorghum starch granules. Carbohydr. Polym. 41, 269–276.

Huber, K.C., BeMiller, J.N., 1997. Visualization of channels and cavities of corn and sorghum starch granules. Cereal Chem. 74, 537–541.

Iio, T., Takahashi, S., Sawada, S., 1993. Fluorescent molecular rotor binding to actin. J. Biochem. 113, 196–199.

Immel, S., Lichtenthaler, F.W., 2000. The hydrophobic topographies of amylose and its blue iodine complex. Starch–Stärke 52, 1–8.

Inouchi, N., Glover, D.V., Fuwa, H., 1987. Chain length distribution of amylopectins of several single mutants and the normal counterpart, and *sugary*-1 phytoglycogen in maize (*Zea mays* L.). Starch–Stärke 39, 259–266.

Jacobs, H., Delcour, J.A., 1998. Hydrothermal modifications of granular starch, with retention of the granular structure: A review. J. Agric. Food Chem. 46, 2895–2905.

Jacobson, M.R., Obanni, M., Bemiller, J.N., 1997. Retrogradation of starches from different botanical sources. Cereal Chem. 74, 511–518.

Jafari, S.M., He, Y., Bhandari, B., 2006. Nano-emulsion production by sonication and microfluidization—A comparison. Int. J. Food Prop. 9, 475–485.

James, M.G., Robertson, D.S., Myers, A.M., 1995. Characterization of the maize gene *sugary* 1, a determinant of starch composition in kernels. Plant Cell 7, 417–429.

Jane, J., Chen, Y.Y., Lee, L.F., McPherson, A.E., Wong, K.S., Radosavljevic, M., Kasemsuwan, T., 1999. Effects of amylopectin branch chain length and amylose content on the gelatinization and pasting properties of starch. Cereal Chem. 76, 629–637.

Jane, J., Shen, L., Wang, L., Maningat, C.C., 1992. Preparation and properties of small-particle corn starch. Cereal Chem 69, 280–283.

Jane, J.L., Kasemsuwan, T., Leas, S., Zobel, H., Robyt, J.F., 1994. Anthology of starch granule morphology by scanning electron microscopy. Starch–Stärke 46, 121–129.

Jane, J.L., Robyt, J.F., 1984. Structure studies of amylose-V complexes and retrograded amylose by action of alpha amylases, and a new method for preparing amylodextrins. Carbohydr. Res. 132, 105–118.

Juszczak, L., Fortuna, T., Wodnicka, K., 2002. Characteristics of cereal starch granules surface using nitrogen adsorption. J. Food Eng. 54, 103–110.

Karim, A.A., Norziah, M.H., Seow, C.C., 2000. Methods for the study of starch retrogradation. Food Chem. 71, 9–36.

Kim, J.O., Kim, W.S., Shin, M.S., 1997. A comparative study on retrogradation of rice starch gels by DSC, X-ray and α-amylase methods. Starch–Stärke 49, 71–75.

Kim, Y.H., Cho, D.W., Yoon, M., Kim, D., 1996. Observation of hydrogen-bonding effects on twisted intramolecular charge transfer of p-(N,N-Diethylamino)benzoic acid in aqueous cyclodextrin solutions. J. Phys. Chem. 100, 15670–15676.

Klucinec, J.D., Thompson, D.B., 2002. Structure of amylopectins from ae-containing maize starches. Cereal Chem. J. 79, 19–23.

Klucinec, J.D., Thompson, D.B., 1999. Amylose and amylopectin interact in retrogradation of dispersed high-amylose starches. Cereal Chem. 76, 282–291.

Klucinec, J.D., Thompson, D.B., 1998. Fractionation of high-amylose maize starches by differential alcohol precipitation and chromatography of the fractions. Cereal Chem. 75, 887–896.

Kong, X., Bao, J., Corke, H., 2009. Physical properties of Amaranthus starch. Food Chem. 113, 371–376.

Kshirsagar, A.C., Singhal, R.S., 2008. Preparation of hydroxypropyl corn and amaranth starch hydrolyzate and its evaluation as wall material in microencapsulation. Food Chem. 108, 958–964.

Kuimova, M.K., 2012. Mapping viscosity in cells using molecular rotors. Phys. Chem. Chem. Phys. 14, 12671–12686.

Kuimova, M.K., Yahioglu, G., Levitt, J.A., Suhling, K., 2008. Molecular rotor measures viscosity of live cells via fluorescence lifetime imaging. J. Am. Chem. Soc. 130, 6672–6673.

Lathe, G.H., Ruthven, C.R.J., 1956. The separation of substances and estimation of their relative molecular sizes by the use of columns of starch in water. Biochem. J. 62, 665–674.

Lazarick, K., Aladedunye, F., Przybylski, R., 2014. Effect of breading and battering ingredients on performance of frying oils. Eur. J. Lipid Sci. Technol. 116, 763–770.

Le Corre, D., Bras, J., Dufresne, A., 2010. Starch nanoparticles: A review. Biomacromolecules 11, 1139–1153.

Lee, E.Y.C., 1971. The action of sweet potato β-amylase on glycogen and amylopectin: formation of a novel limit dextrin. Arch. Biochem. Biophys. 146, 488–492.

Lee, M.H., Baek, M.H., Cha, D.S., Park, H.J., Lim, S.T., 2002. Freeze-thaw stabilization of sweet potato starch gel by polysaccharide gums. Food Hydrocoll. 16, 345–352.

Lei, J., Gao, Q., 2014. Preparation of waxy rice dextrin with β-amylase treatment and study on its properties. Food Ferment. Ind. 10, 005.

Leloup, V.M., Colonna, P., Ring, S.G., Roberts, K., Wells, B., 1992. Microstructure of amylose gels. Carbohydr. Polym. 18, 189–197.

Li, J.Y., Yeh, A.I., 2001. Relationships between thermal, rheological characteristics and swelling power for various starches. J. Food Eng. 50, 141–148.

Lindeboom, N., Chang, P.R., Falk, K.C., Tyler, R.T., 2005. Characteristics of starch from eight quinoa lines. Cereal Chem. 82, 216–222.

Lindeboom, N., Chang, P.R., Tyler, R.T., 2004. Analytical, biochemical and physicochemical aspects of starch granule size, with emphasis on small granule starches: A review. Starch–Stärke 56, 89–99.

Lindgren, M., Sörgjerd, K., Hammarström, P., 2005. Detection and characterization of aggregates, prefibrillar amyloidogenic oligomers, and protofibrils using fluorescence spectroscopy. Biophys. J. 88, 4200–4212.

Liu, H., Arntfield, S.D., Holley, R.A., Aime, D.B., 1997. Amylose-lipid complex formation in acetylated pea starch-lipid systems. Cereal Chem. 74, 159–162.

Lourdin, D., Putaux, J.-L., Potocki-Véronèse, G., Chevigny, C., Rolland-Sabaté, A., Buléon, A., 2015. Crystalline Structure in Starch, in: Nakamura, Y. (Ed.), Starch: Metabolism and Structure. Springer Japan, Tokyo, pp. 61–90.

Lourvanij, K., 1995. Partial dehydration of glucose to oxygenated hydrocarbons in molecular-sieving catalysts. ProQuest Dissertations Publishing.

Loutfy, R.O., Arnold, B.A., 1982. Effect of viscosity and temperature on torsional relaxation of molecular rotors. J. Phys. Chem. 86, 4205–4211.

Malinski, E., Daniel, J.R., Zhang, X.X., Whistler, R.L., 2003. Isolation of small starch granules and determination of their fat mimic characteristics. Cereal Chem. 80, 1–4.

Manners, D.J., 1989. Recent developments in our understanding of amylopectin structure. Carbohydr. Polym. 11, 87–112.

Martin, C., Smith, A.M., 1995. Starch biosynthesis. Plant Cell 7, 971–985.

Mattila-Sandholm, T., Myllärinen, P., Crittenden, R., Mogensen, G., Fondén, R., Saarela, M., 2002. Technological challenges for future probiotic foods. Int. Dairy J., NIZO Dairy Conference on Food Microbes 2001 12, 173–182.

Mazza, G., Biliaderis, C.G., Przybylski, R., Oomah, B.D., 1992. Compositional and morphological characteristics of cow cockle (*Saponaria vaccaria*) seed, a potential alternative crop. J. Agric. Food Chem. 40, 1520–1523.

McDonagh, P., 2012. Native, modified and clean label starches in foods and beverages, in: Baines, D., Seal, R. (Eds.), Natural Food Additives, Ingredients and Flavourings, Woodhead Publishing Series in Food Science, Technology and Nutrition. Woodhead Publishing, pp. 162–174.

McGorrin, R.J., Leland, J.V., 1996. Flavor-food interactions. ACS Publications.

Merkus, H.G., 2009. Particle Size Measurements Fundamentals, Practice, Quality, Particle Technology Series, 17.

Mills, M.S., Thurman, E.M., 1994. Reduction of nonpoint source contamination of surface water and groundwater by starch encapsulation of herbicides. Environ. Sci. Technol. 28, 73–79.

Morris, E.R., Cutler, A.N., Ross-Murphy, S.B., Rees, D.A., Price, J., 1981. Concentration and shear rate dependence of viscosity in random coil polysaccharide solutions. Carbohydr. Polym. 1, 5–21.

Morrison, W.R., Karkalas, J., 1990. Starch, in: Dey, P.M. (Ed.), Methods in Plant Biochemistry. Academic Press, London, pp. 323–352.

Morrison, W.R., Laignelet, B., 1983. An improved colorimetric procedure for determining apparent and total amylose in cereal and other starches. J. Cereal Sci. 1, 9–20.

Muth, J., Hartje, S., Twyman, R.M., Hofferbert, H.-R., Tacke, E., Prüfer, D., 2008. Precision breeding for novel starch variants in potato. Plant Biotechnol. J. 6, 576–584.

Nadiv, O., Shinitzky, M., Manu, H., Hecht, D., Roberts, C.T., LeRoith, D., Zick, Y., 1994. Elevated protein tyrosine phosphatase activity and increased membrane viscosity are associated with impaired activation of the insulin receptor kinase in old rats. Biochem. J. 298, 443–450.

Nelson, O., Pan, D., 1995. Starch synthesis in maize endosperms. Annu. Rev. Plant Physiol. Plant Mol. Biol. 46, 475–496.

Nickels, J.D., Atkinson, J., Papp-Szabo, E., Stanley, C., Diallo, S.O., Perticaroli, S., Baylis, B., Mahon, P., Ehlers, G., Katsaras, J., Dutcher, J.R., 2016. Structure and hydration of highly-branched, monodisperse phytoglycogen nanoparticles. Biomacromolecules 17, 735–743.

Ong, M.H., Jumel, K., Tokarczuk, P.F., Blanshard, J.M.V., Harding, S.E., 1994. Simultaneous determinations of the molecular weight distributions of amyloses and the fine structures of amylopectins of native starches. Carbohydr. Res. 260, 99–117.

Pal, J., Singhal, R.S., Kulkarni, P.R., 2002. Physicochemical properties of hydroxypropyl derivative from corn and amaranth starch. Carbohydr. Polym. 48, 49–53.

Paredes-López, O., Schevenin, M.L., Hernández-López, D., Cárabez-Trejo, A., 1989. Amaranth starch-isolation and partial characterization. Starch–Stärke 41, 205–207.

Patel, B.K., Waniska, R.D., Seetharaman, K., 2005. Impact of different baking processes on bread firmness and starch properties in breadcrumb. J. Cereal Sci. 42, 173–184.

Peat, S., Whelan, W.J., Thomas, G.J., 1952. Evidence of multiple branching in waxy maize starch. J. Chem. Soc. 4546–4548.

Pelletier, S., Hubert, P., Lapicque, F., Payan, E., Dellacherie, E., 2000. Amphiphilic derivatives of sodium alginate and hyaluronate: synthesis and physico-chemical properties of aqueous dilute solutions. Carbohydr. Polym. 43, 343–349.

Peng, M., Gao, M., Abdel-Aal, E.-S.M., Hucl, P., Chibbar, R.N., 1999. Separation and characterization of A- and B-type starch granules in wheat endosperm. Cereal Chem. 76, 375–379.

Peng, X., Yao, Y., 2018. Small-granule starches from sweet corn and cow cockle: Physical properties and amylopectin branching pattern. Food Hydrocoll. 74, 349–357.

Pérez, S., Bertoft, E., 2010. The molecular structures of starch components and their contribution to the architecture of starch granules: A comprehensive review. Starch–Stärke 62, 389–420.

Picton, L., Bataille, I., Muller, G., 2000. Analysis of a complex polysaccharide (gum arabic) by multi-angle laser light scattering coupled on-line to size exclusion chromatography and flow field flow fractionation. Carbohydr. Polym. 42, 23–31.

Pumacahua-Ramos, A., Demiate, I.M., Schnitzler, E., Bedin, A.C., Telis-Romero, J., Lopes-Filho, J.F., 2015. Morphological, thermal and physicochemical characteristics of small granules starch from *Mirabilis jalapa* L. Thermochim. Acta 602, 1–7.

Putseys, J.A., Lamberts, L., Delcour, J.A., 2010. Amylose-inclusion complexes: Formation, identity and physico-chemical properties. J. Cereal Sci. 51, 238–247.

Qian, J., Kuhn, M., 1999. Characterization of *Amaranthus cruentus* and *Chenopodium* quinoa starch. Starch–Stärke 51, 116–120.

Radosavljevic, M., Jane, J., Johnson, L.A., 1998. Isolation of amaranth starch by diluted alkaline-protease treatment. Cereal Chem. 75, 212–216.

Ragaee, S., Abdel-Aal, E.S.M., 2006. Pasting properties of starch and protein in selected cereals and quality of their food products. Food Chem. 95, 9–18.

Rettig, W., 1986. Charge separation in excited states of decoupled systems—TICT compounds and implications regarding the development of new laser dyes and the primary process of vision and photosynthesis. Angew. Chem. Int. Ed. Engl. 25, 971–988.

Ring, S.G., Colonna, P., I'Anson, K.J., Kalichevsky, M.T., Miles, M.J., Morris, V.J., Orford, P.D., 1987. The gelation and crystallisation of amylopectin. Carbohydr. Res. 162, 277–293.

Sajilata, M.G., Singhal, R.S., Kulkarni, P.R., 2006. Resistant starch–A review. Compr. Rev. Food Sci. Food Saf. 5, 1–17.

Sandhu, K.S., Singh, N., 2007. Some properties of corn starches II: Physicochemical, gelatinization, retrogradation, pasting and gel textural properties. Food Chem. 101, 1499–1507.

Schober, T.J., Bean, S.R., Boyle, D.L., Park, S.H., 2008. Improved viscoelastic zein-starch doughs for leavened gluten-free breads: Their rheology and microstructure. J. Cereal Sci. 48, 755–767.

Shi, Y.-C., Seib, P.A., 1992. The structure of four waxy starches related to gelatinization and retrogradation. Carbohydr. Res. 227, 131–145.

Shin, J.-E., Simsek, S., Reuhs, B.L., Yao, Y., 2008. Glucose release of water-soluble starch-related α-glucans by pancreatin and amyloglucosidase is affected by the abundance of α-1,6-glucosidic linkages. J. Agric. Food Chem. 56, 10879–10886.

Shiraishi, K., Matsuzaki, S., Ishida, H., Nakazawa, H., 1993. Impaired erythrocyte deformability and membrane fluidity in alcoholic liver disease: Participation in disturbed hepatic microcirculation. Alcohol Alcohol 28, 59–64.

Singh, N., Inouchi, N., Nishinari, K., 2006. Structural, thermal and viscoelastic characteristics of starches separated from normal, sugary and waxy maize. Food Hydrocoll. 20, 923–935.

Singh, N., Singh, J., Kaur, L., Singh Sodhi, N., Singh Gill, B., 2003. Morphological, thermal and rheological properties of starches from different botanical sources. Food Chem. 81, 219–231.

Soulaka, A.B., Morrison, W.R., 1985. The amylose and lipid contents, dimensions, and gelatinisation characteristics of some wheat starches and their A- and B-granule fractions. J. Sci. Food Agric. 36, 709–718.

Stone, L.A., Lorenz, K., 1984. The starch of Amaranthus—Physico-chemical properties and functional characteristics. Starch–Stärke 36, 232–237.

Szymońska, J., Krok, F., 2003. Potato starch granule nanostructure studied by high resolution non-contact AFM. Int. J. Biol. Macromol. 33, 1–7.

Tamjidi, F., Shahedi, M., Varshosaz, J., Nasirpour, A., 2013. Nanostructured lipid carriers (NLC): A potential delivery system for bioactive food molecules. Innov. Food Sci. Emerg. Technol. 19, 29–43.

Taniguchi, H., Honnda, Y., 2009. Amylases, in: Schaechter, M. (Ed.), Encyclopedia of Microbiology (Third Edition). Academic Press, Oxford, pp. 159–173.

Tari, T.A., Annapure, U.S., Singhal, R.S., Kulkarni, P.R., 2003. Starch-based spherical aggregates: screening of small granule sized starches for entrapment of a model flavouring compound, vanillin. Carbohydr. Polym. 53, 45–51.

Tester, R.F., Karkalas, J., Qi, X., 2004. Starch—composition, fine structure and architecture. J. Cereal Sci. 39, 151–165.

Tester, R.F., Morrison, W.R., 1991. Swelling and gelatinization of cereal starches. I. Effects of amylopectin, amylose, and lipids. Cereal Chem. 67, 551–557.

Thompson, A.J., Herling, T.W., Kubánková, M., Vyšniauskas, A., Knowles, T.P.J., Kuimova, M.K., 2015. Molecular rotors provide insights into microscopic structural changes during protein aggregation. J. Phys. Chem. B 119, 10170–10179.

Thompson, D.B., 2000. On the non-random nature of amylopectin branching. Carbohydr. Polym. 43, 223–239.

Timgren, A., Rayner, M., Dejmek, P., Marku, D., Sjöö, M., 2013. Emulsion stabilizing capacity of intact starch granules modified by heat treatment or octenyl succinic anhydride. Food Sci. Nutr. 1, 157–171.

Tziotis, A., Seetharaman, K., Klucinec, J.D., Keeling, P., White, P.J., 2005. Functional properties of starch from normal and mutant corn genotypes. Carbohydr. Polym. 61, 238–247.

Vamadevan, V., Bertoft, E., Seetharaman, K., 2013. On the importance of organization of glucan chains on thermal properties of starch. Carbohydr. Polym. 92, 1653–1659.

van Esch, F., 1991. The efficiency of hydrocyclones for the separation of different starches. Starch–Stärke 43, 427–431.

Vandeputte, G.E., Vermeylen, R., Geeroms, J., Delcour, J.A., 2003. Rice starches. III. Structural aspects provide insight in amylopectin retrogradation properties and gel texture. J. Cereal Sci. 38, 61–68.

Vogel, M., Rettig, W., 1985. Efficient intramolecular fluorescence quenching in triphenylmethane-dyes involving excited states with charge separation and twisted conformations. Berichte Bunsenges. Für Phys. Chem. 89, 962–968.

Wang, Shujun, Li, C., Copeland, L., Niu, Q., Wang, Shuo, 2015. Starch retrogradation: A comprehensive review. Compr. Rev. Food Sci. Food Saf. 14, 568–585.

Wang, Y., 1993. Endogenous technical change and intra- and inter-industry quality competition. Econ. Lett. 41, 171–177.

Wang, Y.J., Wang, L., 2000. Structures and properties of commercial maltodextrins from corn, potato, and rice Starches. Starch–Stärke 52, 296–304.

Wang, Y.J., White, P.J., Pollak, L.M., Jane, J., 1993. Characterization of starch structures of 17 maize endosperm mutant genotypes with *Oh*43 inbred line background. Cereal Chem. 70, 171.

Wani, A.A., Singh, P., Shah, M.A., Schweiggert-Weisz, U., Gul, K., Wani, I.A., 2012. Rice starch diversity: Effects on structural, morphological, thermal, and physicochemical properties—A review. Compr. Rev. Food Sci. Food Saf. 11, 417–436.

Whistler, R.L., Daniel, J.R., 1984. Chapter VI—Molecular Structure of Starch, in: Whistler, R.L., Bemiller, J.N., Paschall, E.F. (Eds.), Starch: Chemistry and Technology (Second Edition), Food Science and Technology. Academic Press, San Diego, pp. 153–182.

Whittam, M.A., Orford, P.D., Ring, S.G., Clark, S.A., Parker, M.L., Cairns, P., Miles, M.J., 1989. Aqueous dissolution of crystalline and amorphous amylose-alcohol complexes. Int. J. Biol. Macromol. 11, 339–344.

Wiesenborn, D.P., Orr, P.H., Casper, H.H., Tacke, B.K., 1994. Potato starch paste behavior as related to some physical/chemical properties. J. Food Sci. 59, 644–648.

Willenborg, C.J., Johnson, E.N., 2013. Influence of seeding date and seeding rate on cow cockle, a new medicinal and industrial crop. Ind. Crops Prod. 49, 554–560.

Witczak, M., Korus, J., Ziobro, R., Juszczak, L., 2010. The effects of maltodextrins on gluten-free dough and quality of bread. J. Food Eng. 96, 258–265.

Wong, K.-S., Kubo, A., Jane, J., Harada, K., Satoh, H., Nakamura, Y., 2003. Structures and properties of amylopectin and phytoglycogen in the endosperm of *sugary*-1 mutants of rice. J. Cereal Sci. 37, 139–149.

Woodhouse, C.F., 2017. Food lawyers face challenges from 21st century logistics, FSMA, and the clean label movement. Am. Bar Assoc., Food, Cosmet. and Nutraceuticals News Letter, Winter 2017 Issue, 2–10.

Wu, J.G., Wang, P.J., Chen, S.C., 2010. Antioxidant and antimicrobial effectiveness of catechin-impregnated PVA-starch film on red meat. J. Food Qual. 33, 780–801.

Xia, H., Thompson, D.B., 2006. Debranching of β-dextrins to explore branching patterns of amylopectins from three maize genotypes. Cereal Chem. 83, 668–676.

Yao, Y., Thompson, D.B., Guiltinan, M.J., 2004. Maize starch-branching enzyme isoforms and amylopectin structure. In the absence of starch-branching enzyme IIb, the further absence of starch-branching enzyme Ia leads to increased branching. Plant Physiol. 136, 3515–3523.

Yoo, S.H., Jane, J., 2002. Molecular weights and gyration radii of amylopectins determined by high-performance size-exclusion chromatography equipped with multi-angle laser-light scattering and refractive index detectors. Carbohydr. Polym. 49, 307–314.

Yuan, R.C., Thompson, D.B., Boyer, C.D., 1993. Fine structure of amylopectin in relation to gelatinization and retrogradation behavior of maize starches from three *wx*-containing genotypes in two inbred lines. Cereal Chem. 70, 81–81.

Yun, S.H., Matheson, N.K., 1993. Structures of the amylopectins of waxy, normal, amylose-extender, and *wx*: *ae* genotypes and of the phytoglycogen of maize. Carbohydr. Res. 243, 307–321.

Yusoff, A., Murray, B.S., 2011. Modified starch granules as particle-stabilizers of oil-in-water emulsions. Food Hydrocoll. 25, 42–55.

Zhang, B., Davis, S.A., Mann, S., 2002. Starch gel templating of spongelike macroporous silicalite monoliths and mesoporous films. Chem. Mater. 14, 1369–1375.

Zhang, B., Dhital, S., Flanagan, B.M., Gidley, M.J., 2014. Mechanism for starch granule ghost formation deduced from structural and enzyme digestion properties. J. Agric. Food Chem. 62, 760–771.

Zhao, J., Whistler, R.L., 1994. Spherical aggregates of starch granules as flavor carriers. Food Technol. 48, 104–105.

Zobel, H.F., 1988. Starch crystal transformations and their industrial importance. Starch–Stärke 40, 1–7.

VITA

PROFESSIONAL EXPERIENCE

Purdue University, West Lafayette, IN **2014-present**

Graduate Research Assistant, Whistler Center for Carbohydrate Research

Graduate Teaching Assistant, Department of Food Science

China Agricultural University, Beijing, China **2012-2014**

Graduate Research Assistant, Laboratory of Protein Processing and Utilization

China Agricultural University, Beijing, China **2007-2011**

Undergraduate Research Assistant, Sino-Japanese Agricultural Products Processing Research Center

EDUCATION

Ph. D.	Purdue University	Food Science
M. Eng.	China Agricultural University	Food Science
B. Eng.	China Agricultural University	Food Science and Engineering

SELECTED PUBLICATIONS & PRESENTATIONS

1. **Peng X.,** Yao Y**.** (2017). Carbohydrates as fat replacers. ***Annual Review of Food Science and Technology***, 8, 331-351.
2. **Peng X.**, Yao Y. (2018). Small-granule starches from sweet corn and cow cockle: physical properties and amylopectin branching. ***Food Hydrocolloids***, 74, 349-357.
3. **Peng X.**, Yao Y. (2016). Microscale structure and thermal and pasting properties of sweet corn and cow cockle starches, presented at AACC International Annual Meeting, Savannah, 2016.
4. **Peng X.**, Yao Y. (2016). Advances in the use of starch for imparting fat-like texture to foods, presented at AACC International Annual Meeting, Savannah, 2016.
5. **Peng X.**, Alvarez M., Yao Y. (2018). High-throughput platform by single-kernel-screening method in maize, presented at Whistler Center for Carbohydrate Research Industrial Advisory Board Meeting, West Lafayette, 2017.